Institute of Electronic Structure and Laser (IESL),
Foundation for Research and Technology-Hellas (FORTH)
&
Department of Physics, University of Crete

Master Thesis
in
Optoelectronics and Microelectronics

FABRICATION OF 1D AND 2D RELIEF BRAGG REFLECTORS IN RARE EARTH DOPED PHOSPHATE GLASS BY EMPLOYING HOLOGRAPHIC LASER INDUCED STRUCTURAL MODIFICATION

Christos Pappas

Heraklion 2006

ABSTRACT

A high yield patterning technique for the fabrication of 1D relief Bragg reflectors and 2D photonic crystals is going to be demonstrated in the present study. The periodic structures were inscribed in Schott-USA IOG-1 Er/Yb-codoped phosphate glass substrates by employing multiple beam interference and the output of a high intensity pulsed 213nm Nd:YAG laser. The photosensitivity of the IOG-1 samples exposed to ultraviolet irradiation was studied and the nature of the induced damage in the volume of the material was investigated. Spectrophotometric data and diffraction efficiency measurements were employed in order to identify the irradiation induced absorption peaks and estimate the changes in the refractive index. In addition, Kramers-Kronig theoretical model and Urbach empirical rule were applied in order to enhance our understanding upon the defect formation mechanism and reveal possible changes in the structural order of the material.

The relief patterns were formed by following a low-damage method, in which the glass samples were irradiated with laser energy densities below the ablation threshold. A 2-beam elliptical Talbot interferometer and a 4-beam interference setup were employed in order to inscribe 1D and 2D periodic structures, respectively, in the volume of the IOG-1 glass, in the form of a periodic perturbation in the optical and the structural properties of the material. The exposed areas were selectively removed by employing a wet chemical development technique. For characterizing and optimizing the chemical development process, acidic and alkaline solutions were tested of different molar concentrations. The resulting relief gratings were characterized in terms of diffraction efficiency, while atomic force and scanning electron microscopy were employed to investigate the topography of the relief structures. 2D and 1D periodic Bragg structures in rare earth doped phosphate glasses may constitute a nutritious starting base for the realization of high gain lasers or amplification devices with low pumping needs, which can find several applications in telecommunications or optical sensing domains.

Περίληψη

Στην παρούσα εργασία περιγράφεται μια τεχνική κατασκευής ανάγλυφων μονοδιάστατων περιοδικών δομών Bragg και δισδιάστατων φωτονικών κρυστάλλων που βασίζεται στη χρήση ολογραφικής συμβολομετρίας λέιζερ. Οι παραπάνω περιοδικές δομές κατασκευάστηκαν σε υποστρώματα από φωσφορικό ύαλο με προσμίξεις σπανίων γαιών (Ερβίου και Υττερβίου) του τύπου IOG-1 (κατασκευαστής Schott-USA). Η κατασκευή των δομών γίνεται μέσω της έκθεσης του ύαλου σε παλμική ακτινοβολία λέιζερ Nd:YAG, μήκους κύματος 213nm, διάρκειας παλμού 150ps και εντάσεων της τάξης των GW/cm^2 και την μετέπειτα επιλεκτική εγχάραξη των εκτεθειμένων περιοχών μέσω χημικής εκσκαφής σε κατάλληλο οξύ ή βάση.

Αρχικά γίνεται μελέτη της φωτοευαισθησίας του ύαλου IOG-1 στην παλμική ακτινοβολία λέιζερ των 213nm και διερευνώνται οι αλλαγές που προκαλεί αυτή η ακτινοβολία στη δομή του υλικού. Γίνεται χρήση φασματοφωτομετρικών μετρήσεων για το προσδιορισμό και ταυτοποίηση των φασμάτων απορρόφησης που δημιουργούνται μετά την έκθεση. Οι παραπάνω δομικές αλλαγές εναλλακτικά ποσοτικοποιούνται και με την εγγραφή μονοδιάστατων φραγμάτων περίθλασης στον όγκο του ύαλου και την μέτρηση του συντελεστή απόδοσης σκέδασης τους (diffraction efficiency). Επιπροσθέτως, γίνεται εφαρμογή του θεωρητικού μοντέλου των Kramers-Kronig και του εμπειρικού κανόνα του Urbach για να εξετάσουμε αν οι αλλαγές στον συντελεστή απορρόφησης λόγω της έκθεσης στην ακτινοβολία συνδέονται με αλλαγές στον δείκτη διάθλασης, καθώς επίσης και για την αποσαφήνιση του μηχανισμού σχηματισμού ατελειών στον όγκο του υλικού.

Ακολούθως, ανάγλυφες περιοδικές δομές σχηματίζονται στην επιφάνεια του ύαλου, με την εφαρμογή μιας «ήπιας» τεχνικής νανο-εκσκαφής μέσω έκθεσης σε ισχυρή ακτινοβολία λέιζερ και ακόλουθης αφαίρεσης των εκτεθειμένων περιοχών μέσω χημικής κατεργασίας με κατάλληλο οξύ ή βάση. Αρχικά, γίνεται χρήση ενός ελλειπτικού συμβολομέτρου δύο δεσμών τύπου Talbot για την εγγραφή μονοδιάστατων περιοδικών δομών, στον όγκο του ύαλου IOG-1, με τη μορφή μιας περιοδικής διαμόρφωσης των οπτικών και δομικών ιδιοτήτων του. Διαλύματα οξέος HNO_3 και βάσεως KOH, διαφορετικών μοριακών συγκεντρώσεων εφαρμόζονται στη διαδικασία της υγρής εκσκαφής και συγκρίνονται ως προς τα αποτελέσματά τους. Οι ανάγλυφες δομές που προκύπτουν αξιολογούνται με βάση την απόδοσή τους σε πειράματα σκέδασης, το βάθος τους και την τοπολογία της περιοδικότητας τους, μέσω ατομικής (AFM) και ηλεκτρονικής μικροσκόπιας (SEM).

Τέλος, η μέθοδος εφαρμόζεται στην κατασκευή ανάγλυφων δισδιάστατων φωτονικών κρυστάλλων στον ύαλο IOG-1. Η εγγραφή των δομών στον παραπάνω φωσφορικό ύαλο επιτυγχάνεται με τη χρήση ενός συμβολομέτρου τεσσάρων δεσμών και την έκθεση σε ακτινοβολία 213nm Nd:YAG λέιζερ. Η εκσκαφή των πολυδιάστατων περιοδικών δόμων τελείται με κατάλληλη επιλογή των παραμέτρων της χημικής ανάπτυξης όπως αυτές βελτιστοποιήθηκαν σε προηγούμενες μελέτες. Πειράματα μέτρησης σκέδασης και εικόνες μικροσκοπίας SEM και AFM χρησιμοποιούνται για την περαιτέρω μελέτη των ανάγλυφων δισδιάστατων περιοδικών δομών.

Ευχαριστήριο Σημείωμα

Είθισται κάθε πόνημα που ανακεφαλαιώνει κατά κάποιο τρόπο κόπους και προσπάθειες πολλών ετών να αφιερώνεται πρωτίστως στα συγγενικά πρόσωπα. Ως προς αυτό, η δική μου εργασία δεν θα αποτελέσει εξαίρεση. Ευχαριστώ λοιπόν την μητέρα μου Χρύσα, τον πατέρα μου Βαγγέλη και τη μικρή μου αδελφή Ελένη για την αγάπη και τη στήριξη που μου προσέφεραν όλα αυτά τα χρόνια. Ακόμα ευχαριστώ τους κοντινούς μου συγγενείς που ήταν έτοιμοι να προσφέρουν κάθε βοήθεια με κάθε τρόπο.

Μια εργασία, όπως η παρούσα, δεν θα ήταν δυνατόν να περατωθεί, χωρίς την ουσιαστική συμβολή και έμπνευση του επιβλέποντα ερευνητή μου Dr. Σταύρου Πισσαδάκη. Πολλά ευχαριστώ οφείλω στον Σταύρο για την υπομονή του, τον χρόνο που επένδυσε και κυρίως για την πίστη του σε εμένα.

Θέλω ακόμα να ευχαριστήσω τον διευθυντή του Ινστιτούτου Ηλεκτρονικής Δομής και Λέιζερ (ΙΗΔΛ), Dr Κωνσταντίνο Φωτάκη για την ευκαιρία που μου έδωσε να τελέσω την μεταπτυχιακή μου εργασία σε ένα ερευνητικό ίδρυμα μοναδικό για τα ελληνικά δεδομένα και καταξιωμένο στον ευρωπαϊκό χώρο όπως το Ίδρυμα Τεχνολογίας και Έρευνας (ΙΤΕ).

Ευχαριστίες ακόμα και σε όλο το προσωπικό του ΙΤΕ που βοήθησε με κάθε τρόπο και ειδικά στον 'γιατρό' των λέιζερ Απόστολο Ιγγλέζη και την Αλέκα Μανουσάκη που είχε τη υπομονή να δει τόσες εικόνες AFM όσες είδα και εγώ.

Τέλος πρέπει να αποδώσω τα δέοντα και με όλες τις τιμές σε όλη τη τρελοπαρέα της Κρήτης. Σ' αυτούς που μου στάθηκαν στα δύσκολα και έκαναν τις ωραίες στιγμές υπέροχες. Αρχίζοντας από τον σκληρό πυρήνα τον 'Skandzman' Μανόλη, την Έλσα, τον Γρηγόρη. Αλλά και τους πλησιέστερους δορυφόρους Ελένη, Iacopo και τον 'συνάδελφο' Γιώργο. Όλους τους φανατικούς στο deck του La Brasserie, τον 'Ξάδελφο' τον άρχοντα του Desire. Τους 'μουτζαχεντίν' του meeting room Βασιλεία, Όλγα, Μαρία, Αντρέα, Austin. Σε όλους όσους πέρασαν από την μεγάλη παρέα του ΙΤΕ, άλλος για περισσότερο και άλλος για λιγότερο και μιλήσαμε και γελάσαμε μαζί. Σας ευχαριστώ όλους πολύ παιδιά και ξέρω ότι ένα ευχαριστώ είναι πολύ λίγο…

Table of contents

Chapter 1. Introduction

1.1. Ultraviolet laser micro-/nano-patterning for structuring photonic devices

Laser micro-/nano-patterning arises as a reliable, low-cost approach in the fabrication procedure of high performance photonic devices. This patterning approach has attracted great interest, triggered mostly by the widespread availability of high-intensity short-pulse UV laser sources (ex. Excimer, Nd:YAG lasers) and the high quality etching products. Ultraviolet (UV) pulsed laser irradiation enables the straightforward inscription of different kind of modifications in most optical materials. These modifications are usually of the form of permanent changes in the optical or the structural properties of the material, while at high fluencies, short wavelength laser pulses can cause ablation of the material surface, which leads to the fabrication of relief patterns. Relief patterns are desirable in modern photonic applications due to the high contrast in the refractive index that they exhibit. Optical elements that exhibiting high contrast in the refractive index compared with the environment can be used for the efficient manipulation of light in the micro or nano-meter scale.

Laser micro-/nano-patterning exhibits several advantages over other relevant fabrication techniques such as UV, X-ray or electron beam lithography in the fabrication of submicron period grating/crystal structures. UV lithography is a multi-step procedure which demands the use of a hard or soft mask and it is not of high yield when tuning tolerances are needed. Electron beam lithography demands expensive laboratorial equipment and the processing area is rather limited. On the other hand, short laser pulses in combination with interferometric cavities may lead to the straightforward inscription of sub-micron photosensitive or relief periodic structures in several dielectric, metallic or polymeric substrates. 1D and 2D periodic structures inscribed in transparent materials can constitute key elements in the development of functional and high performance planar photonic devices.

1.2. Optical elements for integrated photonic applications: Bragg reflectors and 2D photonic crystals

Bragg gratings in transparent materials are implemented in the form of a periodic perturbation of the effective absorption/or gain coefficient and/or of the refractive index. The name of those diffractive structures comes from Bragg's Law, firstly derived by Sir William Laurence Bragg (1890-1971) in order to explain the reflection of x-ray beams from a crystal lattice. Since then, the law has been successfully applied to study different kind of periodic structures, by means of type of modulation (refractive index, gain etc), and dimension.

Bragg gratings are inevitable optical elements in the design and development of novel and functional photonic devices. Particularly, these structures can play a significant role in photonic devices used in optical communications, sensing and spectroscopy. For applications in the field of optical communications, Bragg gratings –in conjunction with other significant elements and devices- were the driving levers for the development of the wavelength-division multiplexing (WDM) accessing technology. Fibre and waveguide Bragg reflectors operate in devices such as add-drop multiplexers, gain flattening filters, laser mirrors or dispersion compensators. On the other hand, Bragg reflectors inscribed in optical fibres and waveguides constitute backbone elements for the development of structural, environmental, chemical and biological sensors, of enhanced selectivity and functionality.

Relief Bragg gratings are the cavity forming elements of distributed feed-back (DFB) and distributed Bragg reflector (DBR) lasers [1]. DFB lasers are fixed wavelength single mode solid-state lasers. The whole cavity in DFB lasers consists of a periodic structure which acts as a reflector in the wavelength range of laser action and contains the active medium. A π-defect –namely, half of the Bragg periodicity- is introduced in the middle of the grating. This separates the periodic structure into two Bragg mirrors, defining at the same time a resonant state into the laser cavity. DBR lasers are tunable single mode solid state lasers.

The laser cavity in DBR lasers is defined by one or two passive Bragg grating reflectors at the edges of the gain medium. The structure usually includes a joint between the passive and the active regions. Usually, the emission wavelength of the laser can be tuned electro-optically. Most DFB and DBR lasers are based on semiconductor and glass materials.

Relief 2D or 3D periodic structures of high index contrast, inscribed in transparent optical materials, can also find significant applications in sensing and communications. The main characteristic of photonic crystals, is that they exhibit an energy band gap, known as photonic band gap [2][3][4]. The photons whose energy is in the band gap are not allowed to exist inside the photonic crystal. If phase shifted defects are inserted into the periodicity of the photonic crystal, light oscillation cavities are formed, providing action similar to that of the DFB. Such optical scheme constitutes an efficient light trap, allowing long oscillation times. This is one of the reasons why photonic crystals appear to be attractive optical configurations for controlling the flow of light.

Photonic crystals can also be used to realize wavelength de-multiplexers several times smaller than those based on conventional optical devices. A prism made of photonic crystal exhibits dispersion hundreds of times greater than conventional prisms. Additionally to wavelength de-multiplexing, we can exploit the TE and TM polarization sensitivity of the photonic crystal in order to realize polarization de-multiplexers.

1.3. Fabrication methods of 1D and 2D periodic structures in transparent materials: State-of-the-art

During the last decades, the idea of developing of periodic structures in waveguides for the development of devices that could be used in telecommunication and laser applications appeared quite attractive. This interest was mostly triggered by the development of new laser devices based in semiconductors. The theoretical background of Bragg scattering in dielectric media was first developed by Kogelnik in 1969 [5]. Kogelnik had foreseen the possibility that holographic optical components, like gratings or fly eye lenses,

can be used in a variety of optical systems. Few years later, the same researcher [6] studied the feedback mechanism in DFB lasers and another group, led by Nakamura and Yariv [7], developed the first distributed feedback laser in GaAs. UV, X-ray, e-beam and holographic lithography [8][9] are the most important and applicable processes for the fabrication of Bragg structures in a variety of optical substrates. UV and X-ray lithography are time consuming, multi-step processes and rely on the existence of a fixed projection/or contact mask. Both operate in combination with wet or dry etching techniques in which toxic chemical photoresist and developers are used. E-beam lithography is a more versatile process –by means of mask definition- but at the same time is laborious, requiring expensive laboratorial equipment. Also E-beam lithography poses restrictions in the exposure area of the nano-patterning, resulting in difficult patching processes and the possibility of parasitic stitching error insertion in the periodic structure.

Laser micromachining and holographic lithography are efficient optical techniques for the fabrication of 1D gratings and of more complicated photonic crystals. In holographic lithography, we exploit the interference pattern generated by the overlap of two or more monochromatic beams emitted from a single light source and splitted in different parts. Direct fabrication of periodic structures by the above technique has been reported in several studies. Ablation experiments were performed with short pulse high photon energy laser sources, such as F_2-lasers (@157nm) or narrow-linewidth excimer lasers in order to ablate relief patterns in several substrates like borosilicate glass [10], fused silica [11], Niobium Oxide (Nb_2O_5) films [12] or Lithium Niobate ($LiNbO_3$) [13]. In the aforementioned works the irradiation of the sample was done by using an amplitude mask projection setup or by direct two beam interference. Zimmer, *et al*, [14] employed an achromatic Schwarzchild-type reflective objective configuration in conjunction with a process that allows laser-induced etching of transparent materials at the interface of high absorbing liquids, in order to shape relief structures in fused silica. Kawamura *et al*, [15] and Fedosejevs *et al*, [16] used a Ti:Sapphire and a KrF laser respectively and simple beam splitters to inscribe gratings in several substrates. Finally, direct interferometric ablation was used for the fabrication of strong Bragg reflectors in thin film overlaid potassium ion exchanged waveguides [17].

The interest about optical holography techniques was recently triggered by the development of high performance beam splitting elements like phase masks. The phase mask is a one dimensional periodic surface relief element fabricated by e-beam lithography in fused silica plates. The phase mask exhibits many advantages, because it can be easily aligned and placed in an interferometric cavity or can be used directly in contact mode to inscribe periodic patterns in substrates, enabling the use of low coherence laser sources. Phase masks in contact mode have already been employed for the inscription of Bragg gratings in fibers [18]-[20] and glass slabs. P.E Dyer *et al*, [21] employed a low coherence KrF laser and a phase mask in contact mode to inscribe relief gratings in polymers. J. Zhang [22] demonstrated that a similar configuration can lead to effective ablation of fused quartz by coupling of plasma generated from a metal target placed beside the sample, by the same laser. They both demonstrated that the interference of the 0-order and the ±1 orders coming out of the phase mask, results in a structure with the same period as the period of the phase mask. Luo *et al*, [23] employed a phase mask in contact mode and the output of a KrF laser in order to inscribe gratings in $LiNbO_3$. Phase masks have also been incorporated in open interferometric setups. Dyer *et al*, [24] employed the zero and first diffraction orders and the output of an ArF laser (@193nm) in order to inscribe gratings in polymers. Lastly, Wu *et al*, [25] employed the ±1 diffraction orders and a mirror-based beam-folding system to induce surface relief gratings in $LiNbO_3$.

More complicated 2-dimensional and 3-dimensional periodic structures have also been fabricated by employing laser interferometric lithography. Kondo *et al*, [26] described the fabrication of 2D periodic structures in photoresist by multiple beam interference. Klein-Wiele [27] demonstrated that photonic structures with different shapes can be obtained by controlling the phase difference between the interfering beams. Kawamura, *et al*, [28] and Lai, *et al*, [29] demonstrated the fabrication of 2D and 3D photonic crystals by employing a multi-step 2-beam interference technique. In this technique, a 1D periodic crystal is initially inscribed and subsequently the sample is rotated and a second grating is recorded. Lastly, Campell *et al*, [30] fabricated 3D periodic structures in polymer by employing 4-beams interference and the output of a Q-switched Nd:YAG

laser. The phase mask was the key beam-splitting element in most of the cases described above.

1.4. Phosphate glasses as host materials for active devices

Phosphate glasses are promising candidates for the realization of novel and high performance active and passive integrated optical devices. Their main advantage over other type of glasses –i.e silicate glasses- is their capability of hosting ion dopands at high concentrations/solubilities, without deteriorating/degrading other mechanical, structural or optical properties of the glass matrix.

The basic structural unit in phosphate glasses is the PO_4^{3-} group which can be attached to maximum three neighboring groups forming long polymeric chains. Due to the threefold linked structure, the number of cross-links in phosphate glasses is small compared with that in silicate glasses. On the other hand, there is a large number of terminal oxygen atoms (for example the double-bonded oxygen atoms) which allow high degree of flexibility for the orientation of PO_4^{-3} groups. Thus, the phosphate glasses can be doped with large amounts of alkali, metal or rare earth ions providing complete series of products with unique properties which could be used as the base for the development of sophisticated photonic structures.

Phosphate glasses can be classified in categories by the oxygen-to-phosphorous ratio in the bulk of the material [31]. For example metaphosphate glasses correspond to a O/P ratio equal to 3 and polyphosphate glasses correspond to a O/P ratio greater than 3. Both glasses are characterized by long linear polymeric chains which are formed when P-tetrahedra are linked with two neighbors through covalent bridging oxygens. The chains are connected themselves with ionic cross-links between the non-bridging oxygens and the modifying cations. The average chain length decreases when the O/P ration increases. In Ultraphosphate glasses, the O/P ratio is less than 3 and in each tetrahedron correspond three bridging oxygens. The properties of phosphate glasses have been studied by several research groups. Hoppe, *et al*, [32], for example

described the role that the modifier coordination plays in determining the properties and structure of the material while R. Brow, *et al*, [33] studied the composition dependence of the transition temperature.

The high rare-earth doping concentrations that can be hosted in phosphate glasses, allows the development of high gain waveguide lasers and amplifiers with small cavity sizes and low pumping needs. Meshkinfam *et al*, [34] applied an ion exchange process in order to form waveguides in Er/Yb-codoped phosphate glass. Veasey *et al*, [35] fabricated a DBR laser in IOG-1 phosphate glass. Yan *et al*, [36] fabricated Er-doped phosphate glass waveguides by rf sputtering techniques on thermally oxidized silicon substrates. Chan *et al*, [37] employed femtosecond laser pulses in the near-infrared range of wavelengths in order to inscribe waveguides in the bulk of IOG-1 phosphate glass samples.

1.5. Project motivation

Holographic lithography exhibits several advantages compared with other fabrication techniques, used for periodic structures processing in submicron scale. Two- or multiple- beam interference is a single step, mask-less process which allows the straightforward inscription of submicron periodic patterns in a variety of substrates using direct ablation or photodissociation and subsequent developing/etching processes. Depending on the beams combined, the interference conditions –by means of phase and angle- the exposure conditions and the photon-material interaction nature, 1-, 2- or 3-dimensional periodic structures may be formed in "hard" or "soft" optical materials[1].

Even though there are many examples where laser interfering beams were used for defining 1-, 2- or 3-dimensional periodicities in "soft" materials -such as photoresists- there are fewer examples where such approach was applied for the

[1] We categorise optical materials in "hard" and "soft", where in the category of "hard" materials we include glasses, crystals and polycrystalline matrixes; while in the category of "soft" materials we categorise polymers, photoresits, bio-materials and liquid crystals. Such categorisation is generally based on the mechanical, thermal and optical properties –by means of ablation threshold and radiation resistivity- of the materials used in the laser exposure experiments.

structuring of "hard" materials such as glasses or thin, polycrystalline films. In addition, most of the interference patterning methods used for structuring "hard" materials, are based on the application of direct ablation, where high energy densities are used for the explosive material removal from the exposed area.

The fabrication of relief periodic structures in glasses by employing multi-beam interferometric pulsed laser techniques is a rather difficult task because high values of energy density are required in order to ablate the material. Special care must be taken in order to eliminate the energy losses that are taking place in interferometric cavities. For this reason other fabrication techniques have been applied in the case of "hard" materials, such as e-beam lithography.

In the present study, we will demonstrate the fabrication of 1D and 2D relief periodic structures in Er/Yb-codoped phosphate glass, by employing UV laser holography in combination with structural volume modification and selective wet etching. We have used an elliptical Talbot interferometer for defining the 1-dimensional grating patterns, while for defining the 2-dimensional periodicity a four beam interferometric setup was employed. In order not to adopt direct ablation which requires high energy densities and can result in low quality structures due to the explosive interactions between the laser irradiation and the matter, we have followed an easily controllable, low-damage method. By exposing the optical material with conditions (pulse number and energy density) below the ablation threshold, we induce controlled volume damage into the volume of the material. This volume damage may have the form of changes in the optical and the structural properties of the glass. Subsequently, a chemical development technique is applied in order to selectively remove the irradiated/damaged areas. Selective chemical etching is preferable than direct ablation because it constitutes a more controllable process in which explosive interactions between the laser irradiation and the material are avoided and more qualitative structures can be obtained. A similar technique has already been applied in order to shape relief gratings in Ta_2O_5 but the quality of the structures obtained was of the order of the granule size of the polycrystalline material [38].

We decided to study the micro-structuring of Schott USA IOG-1 Er/Yb-codoped phosphate glass. This glass combines unique material properties such as long

emission lifetime and high energy transfer coefficient from the 1000nm band to 1550nm band which is the common operating frequency in optical telecommunications. For this reason the glass can constitute the base for the realization of high gain lasers or amplification devices of low pumping power needs. A more detailed description of the glass properties will be provided in the next chapters, where the photosensitivity and the dissolution of the material in chemical solutions will be extensively studied.

Relief periodic structures are inevitable optical elements for the development of high gain laser cavities or active routing devices. Thus, the demonstration of a versatile and high efficiency laser structuring method in the periodic nano-patterning of such high performance hybrid active glass may attract the interest for commercial applications and large scale production.

1.6. Project outline

In the next chapters we will present in detail the method applied for the fabrication of 1D Bragg reflectors and 2D photonic crystals in IOG-1 Er/Yb-codoped phosphate glass slabs. The light source used for exposures was a quintupled 213nm, 150ps Nd:YAG laser. This laser wavelength is used for the first time for inscription of structures in the certain glass and for that reason we firstly performed an extended study of the photosensitivity of the material examined. The thematic outline of the thesis is the following:

Chapter 1. *Introduction: Photonic crystals, Laser micro-/nano-fabrication techniques and Phosphate glasses.*

Chapter 2. *UV-induced changes in the optical and structural properties of Er/Yb-codoped IOG-1 phosphate glass substrates: measurement of the changes in the absorption Δα induced by the intense UV laser irradiation, identification of the induced absorption bands and quantitative determination of possible structural modifications. Application of theoretical models in order to estimate the*

permanent refractive index changes caused by intense UV irradiation.

Chapter 3. *Inscription of photosensitive Bragg gratings in IOG-1 phosphate glass: inscription of photosensitive Bragg gratings by employing an elliptical Talbot interferometer and the output of the high intensity 213nm, 150ps Nd:YAG laser; characterization of the inscribed holographic gratings by means of real-time probing and post-exposure diffraction efficiency. Application of theoretical models in order to estimated changes in the refractive index and comparison with the results found previously.*

Chapter 4. *Fabrication of Bragg relief gratings in Er/Yb-codoped IOG-1 phosphate glass slabs using post-exposure selective chemical etching: study of the chemical development in acidic and alkaline solutions for different exposure conditions and etchant concentrations; characterization of the fabricated structures in terms of diffraction efficiency and optimization of the parameters of the technique; topological study of the relief structures by employing AFM scans and SEM microscopy. Speculation of the radiation assisted selective etching mechanism.*

Chapter 5. *Fabrication of 2-dimensional Bragg reflectors in Er/Yb-codoped IOG-1 glass substrates: inscription of 2D periodic structures in IOG-1 glass planar substrates by employing a 4-beam interferometric setup; chemical development of the inscribed structure using the optimized parameters found above. Presentation of AFM scans and SEM images and characterization of the sample in terms of diffraction efficiency and the symmetry of the structure.*

Chapter 6. *Conclusions*

1.7. References

[1] L.A. Coldren, S.W. Corzine, Diode Laser and Photonic Integrated Circuits, Wiley Series in Microwaves and Optical Engineering (1995)

[2] E. Yablonovich, Inhibited Spontaneous Emission in Solid-State Physics and Electronics, Phys. Rev. Let., **58**, 2059-2062 (1987)

[3] S. John, Strong Localization of Photons in Certain Disordered Dielectric Supperlattices, Phys. Rev. Let., **58**, 2486-2489 (1987)

[4] J.D Joannopoulos, P.R. Villeneuve, S. Fan, Photonic Crystals: Putting a New Twist on Light, Nature, **386**, 143-149 (1997)

[5] H. Kogelnik, Coupled Wave Theory for Thick Hologram Gratings, The Bell System Technical Journal, **48**, 2909-2947 (1969)

[6] H. Kogelnik, C.V. Shank, Coupled wave theory of distributed feedback lasers, J. Appl. Phys. **43**, 2328 (1974)

[7] Nakamura, A. Yariv, H.W. Yen, S.Somekh, H.L. Garvin, Optical pumped GaAs surface laser with corrugation feedback, Appl. Phys. Lett., **22**,515 (1973)

[8] C.Y. Chang, S.M. Sze, USLI Technology, Mc Graw-Hill Series in Electrical and Computer Engineering (1996)

[9] L.F. Thomson, C.G. Wilson, M.J. Bowden, Introduction to Microlithography, ACS Professional Reference Book, American Chemical Society, Washington, DC (1994)

[10] S. Pissadakis, L. Reekie, M. Hempstead, M.N. Zervas, J.S. Wilkinson, Ablated Gratings on Borosilicate Glass by 193nm Excimer Laser Radiation, Appl. Phys. A, **69**, S739-S741 (1999)

[11] J. Ihlemann, S. Muller, S. Puschmann, D. Schafer, M. Wei, J. Li, P.R. Herman, Fabrication of Submicron Gratings in Fused Silica by F_2-laser Ablation, Appl. Phys. A, **76**, 751-753 (2003)

[12] M.A. Bader, C. Kappel, A. Selle, J. Ihelmann, M.N. Ng, P.R. Herman, Fabrication of Sub-Micron Gratings in Ultra thin Films by 157nm Laser Ablation and their Application as Gratings Waveguides Structures, Proc. Of SPIE, **5578**, 559-567 (2004)

[13] K. Chen, J. Ihlemann, P. Simon, I. Baumann, W. Sohler, Generation of Submicron Surface Gratings on $LiNbO_3$ by Ultrashort UV Laser Pulses, Appl. Phys. A, **65**, 517-518 (1997)

[14] K. Zimmer, R. Bohme, A. Braun, B. Rauschenbach, F. Bigl, Excimer Laser-Induced Etching of Sub-Micron Surface Relief Gratings in Fused Silica Using Phase Grating Projection, Appl. Phys. A, **74**, 453-456 (2002)

[15] K. Kawamura, T. Ogaka, N.Sarukura, M.Hirano, H. Hosono, Fabrication of surface Relief gratings on Transparent Dielectric materials by Two-Beam Holographic Method Using Infrared Femtosecond Laser Pulses, Appl. Phys. B., **71**, 119-121 (2000)

[16] R. Fedosejevs, M.J. Brett, Direct Formation of Grating Structures on Silicon Using KrF Laser Radiation, Appl. Opt., **28**, 1877-1880 (1989)

[17] S. Pissadakis, L. Reekie, M. Hempstead, M.N. Zervas, J.S. Wilkinson, Relief Gratings on Er/Yb-doped Borosilicate Glasses and Waveguides by Excimer Laser Ablation, Appl. Surf. Sci., **153**, 200-210 (2000)

[18] A. Othonos, X. Lee, Novel and Improved Methods of Writing Bragg Gratings with Phase Masks, IEEE Phot. Tech. Let., **7**, 1183-1185 (1995)

[19] B. Malo, D.C. Johnson, F. Bilodeau, J. Albert, K.O. Hill, Single-Excimer- Pulse Writing of Fiber Grating by the use of a Zero Order Nulled Phase Mask: Grating Spectral Response and Visualization of Index Perturbations, Opt. Let., **18**, 1277-1279 (1993)

[20] Y. Qiu, Y. Sheng, Optimal Phase Mask for Fiber Bragg Grating Fabrication, Jour. of Lig. Tec., **17**, 2366-2370 (1999)

[21] P.E. Dyer, R.J. Farley, R. Giedl, Study and Analysis of Submicron-Period Grating Formation on Polymers Ablated Using a KrF Laser Irradiated Phase Mask, Appl. Phys. Lett., **64**, 3389-3391 (1994)

[22] J. Zhang, K. Sugioka, K. Midorikawa, Direct Ablation of Micrograting in Fused Quartz by Laser-Induced Plasma-Assisted Ablation with a KrF Laser, Opt. Lett., **23**, 1486-1488 (1998)

[23] G.P. Luo, Y.L. Lu, Y. Q. Lu, X.L. Guo, S.B. Xiong, C.Z.Ge, Y.Y. Zhu, Z.G. Liu,N.B. Ming, J.W. Wu, D.S. Ding, Z.H. Lu, $LiNbO_3$ Phase Gratings Prepared by a Single Excimer Pulse Through a Silica Phase Mask, Appl. Phys. Lett., **69**, 1352-1354 (1996)

[24] P.E. Dyer, R.J. Farley, R. Giedl, Analysis and Application of a 0/1 order Talbot interferometer for 193nm Laser Grating Formation, Opt. Com., **129**, 98-108 (1996)

[25] B. Wu, P.L. Chu, H. Hu, Z. Xiong, UV-Induced Surface-Relief Gratings on $LiNbO_3$ Channel Waveguides, J.. Quantum. El., **35**, 1369-1373 (1999)

[26] T. Kondo, S. Matsuo, S. Juodkazis, V, Mizeikis, Multiphoton fabrication of Periodic Structures by Multibeam Interference of Femtosecond Pulses, Appl. Phys. Lett., **82**, 2758 (2003)

[27] J. Klein-Wiele, P. Simon, Fabrication of Periodic Nanostructures by Phase-Controlled Multiple-Beam Interference, Appl. Phys. Lett., **83**, 4707-4709 (2003)

[28] K. Kawamura, N. Sarukura, M. Hirano, N. Ito, H. Hosono, Periodic Nanostructure array in Crossed Holographic Gratings on Silica Glass by two Interfered Infrared-Femtosecond Laser Pulses, Appl. Phys. Lett., **79**, 1228-1230 (2001)

[29] N. Lai, W.P. Liang, J.H. Lin, C.C. Hsu, C.H. Lin, Fabrication of Two- and Three-Dimensional Periodic Structures by Multi-Exposure of Two-Beam Interference Technique, Opt. Exp., **13**, 9605-9611 (2005)

[30] M. Campbell, D.N. Sharp, M.T. Harrison, R.G. Denning, A.J. Turberfield, Fabrication of Photonic Crystals for the Visible Spectrum by Holographic Lithography, Nature, **404**, 53-56 (2000)

[31] J. Van Wazer, K. Holst, Structure and Properties of the Condensed Phosphates. I. Some General Considerations about Phosphoric Acids, Jour. Am. Chem. Soc., **72**, 639-644 (1950)

[32] U. Hoppe, A Structural Model for Phosphate Glasses, J. Non-Crystalline Sol., **195**, 138-147 (1996)

[33] R.K. Brow, C.A. Click, T.M. Alam, Modifier Coordinator and Phosphate Glass Networks, J. Non-Crystalline Sol., **274**, 9-16 (2000)

[34] P. Meshkinfam, P. Fournier, M.A. Fardad, M.P. Andrews, S.I. Najafl, Integrated Optics Er-Yb amplifier with Potassium Ion-Exchanged Glass Waveguides, Research Grant Report to the Natural Sciences and Engineering Research Council of Canada, Ecole Polytechnique & Mc Gill University (1996)

[35] D.L. Veasey, D.S. Funk, P.M. Peters, N.A. Sanford, G.E. Obarski, N. Fontaine, M. Young, A.P. Peskin, W. Liu, S.N. Houde-Walter, J.S. Hayden, Yb/Er-codoped and Yb-doped Waveguide Lasers in Phosphate Glass, J. Non-Crystalline Sol., **263&264**, 369-381 (2000)

[36] Y.C. Yan, A.J. Faber, H. de Waal, P.G. Kik, A. Polman, Erbium-Doped Phosphate Glass Waveguides on Silicon with 4.1 dB/cm Gain at 1.535 μm, Appl. Phys. Lett., **71**, 2922-2924 (1997)

[37] J.W. Chan, T.R. Huser, S.H. Risbud, J.S. hayden, D.M. Krol, Waveguide Fabrication in Phosphate Glasses Using Femtosecond Laser Pulses, Appl. Phys. Lett., **82**, 2371-2373 (2003)

[38] S. Pissadakis, A. Ikiades, C.Y. Tai, N.P. Session, J.S. Wilkinson, Sub-micron Periodic Gratings in Ta_2O_5 Thin Oxide Films Patterned Using UV Laser Post-Exposure Chemical Assisted Selective etching, Thin Sol. Films, vol. **453-454C**, 458-461 (2004)

Chapter 2. UV-induced changes in the optical and structural properties of Er/Yb-codoped IOG-1 phosphate glass substrates

2.1. Introduction

Intense ultraviolet irradiation of photon energy comparable with the energy band-gap of a material can cause significant electronic and structural changes into its exposed volume. These changes can lead to absorption bands formation, which in turn may be easily observed by simple spectrophotometric measurements. In the following chapter, the optical density changes induced by the exposure of the Er/Yb-codoped IOG-1 phosphate glass to intense ultraviolet radiation will be investigated and quantified. These optical density changes are associated with colour centre formation and structural modifications that occur into the material matrix, which in turn are usually translated to refractive index changes. Kramers-Kronig theoretical formula will be applied in order to estimate the changes in the refractive index which are correlated with the formation of strong absorption bands. In addition, Urbach empirical rule will be applied in order to provide us with a quantitative approximation about the radiation induced structural changes in the bulk of the material.

Our main aim in this chapter is to identify and examine the nature and the formation mechanism of the UV irradiation induced defects. Changes in the optical density of the glass could be induced in a periodic pattern in order to inscribe photosensitive Bragg structures. Possible structural damages could also be exploited in order to make the glass more vulnerable to specific acidic or alkaline chemical solutions. In this case, we could exploit the different etching rates between the irradiated and the non-irradiated areas of the samples in order form relief patterns on the surface of the IOG-1 glass substrates.

2.2. The UV photosensitivity of phosphate glasses

Laser pulses of high energy densities provoke strong interaction in transparent materials. These interactions usually lead to defect formation in the volume of the material, usually called as electron or color centers, and absorption band generation. The history [1][2] of research into electron centers, starts in the first decades of the previous century from the attempts of mineralogists to interpret the coloration or bleaching of certain minerals caused by heating, electrical charge or irradiation. The term "color center" or "F-center" (from German Farbenzentren) appears for the first time in 1920, first concerning materials of alkali halides, which were studied extensively that period of time. De Boer, in 1937, suggested the model of the F center as an electron trapped in an anion vacancy. By analogy, a "hole center" or "V-center" corresponds to a cation vacancy with a trapped hole. The research into electron-hole centers is closely related to the electron-paramagnetic resonance measurements (EPR) carried out form the middle of 1960s.

During the last 25 years, high power lasers have been employed in order to study the defect formation in several transparent materials. Extensive work has already been performed on materials like SiO_2, CaF_2, alkali halides, germanosilicates, chalcogenides etc. On the other hand, the photosensitivity of phosphate glasses, has only been recently studied, although the unique physical properties and optical characteristics that they exhibit. One possible frustrating reason is that phosphate glasses usually exhibit poor chemical durability in aqueous solutions. However, new melting techniques that were developed, yielded a variety of phosphate based glasses of different compositions with resistance to aqueous corrosion that is comparable to that of silicate glasses. The dissolution of the new generation of phosphate glasses in aqueous solutions was extensively studied by several groups [3][4][5].

The photosensitivity of phosphate based glasses has attracted the interest of several groups. Ehrt *et al,* [6] studied the UV radiation-induced defects in meta-phosphate and fluoride-phosphate glasses. An analogous study was performed by Zhou *et al,* [7] in Nd-doped barium meta-phosphate laser glasses. Watanabe

et al, [8] reported on the photosensitivity in soda-aluminum-phosphate glass doped upon exposure to near-ultraviolet femtosecond laser pulses. Chan *et al,* [9] exposed sodium-aluminum phosphate glass to infrared femtosecond laser pulses. Lastly, in a recent work, Pissadakis *et al,* [10] studied the photosensitivity of Ag^+ ion-exchanged Er-doped phosphate glass using 248nm excimer laser irradiation.

2.3. Er/Yb-codoped IOG-1 Schott phosphate glass: Material details

The phosphate glass used in this project is the Er/Yb-codoped IOG-1 fabricated by Schott-USA. IOG-1 is a sodium-aluminum-phosphate glass developed for hosting high concentrations of rare earth ions and being suitable for waveguide fabrication by potassium and silver ion-exchange processes [11].

IOG-1 glass was specially designed for the realization of waveguide lasers and amplifiers, fact which means that the material properties were optimized in order to support efficient laser action. Thus, the laser transition lifetime is relatively long compared to the lifetime of the pump level (see Table 2.2) and the energy transfer efficiency to Er from the sensitizing ion Yb is near unity. Special care was also taken in order to provide the glass with properties that allow the fabrication of channel waveguides. The most common way to do this is to follow an ion exchange process, where alkali ions in the glass are exchanged for ions with larger polarizability, which finally lead to an increase of the refractive index near the glass surface. Such a process requires that the material contains alkali-oxide components such as Na_2O. Another requirement for materials designed to be used as laser waveguides is that the rare-earth doping concentration must be as large as possible without significantly altering the base glass matrix. Lasting, in the composition of IOG-1 glass, Al_2O_3 was added in order to increase durability since phosphate containing glasses with P_2O_5 grater than 50 mol% normally react with molten salt baths used in waveguide preparation. A representative glass composition is given in Table 2.1. The molarity of phosphoric oxide, sodium and aluminum matrix modifiers, can slightly vary, depending on the rare earth dopand concentration and type. The transformation temperature (T_g) of IOG-1 glass is 474°C. The weight loss of the glass in water

at 50°C is 0.012mg/(cm^2·day). Other properties of the glass are presented in Table 2.2 [12].

Table 2.1

IOG-1 glass composition

IOG-1 glass composition (mol%)	
P_2O_5	60
Na_2O	24
Al_2O_3	13
R_2O_3	3

$R=\sum$ rare earths

Table 2.2

Optical properties	
n_d	1.523
v_d	67.53
n_{1054nm}	1.515
N_{1540nm}	1.513

Erbium Laser Properties	
Emission Peak, λ (nm)	1534.0
Radiative Lifetime, T_{Rad} (msec)	10.7
Emission Cross Section, σ_{em} (10^{-21}cm^2)	6.6
Absorption Peak for the 800nm Pump Band (10^{-21}cm^2)	2.0

Ytterbium Laser Properties	
Emission Peak, λ (nm)	1001.5
Radiative Lifetime T_{Rad} (msec)	1.36
Emission Cross Section σ_{em} (10^{-21}cm^2)	5.4
Absorption Peak for the 980nm Pump Band (10^{-21}cm^2)	14.5

2.4. Exposure of IOG-1 phosphate glass samples to intense pulse UV laser irradiation

The laser source used in the present work is a 213nm, 150ps Nd:YAG laser manufactured by EKSPLA, Lithuania. This system will be employed for studying the photosensitivity of IOG-1 glass and for the inscription of 1D and 2D periodic

structures in the same material. Thus, before continuing with the experimental part, a short description of the laser system will follow.

2.4.1. Laser system

The laser system used, is based on the commercial model SL 312M, fabricated by EKSPLA Lithuania. SL 312M [13] is a Nd:YAG laser which provides high energy picosecond laser pulses. In order to enhance the performance of the laser in short wavelengths, special rearrangements of the optical setup were carried out by EKSPLA technicians. The harmonics generators were placed in a separated chamber and a spatial filter was added for improving the quality of the beam.

The pulse in SL 312M laser system is generated in the master oscillator which consists of a Nd:YAG rod used as an active medium and a high reflectivity Fabry-Perot etalon used for longitudinal mode selection. The oscillator is electro-optically Q-switched in order to provide a nanosecond laser pulse. The pulse is compressed at the picosecond time scale during backward-stimulated Brillouin scattering (SBS). The SBS-cell consists of an optical guiding system and CCl_4 liquid. The linearly polarized pulse coming from the master oscillator passes through a QWP and focused into the SBS-cell in order to be time compressed. The backscattered pulse is phase reversed and is guided to the first amplification stage using polarizer and mirror. After the first amplifier, the pulse double passes a second one. Both amplifiers are based on laser chambers containing Nd:YAG rods pumped by flash lamps.

After amplification, the beam exits the pulse generation chamber and passing through a spatial filter enters in the harmonics generation chamber. The fundamental frequency of the laser is quintupled by inserting into the beam pass non-linear crystals generating the corresponding harmonic. The non-linear crystals are angle-tuned KD*P and KDP crystals mounted in temperature controlled heaters. Lastly, dichroic mirrors are used for separating the harmonic and directing it in a certain output port. The layout of the laser system is presented in Fig. 2.1.

To conclude, the Nd:YAG system used, provides pulsed laser irradiation at 213nm, employing the 5th harmonic of the fundamental output (1064nm). The pulse duration is 150 picosecond. The laser energy was measured to be up to 11mJ per pulse. The repetition rate was kept fixed for all exposures at 10Hz. The coherence length of the laser setup is longer than 2cm, which make it convenient for use in open interferometric setups.

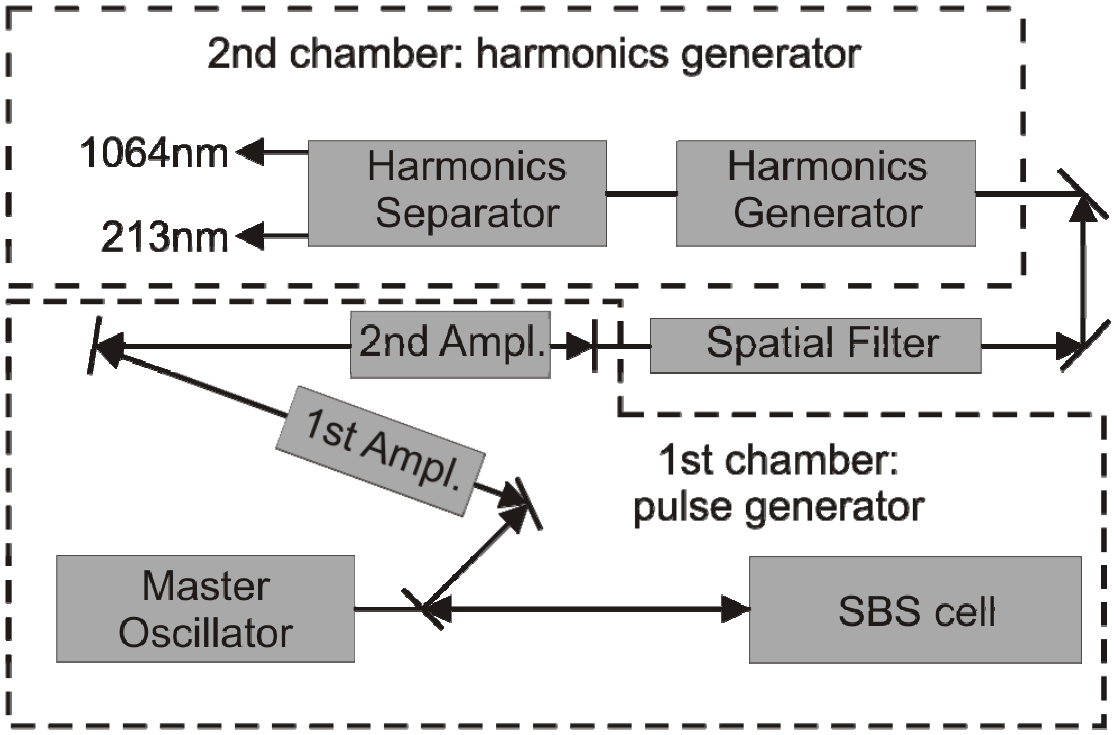

Fig. 2.1 *Layout of the laser system: the setup consists of two main chambers, one for pulse generation and the other for harmonics generation. The pulse duration is 150ps.*

2.4.2. Experimental apparatus and methodology

The electronic changes induced into the IOG-1 glass samples during the laser irradiation, were monitored by employing the following experimental setup. The 5th harmonic (213nm) of the 150ps Nd:YAG laser described above, was focused with a 20cm focal length fused silica lens in order to define spots of different diameters on the sample. Each sample was 1mm thick. The exposure was determined to be 36000 pulses. An oscillatory CaF_2 plate was used to scan the laser beam onto the sample surface for averaging beam irregularities. During

the exposure, the evolution of the 440nm absorption band was monitored in real-time mode by directing the output of a 442nm CW He-Cd laser on the exposure spot, and measuring the power received by the photodiode of a powermeter, which was placed behind the sample. In order to be able to normalize the received signal and ensure that the He-Cd laser power fluctuations will not affect our measurements, a beam-splitter was added in the beam path before the sample, for sending a part of the initial beam to a second photodiode connected with the powermeter. The layout of the experimental setup is shown in Fig. 2.2.

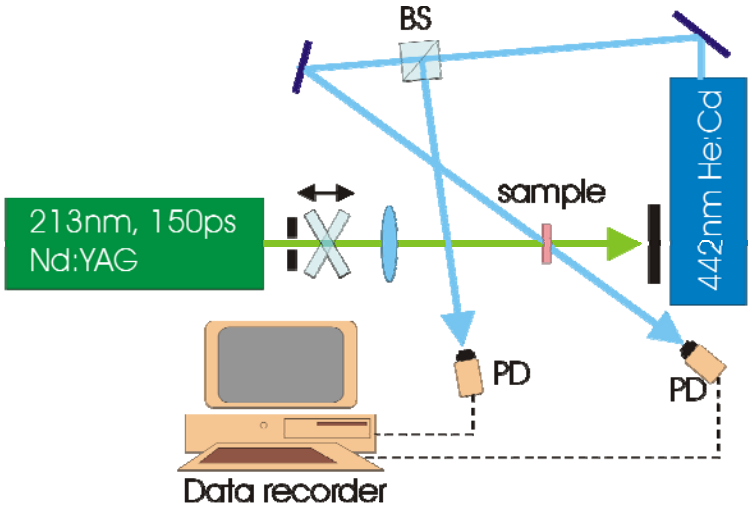

Fig. 2.2 *Experimental setup used for monitoring in real-time mode optical density changes induced into the IOG-1 glass samples during the exposure to 213nm, 150ps Nd:YAG radiation. A He-Cd laser is employed in order to probe the evolution of 440nm absorption band. BS: beam splitter, PD: photodiode.*

A number of samples was exposed to energy densities varying from 32 to 140mJ/cm^2. After the end of the exposure time, the relaxation behavior of the exposure process was further recorded for 20 minutes.

2.4.3. Results on the real-time recording of UV induced optical changes

Using the experimental apparatus, which was described in section 2.4.2, real time monitoring of the growth during exposure of a specific colour centre band was performed. Such a real-time absorption rate recording for the 440nm band is presented in Fig. 2.3.

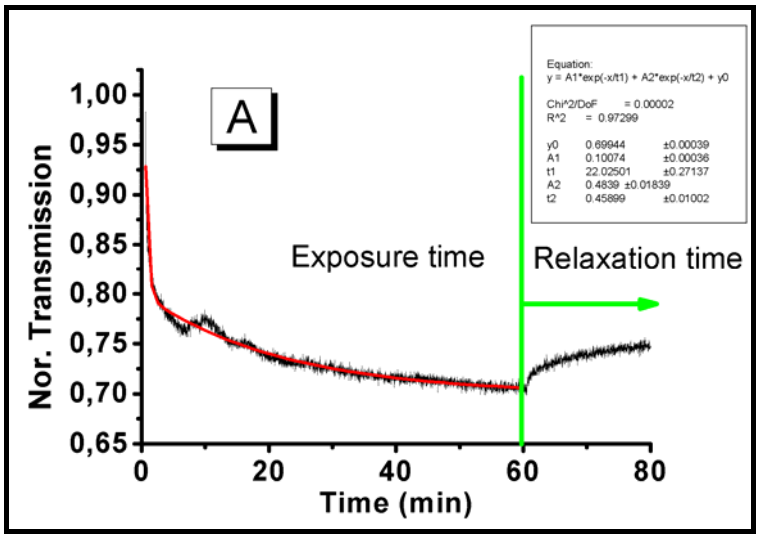

Fig. 2.3 *Normalized transmission signal versus time for a sample irradiated with 80mJ/cm^2 and 36000 laser pulses. A slight recovery of the transmission signal is observed after the end of the exposure. A double exponential function Tr(t) was chosen to fit the experimental data. The function fitted to data is the* $Tr(t)=0.69+0.48e^{-2.22t}+0.1e^{-0.045t}$.

A double exponential curve was used to fit the time dependent experimental data. The double exponential fitting function may imply that two different absorption mechanisms are activated during exposure. The first grows rapidly with an exponent factor of r1=2.2, while the second one -which appears to dominate for prolonged exposures-, grows slower with an exponential factor of r2=0.045. The changes induced by the activation of the quick mechanism appear to be permanent. On the other hand the centers induced by the slow mechanism appear to bleach after some minutes of recovery. For this reason we assume that the remaining absorption bands are principally generated at the first minutes of the exposure and they are mostly connected with the fast response mechanism.

2.4.4. Measurement of the irradiation depth

The irradiated volume in the glass sample surface is easily distinguished by the color difference between the UV exposed and the unexposed areas. The exposed area appears to be darker compared to the color of the rest of the surface. This darkening effect is strongly correlated with color center formation.

The measurement of the irradiation depth of the sample was performed in the following way. A sample irradiated with energy density of 133mJ/cm^2 was incubated in epoxy resin. The cube was then carefully polished down to the irradiated part and a grayscale picture of the cross-section was taken using an optical microscope. The grayscale analysis of the cross-section picture, (see Fig. 2.4), which was analyzed using specialized software (Mathematica), revealed an exponentially decreasing penetration depth, starting from the sample surface and fading out in a depth of 330μm, approximately. An exponential decay function GS(x) was employed for fitting the grayscale coloration experimental data versus the sample depth x. The optimized function fitted to these grayscale data was the GS(x)= 2.4e$^{3.68x}$+30.

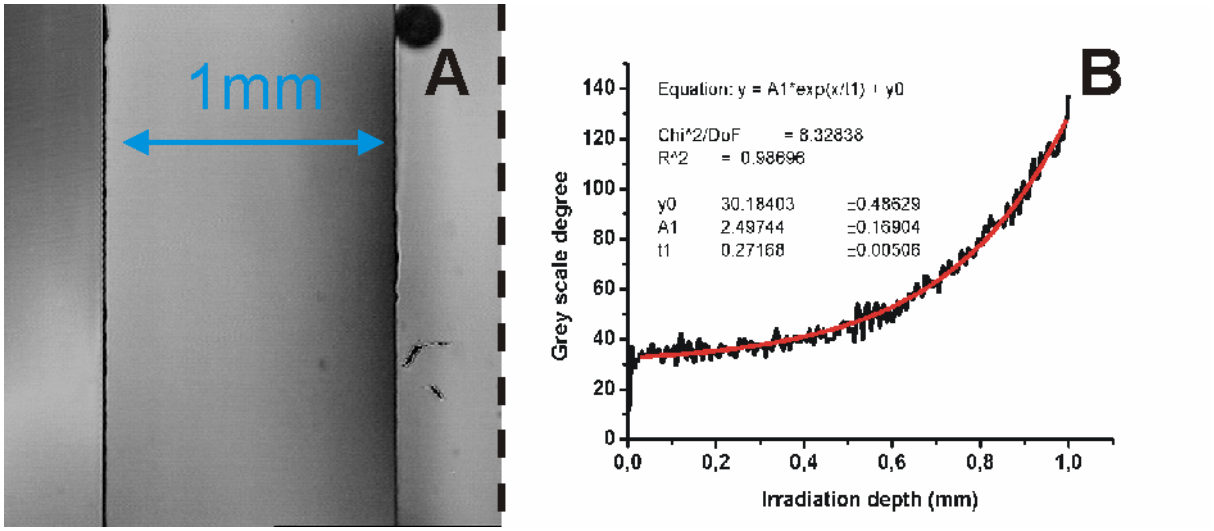

Fig. 2.4 *A) Optical microscope image of sample's cross section. The thickness of the sample is 1mm. The irradiated part is revealed by the darkening near the irradiated surface. B) Grayscale analysis of sample's cross-section. The induced optical changes appear to reduce exponentially, revealing an irradiation depth of approximately 330μm. The exponential function fitted to the data is GS(x)=2.4e$^{3.68x}$+30, where x is the sample depth.*

The data presented in Fig. 2.4 point out that the UV induced defects are mostly accumulated closely to the sample surface. Accordingly, the defect population may decrease with respect to depth with an exponential factor of r=3.68. The value of the irradiation depth constitutes another useful information which we are going to exploit in the following chapters in order to estimate UV induced refractive index changes.

2.5. Spectrophotometric broadband measurements

The spectrophotometric data presented in this chapter were obtained by employing a CARY 50 UV-Visible spectrophotometer. This spectrophotometer incorporates a Xenon flash tube and enables the scanning of the whole wavelength range from 190 to 1100nm. In the following measurements the transmission spectrum configuration was used. A custom made sample holder was designed in order to fit in spectrophotometer cavity, allowing selection/probing of the irradiated area only.

2.5.1. Transmission curves

The transmission curves of samples irradiated with 32, 56, 104 and 133 mJ/cm^2 energy densities and 36000 pulses, for the wavelength range between 190 and 1100nm, are shown in Fig. 2.5.

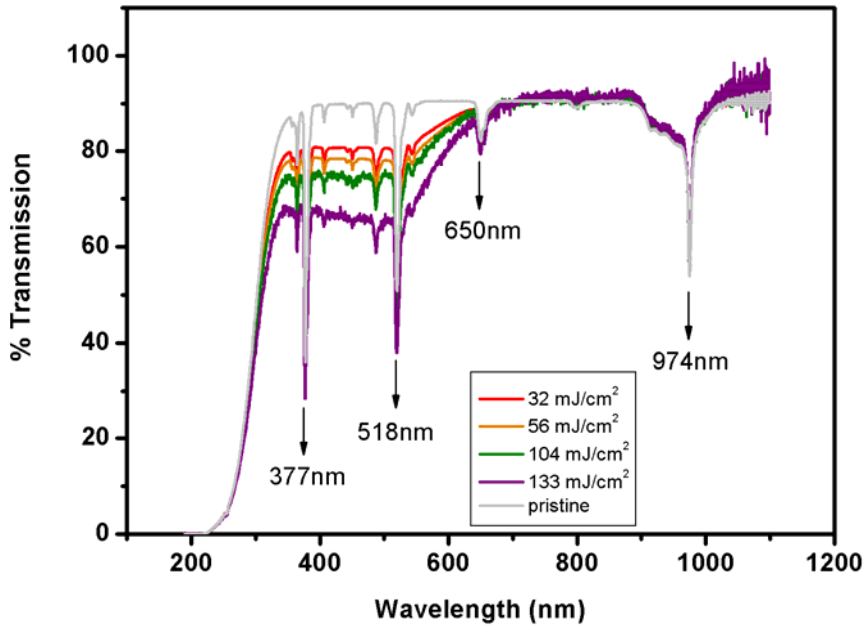

Fig. 2.5 *Transmission spectrum of IOG-1 samples exposed to energy densities of 32, 56, 104 and 133mJ/cm^2 using 36000 pulses. The transmission spectrum of the pristine glass is also presented in the same graph.*

In Fig. 2.5, we observe that the pristine sample is "non-transparent" at 213nm which is the wavelength of the Nd:YAG laser (the transparency factor of the material at 213nm was estimated from the data presented in Fig. 2.5 to be a=7.7mm^{-1} approximately). This means that the photon energy we use is comparable to the energy band-gap of the material. We assume that a single-photon process takes place during the exposure, in which the electrons of the valence band are excited directly to the conduction band. This can result in the formation of free electron and holes centres depending on the retrapping of the excited species. Thermal ionization of the swallow trapped electron might be another possible way for free electrons generation but we expect that photo-ionization is the main reason for the laser induced darkening [7][14]. The absorption at short wavelengths (190-400nm) increases rapidly. For the irradiated samples, this short wavelength "tail" is slightly displaced with regard to the pristine sample. This effect will feed our analysis in paragraph 2.6.1. Strong absorption changes are observed in the visible range of wavelengths. Other researchers have found that these absorption changes located in the visible band, are strongly correlated with electron centre formation. Their exact identification and physical origin will be discussed extensively in paragraph 2.5.3. The four discrete and strong absorption peaks which are observed in the transmission spectrum, with spectral locations at 377, 518, 650 and 974nm, are attributed to the Er and Yb doping [15].

2.5.2. UV induced absorption bands

Further investigating the spectral shape and growth of the absorption bands we plot the difference in the absorption coefficient between the irradiated areas and the pristine sample as a function of the photon energy. The plot is illustrated in Fig. 2.6. The absorption coefficient is calculated according to the equation:

$$I_t = I_0(1-R)^2 e^{-ad} \Leftrightarrow a = -\frac{1}{d}\lambda n\left(\frac{T}{(1-R)^2}\right) \quad \textbf{Eq. 2.1}$$

Where I_t is the intensity transmitted by the sample, I_0 the reference intensity and R is the reflectivity at normal incident given by the

equation $R = (n-1)^2/(n+1)^2$, where n is the refractive index. The dependence of the refractive index on the wavelength is expected to induce an error factor less than 0.01 to the evaluation of the absorption coefficient.

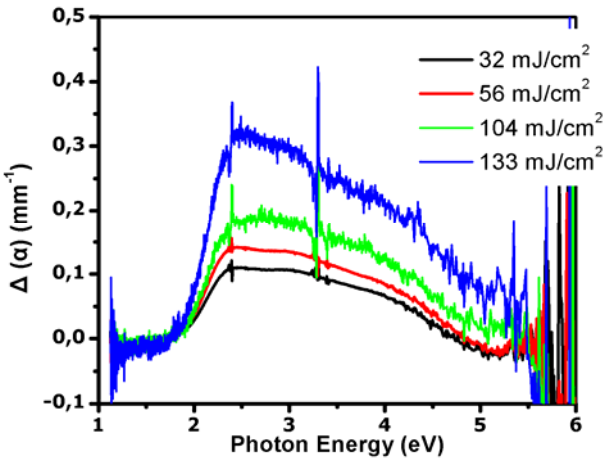

Fig. 2.6 *UV induced differences in the absorption coefficient of IOG-1 glass samples, irradiated with different energy densities (32, 56, 104 and 133mJ/cm^2) and 36000 pulses, versus photon energy.*

2.5.3. Color center peak identification

A band separation of the radiation-induced absorption, shown in Fig. 2.6, is presented in Fig. 2.7. In this graph, three well defined absorption bands are distinguished at 534nm (2.32eV), 436nm (2.84eV) and 331nm (3.74eV). The measured absorption spectral features are analyzed/approximated using a Gaussian band superposition. The resolved Gaussian bands were correlated with defect centers detected by EPR measurements, performed by Ehrt, *et al* [6]. In Table 2.3 the paramagnetic constants (A,g) and optical absorption of radiation-induced P-related defects are summarized.

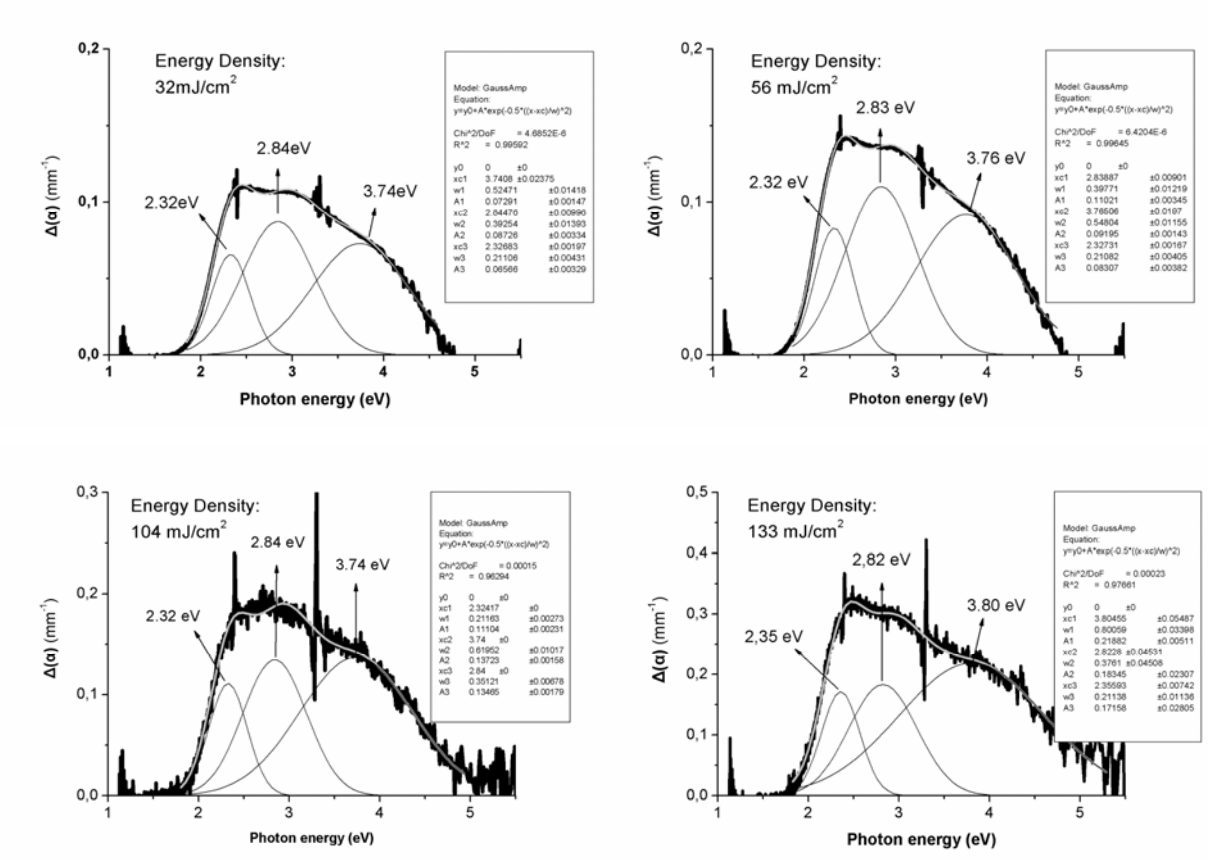

Fig. 2.7 *Band separation of the irradiation-induced absorption for samples exposed to 32, 56, 104 & 133 mJ/cm^2 energy density. All exposures were performed using 36000 pulses. In each graph the experimental data were fitted with Gaussian functions. Three well defined absorption bands are distinguished at 2.32, 2.84 & 3.74 eV. The continuous grey line represents the sum of the three Gaussian curves.*

Table 2.3

D.Ehrt et al, / Journal of Non-Crystalline Solids 263&264 (2000) 240-250

Paramagnetic constants and optical absorption of radiation-induced defects in phosphate groups[a]

Defect	Type	EPR-parameter		Optical absorption			Structure [28]
		A_{iso}[b] (mT)	g-value[c]	λ (nm)	E (eV)	W (eV)	
POHC	HC	4.0 ± 0.3	2.008 ± 0.003	540 ± 5	2.30 ± 0.02	0.44 ± 0.02	
				430 ± 10	2.88 ± 0.06	1.16 ± 0.08	
				300 ± 7	4.13 ± 0.08	1.38 ± 0.07	
PO_3	EC	86 ± 2	2.064 ± 0.005	210 ± 3	5.90 ± 0.06	1.55 ± 0.07	
PO_4	EC	126 ± 3	2.142 ± 0.008	242 ± 3	5.12 ± 0.06	1.42 ± 0.09	
PO_2	EC? HC?	27 ± 2	2.006 ± 0.003	266 ± 5	4.66 ± 0.08	1.35 ± 0.12	

[a] Symbols: O = oxygen ion; P = phosphorus ion; ⊕ = positive charge; ⊖ = negative charge; • = paramagnetic electron.
[b] A_{iso} ≡ isotrope hyperfine splitting due to ^{31}P, the distance (in mT) between two signals of the doublet.
[c] g-value ≡ the middle g-value between g-values of both signals of doublet: $g_{mid.}(g_1 + g_2)/2$.

Table 2.3 correlates the absorption bands at 2.32eV and 2.84eV with phosphorus related hole centers (POHC) in the visible range. A POHC appears when a double covalent bond between a phosphorous ion and an oxygen ion breaks to form a $(P^{+5})^{+}$ hole center (HC). To illustrate the underlying formation mechanism we plot the induced absorption at 436nm (2.84eV) as a function of the incident energy density. As it is demonstrated in Fig. 2.8, a linear function provides a satisfying fit to the experimental data. This may constitute an evidence that a single photon mechanism dominates the evolution of the absorption bands in the visible range. The linear increase in Fig. 2.8 leads us also to the assumption that the population density of colors centers increases proportionally with the incident energy density [8].

Other defect centers, like electron centers are not detected in the absorption analysis described above. As we can see in Table 2.3 electron centers correspond to photon energies over 4.6eV. We are relying in the analysis of the absorption "tail", which will be presented in the next paragraph, in order to obtain additional information about the generation of such kind of defects.

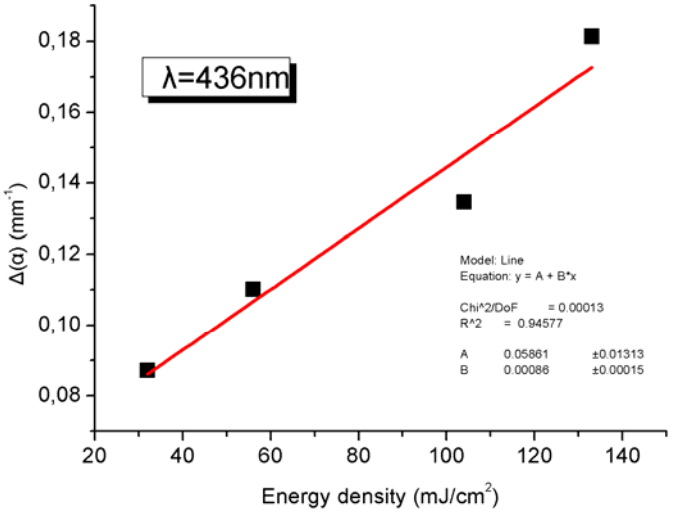

Fig. 2.8 *Radiation-induced absorption $\Delta\alpha$ versus energy density F at 436nm; A linear function was used to fit the experimental data. The linear function fitted to the data is the $\Delta\alpha(F)=0.00086F+0.058$.*

2.6. Quantification of structural modifications and estimation of the refractive index changes using theoretical and empirical models

The short wavelength "tail" of an absorption spectrum is strongly related with the electron absorption process that takes place when irradiation of sufficient photon energy interacts with the volume of a transparent material. Only electromagnetic irradiation with sufficient energy to cause an electron to transfer form the valence to the conduction band will be absorbed by this mechanism, which is known as intrinsic absorption. Additionally, to the intrinsic absorption the higher frequency end of the absorption spectrum may be related with extrinsic absorption, where the transitions occur between the valence or conduction band and donor sites in the band gap or with energy states caused by defects or impurities.

Generally, the profile of the electronic absorption edge is known as the Urbach tail. In the presence of impurities or other defects the Urbach tail shifts towards longer wavelengths. Experimental studies during the last decades [18][19] have strongly suggested that changes of the Urbach tail slope provide an indication of structural modifications induced into the material. In the following paragraphs

we will focus on these changes in order to investigate further the defect formation caused by the intense UV irradiation. Furthermore, Kramers-Kronig theoretical model is going to be applied in order to connect the absorption bands shown in Fig. 2.6 with possible changes in the refractive index of the material.

2.6.1. Urbach tail theory

In 1953, Urbach firstly proposed an empirical rule governing the short wavelength absorption slope, based on observations of the absorption spectrum of alkali halides. He pointed that the tail of the plot of the logarithmic absorption coefficient α, versus photon energy approaches a straight line [16][17]. It has been estimated that the slop of the line is proportional to 1/kT where k is Boltzmann's constant and T is the temperature in Kelvin degrees. The absorption coefficient α is then given by the Eq. 2.2

$$a = a_0 \exp\left[\sigma\left(\eta\omega - \eta\omega_0\right)/kT\right], \textbf{ Eq. 2.2}$$

where α_0 , ω_0 and σ are parameters of the material. More precisely, σ is the steepness of the absorption edge. The factor E_{Ur}=kT/σ is known as Urbach energy and can be easily derived from the logarithmic form of the, **Eq. 2.2**:

$$\ln(a) = \left(\ln a_0 - E_0 \frac{\sigma}{kT}\right) + \frac{\eta\omega\sigma}{kT} = const. + \left(\frac{\eta\omega}{E_{Ur}}\right), \textbf{ Eq. 2.3}$$

Many attempts were made in order to theoretically explain the exponential dependence of the absorption change, near the energy band gap of a material. Some of them are presented in Kurik's [17] review paper on Urbach law. The majority of the studies are focused on the dependence of the absorption slop upon the temperature. The main idea behind these studies is that the energy of the excited electron state changes due to the lattice deformation by thermal vibrations. Many models have been proposed, based mainly on exciton absorption bands or phonon-photon interaction. Other groups have proposed

that another possible explanation of the exponential shape of the fundamental absorption edge could be the presence of impurities or lattice defects like bond cleaving. It has been confirmed a close relationship between the σ parameter in Eq. 2.2 and the concentration of such kind of defects. Today it is universally accepted that the Urbach energy, which can be estimated from Eq. 2.3, characterizes the state of the structural order in an optical material [18][19][20].

2.6.2. Estimation of Urbach energy

Focusing on the short wavelength regime, we are applying the Urbach rule in order to investigate the structural modifications induced inside the IOG-1 glass matrix by the exposure to intense UV radiation. The plot of the logarithm of the absorption coefficient (lnα) as a function of the photon energy, for the samples of Fig. 2.5, is shown in Fig. 2.9. In addition, the plot of the E_{Ur} derived from Eq. 2.3, as a function of the incident energy density for exposures of 36000 pulses and different energy density, is presented in Fig. 2.10.

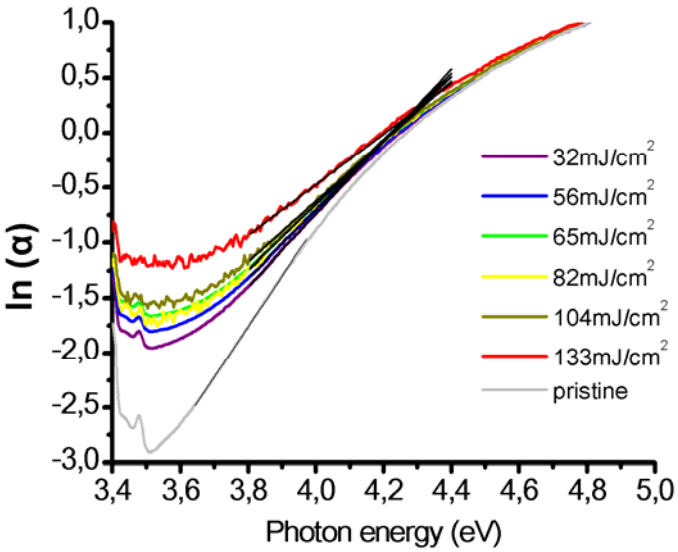

Fig. 2.9 *Urbach tail absorption (α) for IOG-1 samples irradiated with different energy density each. The black lines indicate the slop of the curves.*

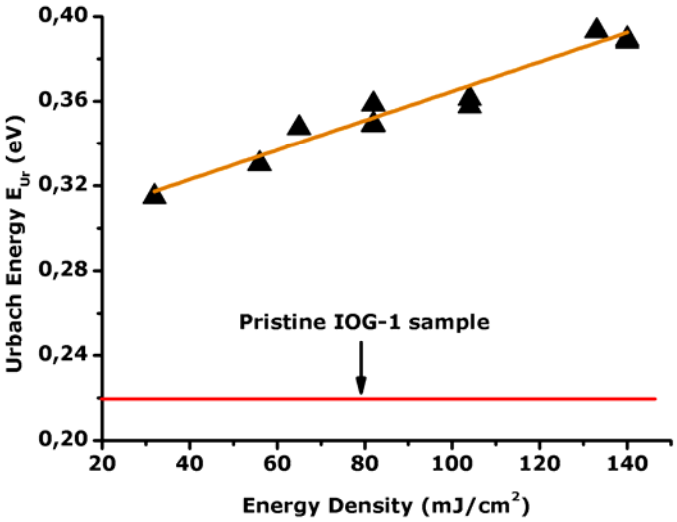

Fig. 2.10 *Urbach energy E_{Ur} versus energy density F for IOG-1 samples irradiated with 36000 pulses. The red continuous line indicates the value E_{Ur} of the pristine sample. The line fitted to the experimental data is the $E_{Ur}(F)=0.0007F+0.2952$*

As it is illustrated in Fig. 2.9, the slope of the measured quantity ln(α) changes for glass samples exposed to 213nm radiation of different energy density.

Furthermore, in Fig. 2.10 the estimated energies E_{Ur} –as these calculated from the data of Figure 2.9- appear to be a linear function of the energy density F of the exposure. The linear function optimally fitted to the experimental data is the $E_{Ur}(F)=0.0007F+0.02952$. The change of the E_{Ur} provides strong evidence that significant modifications are induced into the volume of the IOG-1 glass by the intense UV laser irradiation. Such modifications may be associated with bond-cleaving, compaction or extensive ionization and electron re-trapping processes. Compaction may induce birefringence or additional changes to the refractive index. Bond cleaving may dissociate the long polymeric chains in IOG-1 glass into shorter parts. In this case the irradiated areas located closer to the surface of the material may be more dissolvable than the unexposed areas, in the presence of alkaline or acidic aqueous solutions.

In Table 2.3, we observe that electron related centers, corresponding to an electron trapped in a broken double bond (PO_4EC) or an electron trapped in a cleaved bond (PO_3EC and PO_2EC) between a phosphorous and an oxygen ion, can be found in the same range of energies where Urbach Tail appears. This

provides an evidence, that the structural changes observed previously can be correlated with cleavage of the long polymeric chains in the phosphate glass in shorter parts. However, whatever the nature of these defects is, their generation mechanism is connected with a single-photon process, as this may be extracted from the linear dependence of E_{Ur} on energy density,.

2.6.3. Kramers-Kronig theory

Kramers-Kronig (KK) technique, which was firstly introduced by Kramers (1929) and then improved by Kronig (1931), is one of the most powerful techniques for the accurate determination and cross-correlation of optical constants [21]. This technique makes use of the spectral distribution of one or more optical functions, over a wide range of frequencies. The optical functions used in Kramers-Kronig calculations can be reflectance, transmittance; or phase change on reflection or transmission.

Kramers-Kronig analysis is based on the premise that for an optical function consisting of both real and imaginary parts, if the variation of the real part with the frequency is known, the imaginary part, also as a function of the frequency, can be calculated and vice versa. For example introducing the complex frequency, $\omega = \omega_r - i\omega_i$, in the wave equation for light traveling in a transparent medium we obtain:

$$E = E_0 \exp[i(\omega t - \mathrm{K}x)] = E_0 \exp(\omega_i t) \exp[i(\omega_r t - Kx)], \quad \textbf{Eq 2.4}$$

where the imaginary exponential term represents the oscillating part of the wave as a function of both time and position, while the real exponential is a time depended decay term. As a next step, a complex frequency plane may be constructed with the real part ω_r as the ordinate and the imaginary part ω_i as the abscissa. Kramers–Kronig analysis deals with the integration of a certain function round a close loop in the complex frequency plane. During this procedure, it is necessary to investigate the restrictions which must be placed on

the zeros and the poles of the function in order to obtain a real solution which can then be compared with actual measurements.

Index changes induced in transparent materials by UV irradiation can be calculated from the Kramers-Kronig relation given by the following formula:

$$\Delta n_{eff}(\lambda) = \frac{1}{2\pi^2} P \int_0^{\infty} \frac{\Delta\alpha_{eff}(\lambda')}{1-(\lambda'/\lambda)^2} d\lambda' \text{ , } \textbf{Eq. 2.5}$$

where P is the principal value of the integral, λ is the wavelength and $\Delta\alpha_{eff}(\lambda)$ is the effective change in the absorption coefficient of the defect. The change in the absorption coefficient can be related to the sample's transmittance before and after the irradiation by

$$T_{bl}(\lambda) = \mathrm{T}_{unbl}(\lambda)\exp[\Delta\alpha_{eff}(\lambda)L] \text{ , } \textbf{Eq. 2.6}$$

Eq. 2.5 was derived from the rigorous Kramers-Kronig relation connecting the real (ε') and the imaginary part (ε'') of the dielectric permittivity. Thus, index changes calculated with Kramers-Kronig relationship are strongly connected with color centers related changes.

2.6.4. Estimation of refractive index changes induced in the IOG-1 glass using Kramers-Kronig formula

The Eq. 2.5 was used for calculating the index change induced in IOG-1, related with colour centres formation [22][23]. In this calculation, $\Delta\alpha_{eff}(\lambda)$ was calculated from the curves of Fig. 2.6 using interpolating functions. The resulting data were used in the integral of Eq. 2.5. The Cauchy principal value of the integral, multiplied by a factor of $(1/2\pi^2)$ corresponds to the effective index change $\Delta n_{eff}(\lambda)$. The refractive index change dependence on the incident energy density during the irradiation procedure as this was estimated using KK transformation at the wavelength of 436nm, is presented in Fig. 2.11.

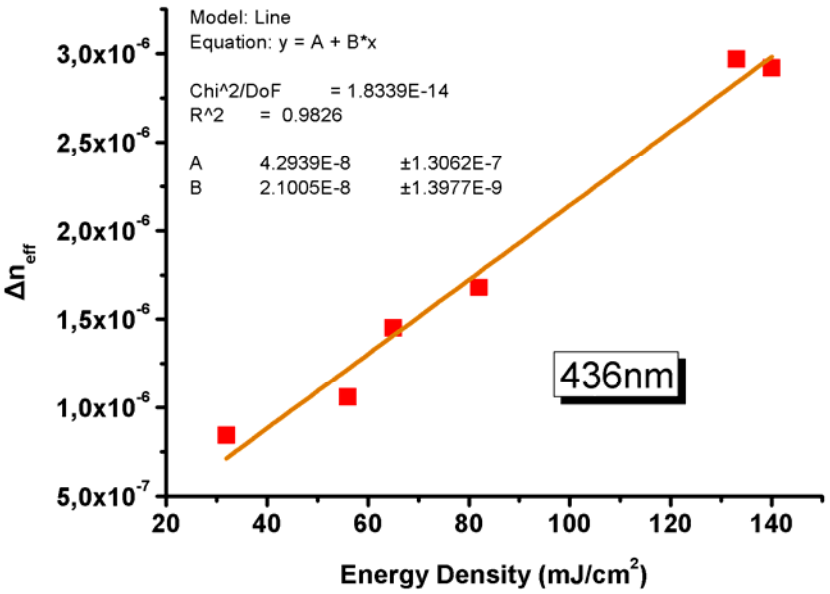

Fig. 2.11 *Refractive index changes Δn in IOG-1 glass induced by intense UV irradiation (213nm, 150ps, 36000 pulses) using different energy densities F (32, 56, 65, 82 & 104mJ/cm^2). The data were extracted by employing Kramers-Kronig formula. All results correspond to a wavelength of 436nm. The linear function fitted to data is the $\Delta n(F)=2.10\cdot10^{-8}F+4.29\cdot10^{-8}$.*

The results, presented in Fig. 2.11, depict that index changes of the order of $\Delta n=3.6 \times 10^{-6}$ can be induced at 436nm, using 213nm radiation. A linear growth behaviour characterizes the UV induced index changes varying as a function of energy density, providing evidence that the underlying index modification mechanism is associated with an one-photon absorption process. Based on the above observation, the refractive index changes measured previously could be attributed to the generation of laser induced electron defects.

2.7. Conclusions

The photosensitivity of Yb/Er-codoped IOG-1 Schott phosphate glass was investigated by using 213nm, 150ps Nd:YAG laser radiation. The photon energy of the laser used is greater then the material energy band gap, allowing direct electron excitation from the valence to conduction band. The samples were exposed to different values of energy density (varying from 32 to 140mJ/cm^2) and 36000 laser pulses. The irradiation/colouration depth was found to fade

exponentially, starting from sample surface and reaching a final value of about 330μm. Two absorption mechanisms were observed during real-time probing of the UV exposure, with the permanent changes in absorption mostly connected with the faster growing mechanism.

The spectrophotometric measurements of the pristine and the exposed to UV samples, revealed well distinguished absorption bands in the visible range. These absorption bands were attributed to hole-related centers generated when a P^{+5} phosphorus ion located in a double P=O bond losses an electron. This assumption was based on EPR measurements performed by other groups [6]. Also, the changes of the optical density were found to increase linearly with the energy density of the exposure. A similar linear type dependence possibly holds for the defect population induced by the UV radiation.

The UV radiation induced volume matrix damage was studied by using the Urbach tail empirical rule. The Urbach energy E_{Ur} was extracted from spectrophotometric measurements and it was found to exhibit a linear increase with respect to the energy density Urbach energy provides a strong indication that measurable changes in the structural order of the material were induced by intense UV radiation. Based on EPR measurements performed by other groups, we assume that this kind of structural damage can be correlated with cleavage of the P-O bonds. Kramers-Kronig formula was employed in order to estimate the induced refractive index change. Refractive index changes of the order of $\Delta n = 3.6 \cdot 10^{-6}$ were extracted by the KK estimation. These changes in the refractive index are associated with absorption band generation. All measured quantities in this chapter, which are the evolution of 436nm hole-center related absorption band, the Urbach Energy and the refractive index change at 436nm, were found to exhibit a linear dependence on the energy density. For this reason we suggest that all the quantities mentioned above are probably connected with a single photon process.

2.8. References

[1] A.S. Marfunin, Spectroscopy, Luminescence and Radiation Centers in Minerals, Springer-Verlag, Berlin Heidelberg New York (1979)

[2] S.Amelinckx, R. Gevers, J. Nihoul, Electronic and Vibrational Properties of Point Defects in Ionic Crystals, North-Holland Publishing Company (1979)

[3] N.E. Alekseev, A.A. Izyneev, V.B. Kravchenko, Yu.S. Milyavskif, S.P. Rozman, Etching of Phosphate glasses, Translated from Steklo I Keramika, **7**, 11-12 (1983)

[4] B.C. Bunker, G.W. Arnold, J.A. Wilder, Phosphate Glass Dissolution in Aqueous Solutions, Jour. of Non-Crystalline Sol., **64**, 291-316 (1984)

[5] A.S. Barnes, C.G. Pantano, S.D. Conzone, Surface Cleaning and Etching of Rare-Earth Doped Phosphate Glass, proc. SPIE, Inor. Opt. Mat., **4452**, 115-125 (2001)

[6] D. Ehrt, P. Ebeling, U. Natura, UV Transmission and Radiation Induced Defects in Phosphate and Fluoride-phosphate glasses, J. of Non-Crystalline Sol., **263&264**, 240-250 (2000)

[7] Qinling Zhou, Lei Xu, Liying Liu, Wencheng Wang, Congshan Zhu, Fuxi Gan, Study of the Laser-induced Darkening in Nd-doped Laser Glasses, Optical Materials, **25**, 313-319 (2004)

[8] Y. Watanabe, G. Namikawa, T. Onuki, K. Nishio, T. Tsuchiya, Photosensitivity in Phosphate Glass Doped with Ag^{+} upon exposure to near-ultraviolet femptosecond laser pulses, Appl. Phys. Lett., **78**, 2125-2127 (2001)

[9] J.W. Chan, T.R. Huser, S.H. Risbud, J.S. Hayden, D.M. Krol, Waveguide Fabrication in Phosphate Glasses Using Femptosecond Laser Pulses, Appl. Phys. Lett., **82**, 2371-2373 (2003)

[10] S. Pissadakis, A. Ikiades, P.H. Anna, K. Sheridan, J.S. Wilkinson, High Photosensitivity of ion-exchanged Er-doped Phosphate Glass Using 248nm Excimer Laser Radiation, Opt. Express, **12**, 3131-3136 (2004)

[11] D.L Vasey, D.S. Funk, P.M. Peters, N.A. Sanford, G.E. Obarski, N. Fontaine, M. Young, A.P. Peskin, Wei-Chic Liu, S.N. Houde-Walter, J.S. Hayden, Yb/Er-codoped and Yb-doped waveguide lasers in phosphate glass, J. of Non-Crystalline Solids, **263&264**, 369-381 (2000)

[12] www.schottglasstech.com

[13] www.ekspla.com

[14] D.Du, X.Liu, G. Kom, J. Squier, G. Mourou, Laser Induced Breakdown in SiO_2 with Pulse Widths from 7ns to 150fs, Appl. Phys. Lett., 64, 3071 (1994)

[15] E. Desurvire, Erbium-Doped Fiber Amplifiers, Principles and Applications, John Wiley & Sons, Inc.,Publications (2002)

[16] F. Urbach, The Long-Wavelength Edge of Photographic Sensitivity and of the Electronic Absorption of Solids, Physical Review, **92**, 1324 (1935)

[17] M.V. Kurik, Urbach Rule, Phys. Stat. Soli. A, **8**, 9 (1979)

[18] I.A. Vainshtein, A.F. Zatsepin, V.S. Kortov, Specific Features of the Urbach Rule Manifestation in Vitreous Materials, Glass Phys. Chem., **25**, 67 (1999)

[19] F. Kuhnlenz, S. Bark-Zolimann, H. Stafast, W. Triebel, VUV Absorption Tail Changes of Fused Silica During ArF Laser Irradiation, Journal of Non-Crystalline Sol.,**278**, 115-118 (2000)

[20] S. John, C. Soukoulis, M. Cohen, E.N. Economou, Physical Review Letters, **57**, 1777 (1986)

[21] L. Ward, The optical Constants of Bulk Materials and Films, The Adam Hilger Series on Optics and Optoelectronics

[22] J.E. Roman, K.A. Winick, Photowritten Gratings in Ion-Exchanged Glass Waveguides, Opt. Lett., 18, 808-810 (1993)

[23] B. Laconte, W.X. Xie, M. Douay, P. Bernage, P. Niay, J.F. Bayon, E. Delevaque, H. Poignant, Analysis of Color-Center-Related Contribution to Bragg Grating Formation in Ge:SiO_2 Fiber Based on a Local Kramers-Kronig Transformation of Excess Loss Spectra, Appl. Opt., **36**, 5923-5930 (1997)

Chapter 3. Inscription of photosensitive Bragg gratings in IOG-1 phosphate glass

3.1. Introduction

In chapter 2 we demonstrated that measurable refractive index, spectral and structural changes can be induced in the IOG-1 glass by exposure to intense 213nm, 150ps radiation. In the present chapter we will exploit the interference pattern of two monochromatic waves coming from the same light source, in order to induce such a kind of modifications in the form of a grating. The light source used is the 213nm Nd:YAG laser, described previously. The diffraction efficiency of the inscribed gratings is measured and the induced refractive index changes are evaluated by employing the thick absorption phase-grating diffraction efficiency equation. This equation provides values for the total induced refractive index change and it is expected to enhance our understanding upon the damage mechanisms that are activated during the exposure of IOG-1 glass to intense UV irradiation.

3.2. Formation of grating patterns in IOG-1 phosphate glass

The grating structures were fabricated by employing an elliptical Talbot interferometer and the output of the 213nm Nd:YAG laser used before. With the above experimental configuration we exposed a number of Er/Yb-codoped IOG-1 glass samples with different energy densities. The inscription process probed in real time, by adding a simple diffraction setup into the cavity of the interferometer. Finally, a more accurate diffraction efficiency measurement of the photosensitive gratings was carried out after the end of the UV exposure, for characterizing the inscribed structures. The experimental procedure will be described in detail in the next paragraphs.

3.2.1. Experimental apparatus: Elliptical Talbot interferometer.

The elliptical Talbot interferometer is an alternative two-mirror version of the Talbot interferometer, which employs a transmission phase grating as the beam-splitting element and a face polished silica block or two parallel mirrors for beam refolding and fringe formation in the sample. The typical Talbot optical configuration suffers from certain disadvantages, since specially optimized beam refolding components are required for operation at high incident angles. In order to eliminate these problems and to reduce the cost of the experimental setup, an elliptical configuration of the Talbot interferometer is applied in the present study.

The cavity of an elliptical Talbot interferometer [1] is presented in Fig. 3.1. A transmission phase grating which is placed on the one of the poles (O) of the ellipse, sends the +1 and -1 diffraction orders of the incident beam towards the two folding mirrors placed on ellipse perimeter. The two reflected beams are then recombined on the other pole (O΄) of the ellipse, where the sample lies, as it is predicted by Euclidean geometry. With this configuration, the beams are reflected at 90° by the mirrors.

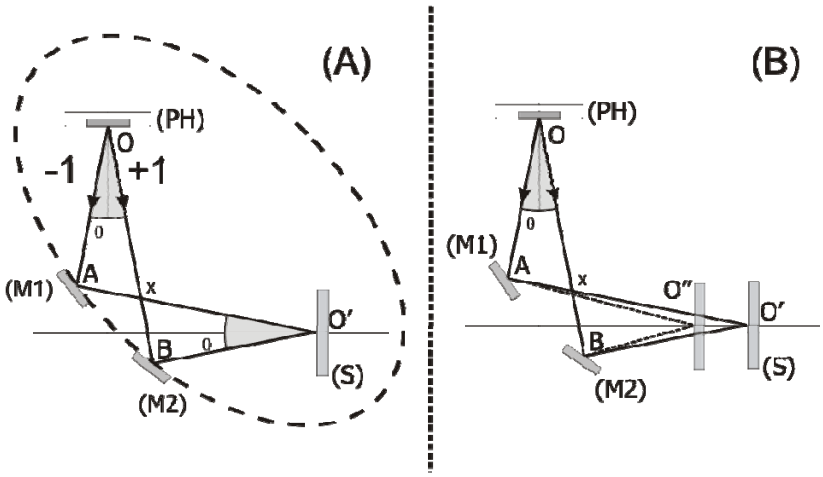

Fig. 3.1 *Schematic diagram of the elliptical Talbot Interferometer (A) aligned for the same period as the half of the phase mask and (B) aligned for shorter period than the half of the phase mask. The dashed line represents the ellipse which defines the dimensions of the cavity: O, O΄the poles of the ellipse, (PH): Phase mask, (M1),(M2) 45° beam folding mirrors, (S) Sample.*

This is a quite important detail because dielectric mirrors that are customized for reflectivity angles of 45° are stock, reasonable cost optical components. Furthermore, modest reflection angles with respect to the mirror planes, allow convenient accommodation of large diameter beams.

An elliptical Talbot interferometer is easily aligned. Special care must be taken to ensure the balance of the optical paths OAO' and OBO'. As it can be easily seen in Fig. 3.1, the interferometer is balanced when OA=BO' and OB=AO'. If we set OA=L, the distance OB, employing Euclidean geometry arguments is evaluated to be:

$$OB = Ox + xB = L\sec(\theta) + L\tan(\theta) = L\left(\frac{1+\sin(\vartheta)}{\cos(\vartheta)}\right), \quad \textbf{Eq. 3.1}$$

Thus, in order to align the cavity, first we place the mirrors at fixed positions OA and OB and align them to retro-reflect the +1 and -1 diffraction orders. Then, by just rotating the mirrors at 45°, the diffracted beams can be easily sent to intersect at point O'. This way, we also ensure that the interference angle is the same as the diffraction angle θ°.

It can be proved, following a simple k-vector analysis that the period of the gratings inscribed with the configuration described above, is half of the period of the phase mask. Longer or shorter periods may be inscribed, by readjusting the mirrors M1 and M2 by the same angle α/2, as it is presented in Fig. 3.1.

3.2.2. Experimental apparatus for the inscription of Bragg gratings

In the present work, a 1070nm period fused silica phase mask, inscribed in a 2mm thick substrate and optimized for 248nm operation, was used as beam splitting element. The diffraction angle θ/2 was 11.48° for the 213nm radiation. The Talbot interferometer cavity was aligned for inscription of gratings with periodicity being approximately the half of the phase mask (535nm). A CaF_2 lens

of 1000mm focal length was placed before the phase mask in order to enable us to adjust the energy density on sample surface. The experimental setup is presented in Fig. 3.2 and a camera picture of the setup in Fig. 3.3. A number of gratings was inscribe in IOG-1 glass substrates, with energy densities varying from 62 to 208mJ/cm^2. All gratings were inscribed with 36000 laser pulses.

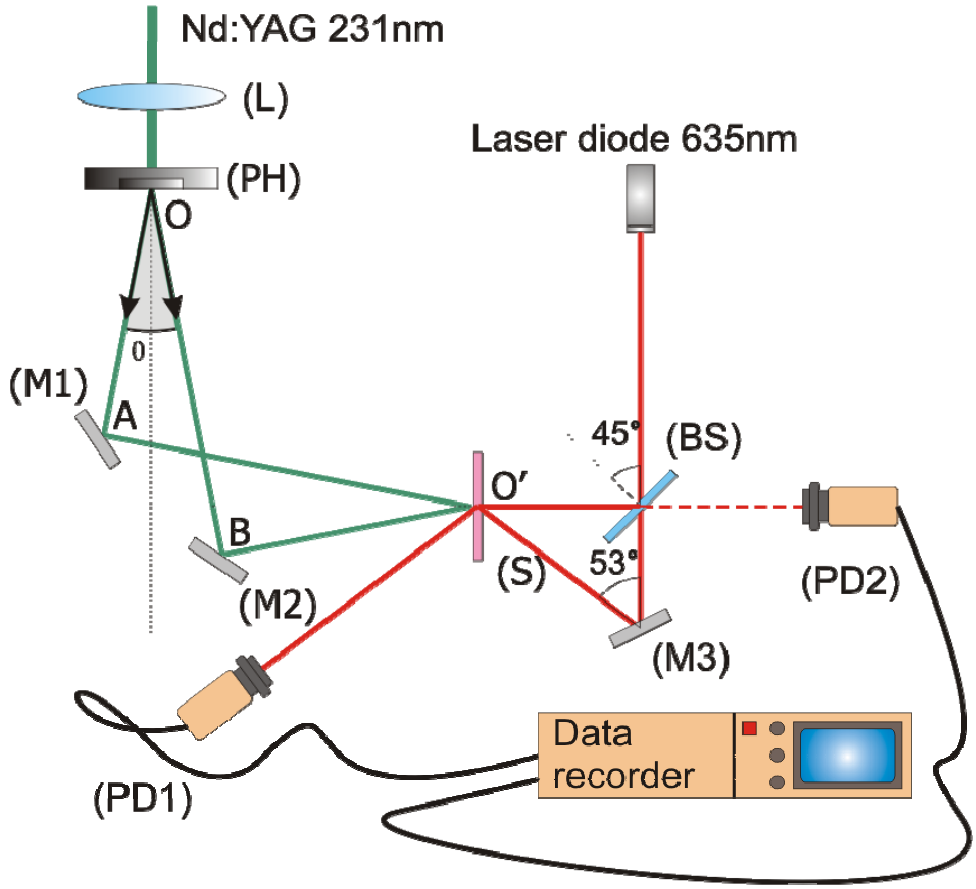

Fig. 3.2 Experimental setup used for the inscription of Bragg gratings in IOG-1 glass. The gratings are inscribed by employing an elliptical Talbot interferometer and the output of a 213nm, 150ps Nd:YAG laser. A simple diffraction setup is added to record the evolution of the inscription. A mirror (M3) sends the beam coming from a 635nm laser diode onto the grating at Bragg angle and the diffracted signal is recorded by a photodiode. A second photodiode is used for signal normalization. (M1), (M2): dielectric mirrors, (M3): metal coated mirror, (PH): phase mask, (BS): beam splitter, (PD1), (PD2): photodiodes, (L): lens with 1000mm focal length, (S): IOG-1 sample.

A simple diffraction setup was added into the interferometer cavity in order to provide us with on-line data concerning the inscription process. A metal coated mirror (M3) is used to reflect a 635nm laser diode beam onto the grating at Bragg angle (37°). The diffracted signal is recorded by a photodiode (PD1). A simple glass beam splitter (BS), placed at 45° with respect to the laser diode beam, is used for assisting alignment and for sending a part of the initial beam

into the input of a second photodiode (PD2) for monitoring variations. The measured power at PD2 was used as a reference. Finally, the recovery period of the next 30 minutes after the exposure was also recorded.

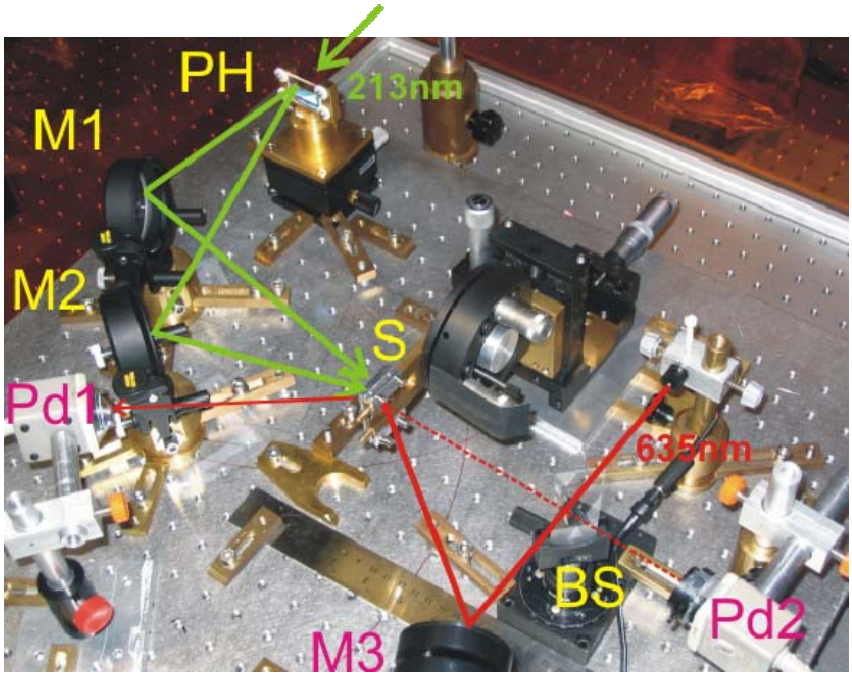

Fig. 3.3 *Photograph of the experimental setup described in Figure 3.2. (PH) phase mask, (M1) & (M2) dielectric mirrors, (M3) metal coated mirror, (Pd1),(Pd2) photodiodes, (BS) beam splitter, (S) sample.*

3.2.3. Real time measurements of the evolution of the diffracted signal during grating inscription

The evolution of the diffracted signal during the exposure, for gratings inscribed with energy density of 84, 124 and 208mJ/cm^2 is presented in Fig. 3.4. All gratings were exposed to 36000 pulses. It should be pointed out that the following graphs should be used to study the trend of the inscription process and they are not indicative for the estimation of the maximum value of the diffracted signal.

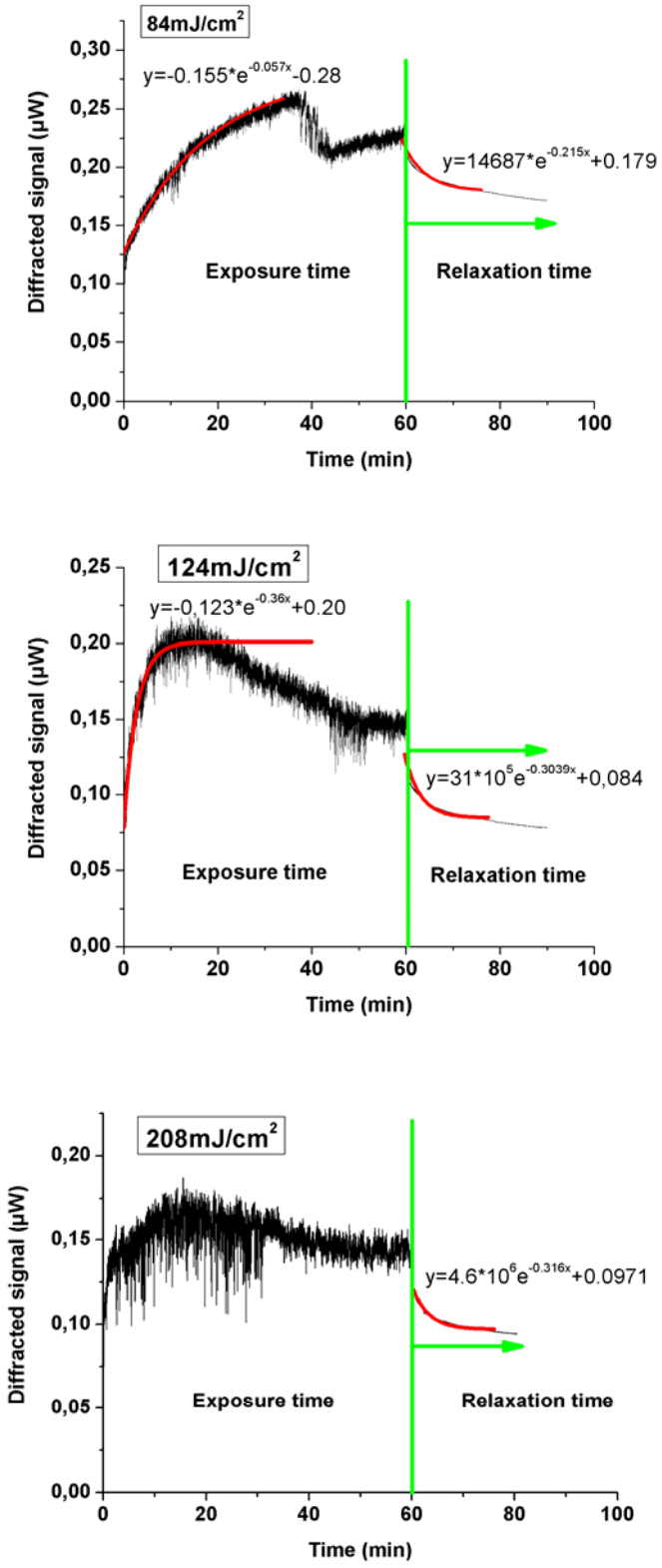

Fig. 3.4 *The evolution of the diffracted signal during the exposure, for gratings exposed to 84, 124 and 208mJ/cm^2 energy densities and 36000 pulses (1 hour). The signal measured during the recovery is also shown. Exponential decay functions were chosen to fit the experimental data at the begging of the exposure and the beginning of the relaxation time.*

For the first two graphs in Fig. 3.4, exponential curves were used to fit the experimental data. We observe that when we increase the energy density from 84 to 124mJ/cm^2, the exponential factor which describes the growth of the diffracted signal increases almost one order of magnitude (from 0.057 to 0.36). For the sample irradiated with 208mJ/cm^2, we observe that the diffraction signal at the beginning increases almost instantly. In all graphs the signal, after reaching a maximum value, starts decreasing. This is maybe due to bleaching of specific absorption bands after prolonged UV irradiation. However, such a phenomenon was not observed in paragraph 2.5. Another assumption could be that heating of the sample due to UV irradiation disturbs the grating structure. Thermal diffusion in non-irradiated areas could induce permanent or non-permanent defects which could alter the shape of the inscribed pattern. However, the above assertions need further investigation.

The signal noise increases as we are moving towards higher energy densities, illustrating the intensity of the interaction between the UV-irradiation and the material. For the case of 208mJ/cm^2 the noise is significantly elevated implying strong interaction with the matter which could lead to ablation initiation at hot spot points of the beam. Indeed, we observed small ablated areas for some samples irradiated with that value of energy density. Finally, we must notice that when exposure time ends, the signal decays exponentially and saturates after a time period of more than 30 minutes, with almost the same exponential factor for all of the samples.

3.3. Post-exposure diffraction efficiency measurements of the gratings

After photosensitive grating inscription, a simple diffraction setup was used in order to measure with accuracy the diffraction efficiency of the samples. As it is illustrated in Fig. 3.5 the samples were mounted on a rotating holder and the output of a 635nm diode laser was used for probing the volume photosensitive grating, at Bragg angle. Following a simple k-vector analysis, for gratings with periodicity of 535nm and incident beam at 635nm, the Bragg condition is satisfied at 36.4^o. The above result was experimentally verified. A

lens with 500mm focal length was added to focus and match the beam size with that of the irradiated area. The last is a quite important parameter, in order to proceed to accurate diffraction efficiency measurements (Incident Power/ Diffracted Power), which will enable us to compare and characterize the structures. Special care was also taken in order to polarize the incident beam perpendicular to the plane of the incidence.

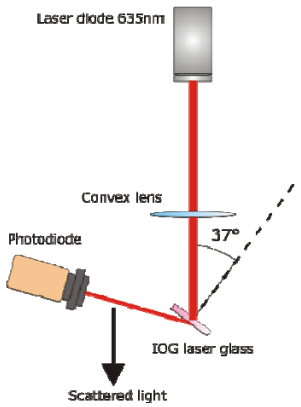

Fig. 3.5 *Experimental setup used for performing diffraction efficiency measurements. The beam coming from the output of a 635nm laser diode is focused on the gratings with a convex lens (500mm focal length). The samples are rotated at Bragg angle from the incidence. A photodiode is used for measuring the diffracted power.*

The diffracted signal for samples irradiated with 36000 pulses and different values of energy density, is presented in Fig. 3.6. The incident power from the laser diode was 1.250 mW. The maximum diffraction efficiency measured, reaches a value of about 0.0025 for the grating inscribed with 208mJ/cm^2. A linear function optimally fits these experimental data. The above implies once more that a single-photon absorption mechanism is activated during grating inscription. This is in agreement with the data measured for the case of absorption bands generation.

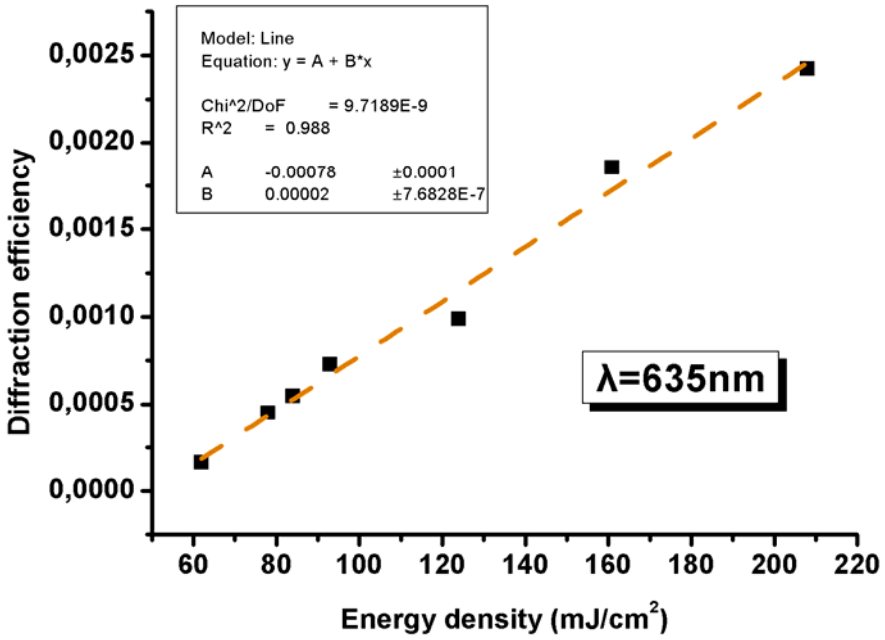

Fig. 3.6 *Diffraction efficiency η for gratings exposed to different energy densities F and 36000 pulses. All data correspond to a wavelength at 635nm. A linear function was chosen to fit the experimental data. The function fitted is the* $\eta=2\cdot10^{-5}F-7.8\cdot10^{-4}$.

3.4. Coupled wave theory for describing thick hologram gratings

Coupled wave theory was first introduced by Kogelnik in 1969 [2], in order to describe the problem of light diffraction from thick phase holograms. A thick or volume hologram is the hologram for which the thickness of the recording medium is of the order or of greater than the fringe spacing. On the contrary, in a thin grating the thickness of the recording medium is small compared to the fringe spacing [3]. The high diffraction efficiency of light which is achieved with thick dielectric holograms, renders them attractive in modern holographic components like Bragg gratings. The distinction between thick and thin holograms is accurately described by the Q-parameter defined as:

$$Q \equiv 2\pi\lambda d/\left(n\Lambda^2\right), \textbf{ Eq. 3.2}$$

where λ is the illuminating wavelength, n the index of the recording material, d the effective thickness of the grating and Λ the spacing of the recorded fringes. The thick hologram theory was found to be accurate for Q values greater than 1.

Couple wave theory predicts that only light incident on the hologram grating at or near the Bragg angle and polarized perpendicular to the plane of the incidence will yield high diffraction efficiency. It is assumed that the grating is relatively thick so that there are only two waves in the medium to be considered: the incoming reference wave R and the outgoing signal S. From this starting point, closed form results for the maximum achievable diffraction efficiency can be obtained for all possible types of holograms like transmission or reflection, amplitude or phase, with or without loss and with slanted or unslanted fringes planes.

In general, gratings inscribed in a variety of recording materials may belong to more than one of the aforementioned types. In mixed gratings, for example, both the refractive index (characterizing the phase gratings) and the absorption coefficient (characterizing the amplitude gratings) are spatially modulated. This is the case where the development of strong absorption peaks causes measurable refractive index changes according to a Kramers-Kronig analysis. The equation for the diffraction efficiency for the case of an unslanted mixed dielectric grating with losses, is [3]:

$$\eta = \left[\sin^2\left(\pi m_1 d_{eff} / \lambda\cos\Theta_0\right) + \sinh^2\left(a_1 / 2\cos\Theta_0\right)\right] e^{-2ad/\cos\Theta_0}, \textbf{ Eq. 3.3}$$

where η is the diffraction efficiency, a is the absorption coefficient, n_1 is the modulation of the refractive index, a_1 is the modulation of the absorption coefficient, d is the thickness of the sample, d_{eff} is the effective thickness of the grating, λ is the wavelength and Θ_0 is the Bragg angle. Thick absorbing phase-grating equation is frequently employed for the evaluation of laser induced refractive index changes in transparent materials [4]-[8].

3.5. Estimation of refractive index changes by employing thick absorption phase-grating equation

In our previous analysis, in Chapter 2, we indicated that the strong absorption peaks induced in IOG-1 glass by intense UV irradiation caused significant refractive index changes. These changes where estimated following a Kramers-Kronig analysis. Thus, we expect that the gratings inscribed here, constitute a periodic variation in both the refractive index and the absorption. Another basic characteristic of the inscribed structures in the IOG-1 glass, is their thickness, estimated to be 330μm (see paragraph 2.4.4), which is greater than the fringe spacing of 535nm. Thus, the Q factor that is evaluated for these gratings using the , Eq. **3.2** was estimated to have a figure of approximately ~3. For these reasons the grating structures inscribed here are classified in mixed holograms category. The refractive index changes can then be evaluated by rewriting the , Eq. **3.3** in the form:

$$\Delta n = \frac{\lambda \cos\Theta_0}{\pi d_{eff}} \arcsin\left[\sqrt{\eta e^{2ad/\cos\Theta_0} - \sinh^2\left(a_1/2\cos\Theta_0\right)}\right], \textbf{ Eq. 3.4}$$

The effective thickness d_{eff} of the grating was measured (see paragraph 2.4.4) to be 330μm approximately. The diffraction efficiency η is given in Fig. 3.6 and the modulation of the absorption coefficient α_1 was taken from the spectrophotometric measurements in paragraph 2.5. The refractive index changes evaluated using, Eq. 3.4 for grating inscribed with different energy densities, are presented in Fig. 3.7. In the same graph are presented the changes in the refractive index which are estimated by employing the Kramers-Kronig formula.

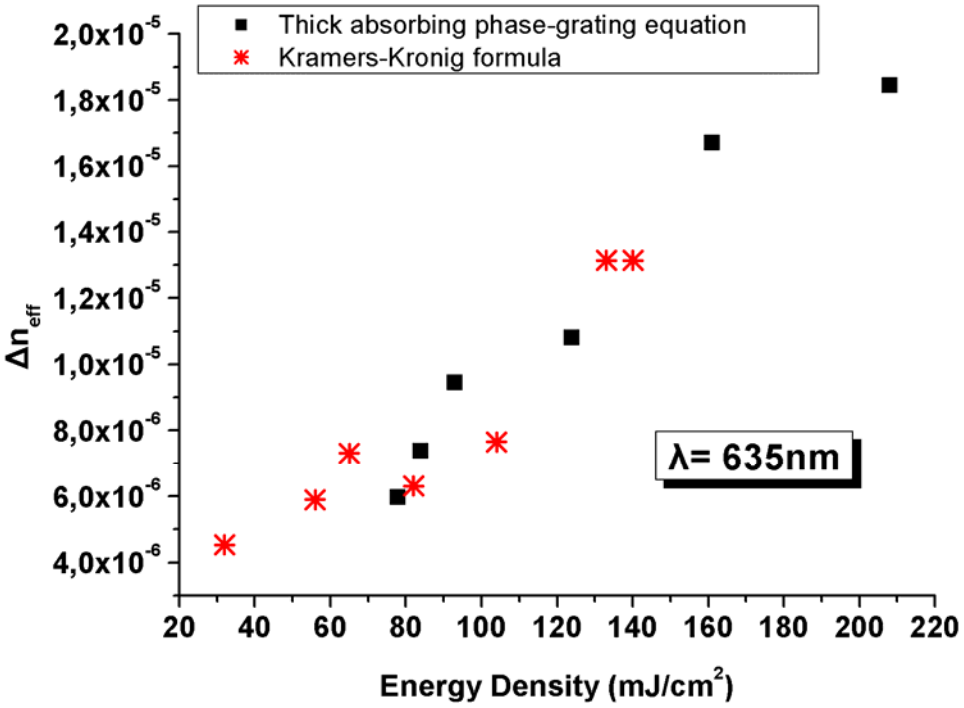

Fig. 3.7 *Induced refractive index change for gratings inscribe with different values of energy density and 36000 pulses. The black square points were evaluated using the thick absorbing phase-grating equation while the red asterisks were evaluated using the Kramers-Kronig formula. All data correspond to a wavelength at 635nm.*

The black squares in Fig. 3.7 denote the values for the refractive index change obtained using the thick absorbing phase-grating equation, while the red asterisks denote the values obtained using Kramers-Kronig formula. All data correspond to refractive index changes at 635nm. A good agreement is observed for the values calculated with these two different models. This may assist the understanding of the mechanism associated with the UV induced refractive index modulation. Hence, we may speculate that possible compaction or structural changes induced during the UV exposure do not result in significant changes in the refractive index.

3.6. Conclusions

Photosensitive Bragg, volume gratings, having periodicities of 535nm, were successfully inscribed in IOG-1 Er/Yr-codoped glass by employing an elliptical Talbot interferometric setup and the output of a 213nm, 150ps Nd:YAG

laser. The gratings were exposed to energy densities varying from 62 to 208mJ/cm^2. The evolution of the inscription process was online recorded, and analyzed. Post-exposure diffraction efficiency measurements revealed that the UV induced index changes were found to increase linearly in accordance to the energy density. The last denotes that the same inscription mechanism was activated no matter the value of the incident energy density. This mechanism is connected with a single-photon process.

The inscribed structures were classified as thick-mixed, lossy, holographic gratings. The thick absorbing phase-grating equation was subsequently applied in order to estimate the total induced refractive index change. The values of the refractive index evaluated, were found to be in good agreement with those estimated using Kramers-Kronig transformation. Thus, we assume that the refractive index changes can be attributed to the generation of the UV-induced absorption bands. Compaction or other structural changes do not seem to contribute to the overall modulation of the refractive index.

3.7. References

[1] S. Pissadakis, L. Reekie, An Elliptical Talbot Interferometer for fiber Bragg Grating Fabrication, Rev. Sci. Instr., **76**, 066101-066103 (2003)

[2] H. Kogelnig, Coupled Wave Theory for Thick Hologram Gratings, The Bell System Technical Journal, **48**, 2909 (1969)

[3] H.M. Smith, Holographic Recording Materials 20, Springer-Verlag (1977)

[4] S. Pissadakis, A. Ikiades, P.H. Anna, K. Sheridan, J.S. Wilkinson, High Photosensitivity of ion-exchanged Er-doped Phosphate Glass Using 248nm Excimer Laser Radiation, Opt. Express, **12**, 3131-3136 (2004)

[5] M. Kosters, Hung-Te Hsieh, D. Psaltis, K. Buse, Holography in Commercially Available Photoetchable Glasses, Appl. Opt., **44**,3399-3402 (2005)

[6] M.C. Wengler, B. Schreder, E. Soergel, J. Zimmer, K. Buse, Spectral Photosensitivity and Holographic Performance of Europium-Doped Fluorophosphate Glass, Appl. Phys. B, **79**, 597-601 (2004)

[7] C. Neipp, I. Pascual, A. Belendez, Experimental Evidence of Mixed Gratings with a Phase Difference Between the Phase and the Amplitude Grating in Volume Holograms, Opt. Expr., **23**, 1374-1383 (2002)

[8] Q. Zhao, J. Qiu, X. Jiang, C. Zhao, C. Zhu, Controllable Precipitation and Dissolution of Silver Nanoparticles in Ultrafast Laser Pulses Irradiated Ag^{+}-doped Phosphate Glass, Opt. Expr., **12**, 4035-4040 (2004)

Chapter 4. Fabrication of Bragg relief gratings in Er/Yb-codoped IOG-1 phosphate glass slabs using post-exposure selective chemical etching

4.1. Introduction

In previous chapters we presented that strong absorption bands can be induced in the IOG-1 glass substrates after exposure to intense 213nm laser radiation. These bands were attributed to the generation of electron centers. Strong indications about the creation of significant structural changes into the glass volume -which strength was dependent upon the energy density of the exposure- were also found by employing Urbach tail empirical rule. Next, we inscribed a number of photosensitive Bragg gratings in the IOG-1 glass using a Talbot interferometer, which exhibited index changes of the order of 10^{-6}. However, Bragg structures with index contrast of the order of 10^{-6} are rather inapplicable for practical use. Thus, the need for higher contrast periodic structures emerges, for attaining greater diffraction efficiencies. Relief Bragg gratings inscribed in "hard" optical materials are excellent diffractive elements of high index contrast and hence, diffraction efficiency.

We are presenting a wet etching laser assisted method for patterning arbitrary shape relief structures in phosphate glasses, however, the method is demonstrated for the patterning of sub-micron periodicity Bragg reflectors. Here we will exploit the volume damage induced into the glass by intense UV irradiation, in order to selectively remove the exposed areas by following a chemical development process. To be more precise, the chemical etching agent will selectively attack the UV exposed regions at higher etching rates, allowing differential patterning/etching process between the bright and dark fringes of interference.

Two different kinds of chemical solutions were tested in the following experiments: an acidic one (HNO_3) and an alkaline one (KOH), of different molar concentrations. The evolution of the relief grating pattern was monitored at fixed time intervals and the dependence of grating depth upon the etching time and the exposure conditions was also investigated. Finally, atomic force microscope (AFM) scans and scanning electron microscopy (SEM) images are presented in order to investigate the relief topology of the structures.

4.2. Chemical development of the IOG-1 glass in acidic solution

The dissolution of phosphate glasses in aqueous solution has already been studied in a number of works, carried out by several groups [1][2][3]. In our case, we used HNO_3 acidic solution with concentrations of 2M and 3M. HNO_3 acid is also used for the definition of the Acidic Resistance Standard [4]. The glass samples were mounted on a specially designed Teflon holder and they were immersed in a container with HNO_3. The acid container was placed in a beaker with water for sustaining constant temperature. The temperature of development was kept stable at 40^{o}C. At fixed time intervals the samples were unloaded from the holder, washed with deionized water and dried by using a nitrogen gun. Subsequently, the diffraction efficiency of the relief grating was measured by employing the diffraction setup presented in Fig. 3.5. The whole procedure was repeated until the diffracted signal was reaching saturation.

4.2.1. Evolution of the etching depth of the relief gratings

Firstly, we examined the dependence of the diffraction efficiency and etching depth on the molecular concentration of the acidic solution. Two grating samples were irradiated with a fixed energy density of 93mJ/cm^2 and 36000 pulses, and after they were developed in HNO_3 aqueous solutions with different concentrations (3M and 2M). The results obtained are presented in Fig. 4.1. Afterwards, gratings were inscribed with different values of energy density (161, 93 and 64mJ/cm^2) and they were developed in a 3M concentration HNO_3 solution. The dependence of the diffraction efficiency and etching depth on the

energy density during the inscription is presented in Fig. 4.2. Barnes *et al*, [2] studied the dissolution of phosphate glass in acidic solutions and found a slow dissolution rate of about 2nm/hr. Based on this result, we fixed the time interval between sequent measurements at 20 minutes. The grating inscribed with 64mJ/cm^2 energy density, needed more than 40 hours in order to reach saturation and so, the full data are presented separately in Fig. 4.3.

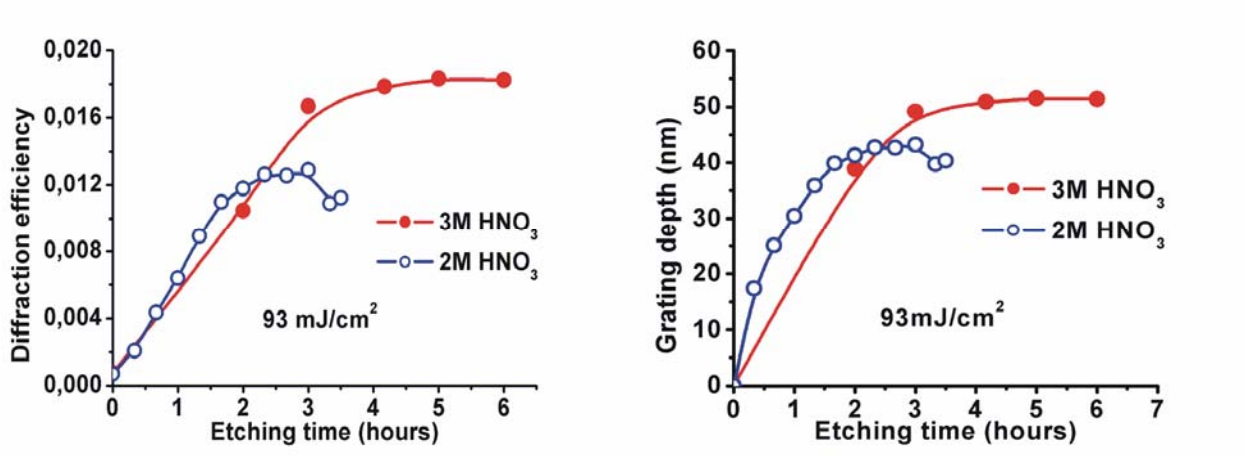

Fig. 4.1 *Diffraction efficiency and grating depths curves versus etching time for gratings exposed to 93mJ/cm^2 energy density and developed in 3M and 2M concentration HNO_3 acidic solution.*

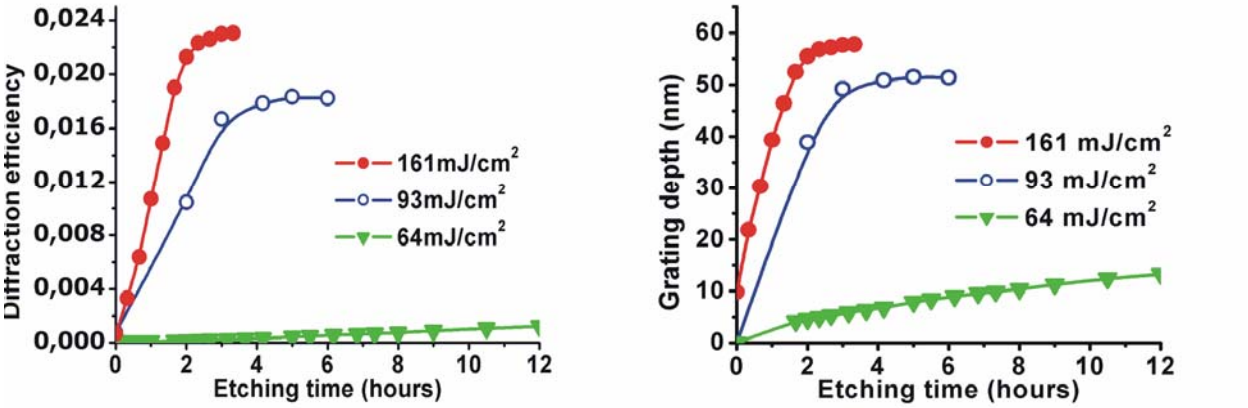

Fig. 4.2 *Diffraction efficiency and grating depth curves versus etching time for gratings developed in 3M concentration HNO_3 aqueous solution.*

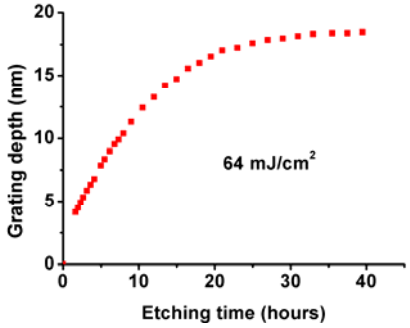

Fig. 4.3 *Grating depth versus etching time for a grating exposed to 64mJ/cm^2 and developed in 3M concentration HNO_3 aqueous solution.*

In Fig. 4.1, we observe that for an etching period of almost two hours the diffraction signal and etching depth of the two samples developed in 2M and 3M HNO_3, evolutes in a rather similar way. After this time interval, the grating developed in the 2M solution saturates, whereas the grating developed in the 3M solution is still increasing in depth, even with a decreasing rate. The maximum diffraction efficiency obtained for those exposures and developing conditions is almost 0.020 corresponding to an average grating depth of about 50nm. Continuing, we used the 3M concentration acidic solution in order to investigate the dependence of the diffraction efficiency on the energy density of the exposure thus, the UV induced structural damage. In the Fig. 4.2 we observe that the grating exposed to the higher value of energy density (161mJ/cm^2), exhibits deeper relief features and saturates faster. Moreover, for lower energy densities (Fig. 4.3), the saturation time increases by one order of magnitude approximately and the saturated grating depth is not grater than 20nm. In comparison with our previous results, the diffraction signal increased at 0.024 corresponding to a grating depth of about 60nm and 3 hours etching time.

As it is illustrated in Fig. 4.4, there are not significant differences in the grating depth between gratings that have been exposed to 161mJ/cm^2 and 93mJ/cm^2. A possible explanation may be that exposures at high energy densities can result in extensive formation of absorbing centers that are accumulated close to the samples surface, which in turn reduce the absorption depth of the incident radiation limiting the induced damage at shallower depths.

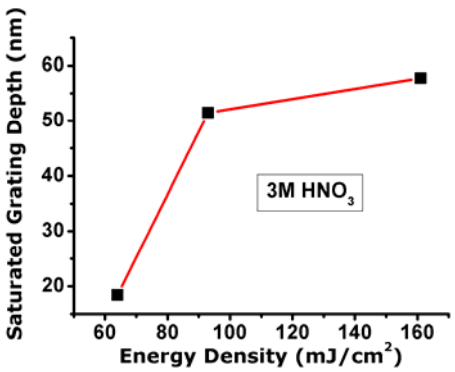

Fig. 4.4 *Saturated grating depths of the wet-etched gratings in HNO_3 solution vs. the incident energy density. All exposures were performed with 36000 pulses. The above result refers to glass samples exposed to 63, 93 and 161 mJ/cm^2 energy densities and developed in the acidic solution until saturation in diffraction efficiency is observed.*

4.2.2. AFM scans and SEM images of the 1D relief gratings

In Fig. 4.5 are presented the AFM scans and the profile analysis of the gratings inscribed with 93mJ/cm^2 and 161mJ/cm^2 energy density and developed in 3M HNO_3 aqueous solution.

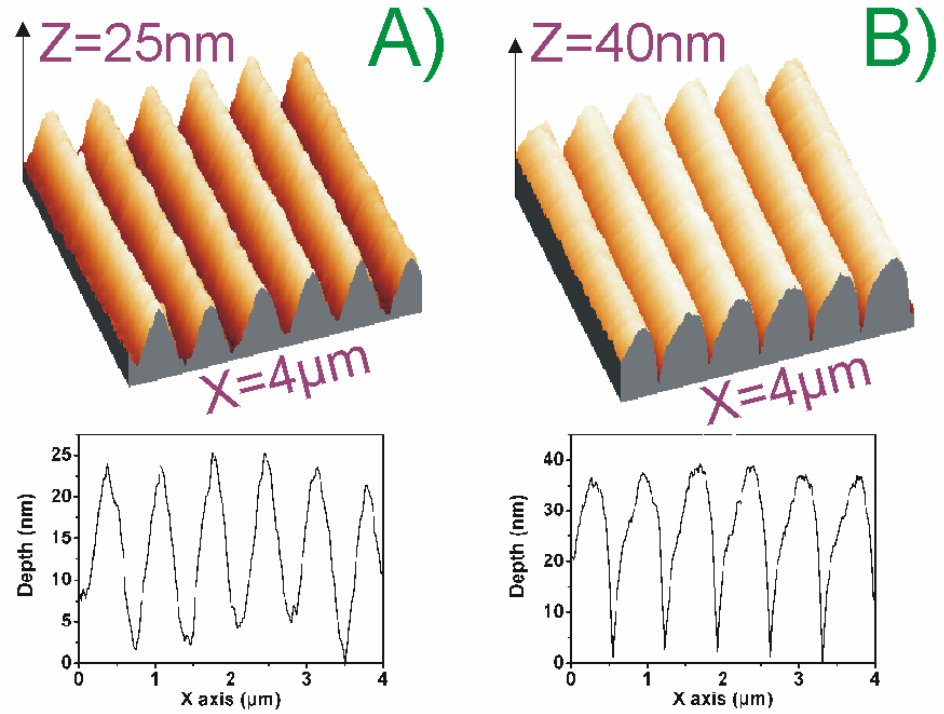

Fig. 4.5 *AFM scans and profile analysis of two gratings developed in 3M HNO_3 aqueous solution: A) grating inscribed with 93mJ/cm^2 and developed for 6 hours in the acidic solution, B) grating inscribed with 161mJ/cm^2 and developed for 3 hours in the acidic solution.*

There are obvious differences in the shape of the profile of these two gratings. The profile of the grating inscribed with 93mJ/cm^2 is sharper compared to that of the grating inscribed with 161mJ/cm^2. On the other hand, the profile of the grating inscribed with the higher value of the energy density is more identical to the theoretically expected (see paragraph 4.4).

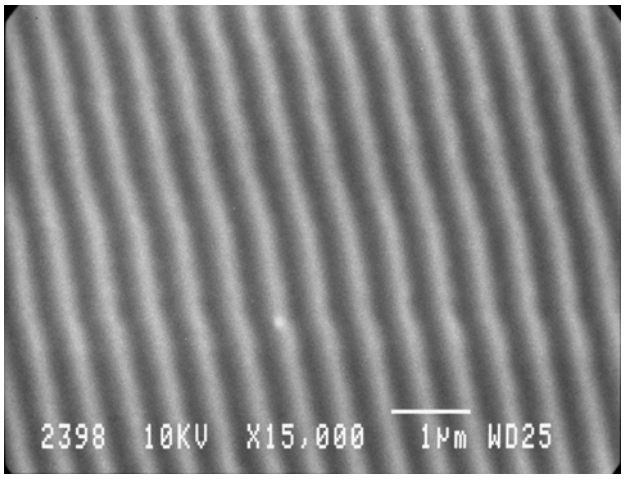

Fig. 4.6 *SEM scan of grating exposed using 36000 pulses and energy density of 161mJ/cm^2, after 6 hours of etching in 3M HNO_3 aqueous solution. The wavy pattern observed in the SEM scan is due to an apparatus artifact.*

A SEM image of the grating inscribed with 161mJ/cm^2 and 36000 pulses, after the end of the development period (6 hours) in 3M HNO_3 solution, is presented in Fig. 4.6. A quite smooth structure is observed without debris deposition or other stitching error features.

4.3. Chemical development of the IOG-1 glass in alkaline solution

The above experiments were repeated, using now an alkaline solution. It was decided to use KOH aqueous solutions of different molar concentrations. In an older study, Barnes *et al*, [2] pointed out that the dissolution rate of phosphate glass in KOH is significantly greater and faster than in an acidic solution of the same molarity. In the same study, it was also pointed out that etch products were deposited on the chemically treated surface. To prevent/eliminate this, they added an organic acid called ethylene-diamine-tetra-acetic acid (EDTA) in the KOH solution, where EDTA acted as a

decomplexing agent. For the aforementioned reason, we added 0.4M Disodium EDTA (Na_2EDTA) in all alkaline solutions we used.

Due to the fact that phosphate glasses appear to be more vulnerable to KOH solutions, we performed a number of chemical developments of the pristine glass in order to roughly estimate the etching rate. For performing the above, IOG-1 glass samples were half-covered with a 200nm Chromium-Nikelium layer in order to define a reference level. Special care was taken in order to form a sharp step between the covered and uncovered surface. The height of the step was measured by employing an alpha-step scanner. The samples were immersed in KOH solutions of different concentrations and the increase in the height between the covered and uncovered areas was measured at fixed time intervals. The results obtained are shown in Fig. 4.7. In all solutions the temperature was kept stable at 40°C. The Chromium-Nikelium layer exhibited tolerance in 1M and 1.5M concentrations of KOH for 1 hour or more. On the contrary, in 2M concentration the layer corroded after the first 20 minutes.

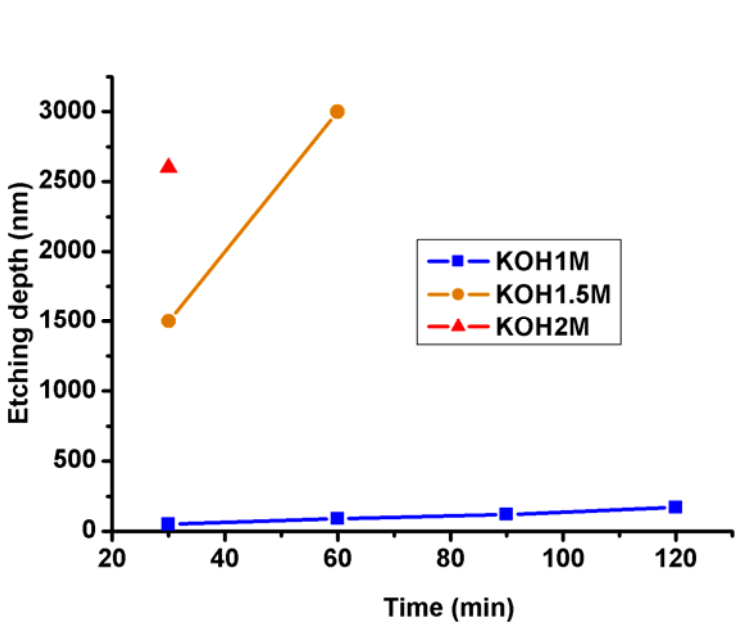

Fig. 4.7 *Etching depth as a function of time for IOG-1 samples immersed in KOH aqueous solutions. Three different concentrations of KOH solutions (1M, 1.5M and 2M) were used. In all occasions the temperature was kept stable at 40°C. The IOG-1 glass samples were half-covered with a Chromium-Nikelium layer in order to define a reference level. No more points were taken when the Chromium-Nikelium layer started to corrode.*

The data presented in Fig. 4.7 depict that quite high etching rates of the IOG-1 phosphate glass can be achieved by using alkaline solutions. Thus, it is expected that the developing time required for reaching the maximum diffraction efficiency signal from the relief gratings etched, should be much shorter than in the case of the acidic solution. The above information assisted in order to determine the time intervals between sequent measurements during the chemical development procedure.

4.3.1. Evolution of the etching depth of the relief gratings

The development of the grating structures in alkaline environment was recorded using the same procedure and apparatus as those used for the case of the acidic solution. Initially, the gratings were inscribed with 124mJ/cm^2 energy density and 36000 pulses, and they were developed in KOH solutions, of different molecular concentration. These diffraction efficiency and grating depth measurements are presented in Fig. 4.8. A similar experiment was performed in order to investigate the dependence of the grating depth upon the value of the energy density during the inscription process. Four gratings, which were inscribed with 84, 124, 161 and 208mJ/cm^2 energy densities, were developed in a 2M concentration KOH solution and the resulting data are shown in Fig. 4.9.

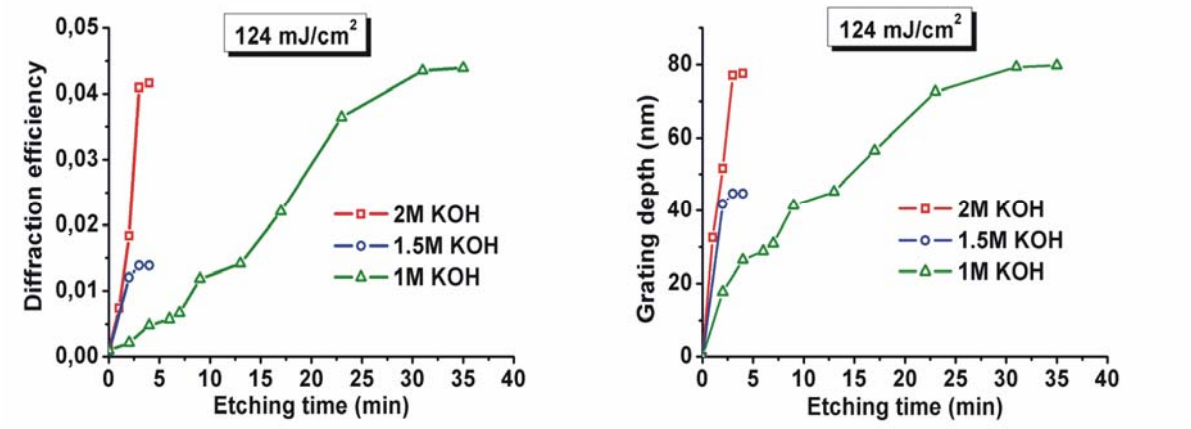

Fig. 4.8 *Diffraction efficiency and grating depth curves versus etching time for gratings exposed to 124mJ/cm^2 and 36000 pulses. The gratings were developed in KOH aqueous solutions of different concentrations (2M, 1.5M and 1M).*

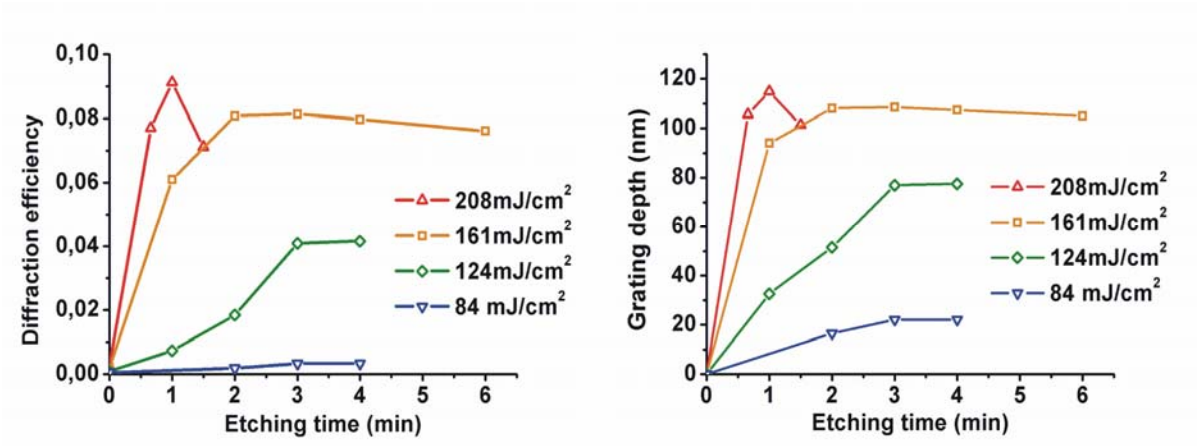

Fig. 4.9 *Diffraction efficiency and grating depth curves versus etching time for gratings exposed to different values of energy density (84, 124, 161 and 208mJ/cm^2).The gratings were developed in 2M KOH aqueous solution.*

As it was indicated in paragraph 4.3 the developing time in alkaline solution appears to be much shorter than that observed for the acidic solution of the same molarity. This difference -having a range of one order of magnitude approximately-, implies that alkaline solutions are more aggressive to IOG-1 glass, thus, the etching process is of reduced selectivity. Furthermore, comparing the 161mJ/cm^2 curve in Fig. 4.9 with the corresponding curve in Fig. 4.2, we conclude that the diffraction efficiency increases by a factor of 4. It should be also underlined the fact that the maximum value for the diffraction efficiency obtained is almost 0.1 (Fig. 4.9) which is considered to be rather high. This value of diffraction efficiency corresponds to an average grating depth of about 120nm. The saturated etching depth versus the incident energy density for the gratings developed in 2M KOH aqueous solution is presented in Fig. 4.10. Lastly, another interesting point is the evolution of the diffracted signal of the grating developed in 1M KOH, as presented in Fig. 4.8. At low concentrations the grating takes significantly longer time in order to saturate. On the other hand, the final diffracted signal is slightly higher than that measured for the grating developed in 2M KOH.

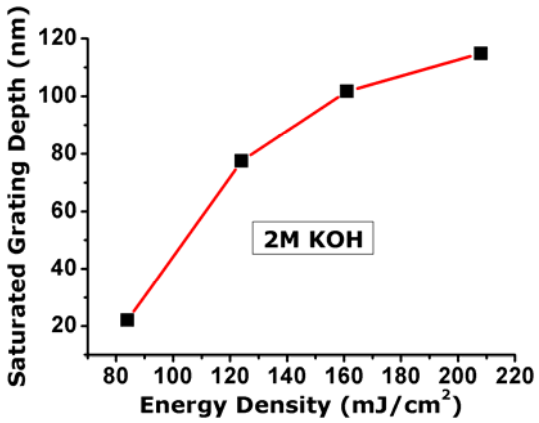

Fig. 4.10 *Saturated grating depths of the wet-etched gratings in KOH solution vs. the incident energy density: All exposures were performed with 36000 pulses. The above result refer to glass samples exposed to 84, 124, 161 and 208 mJ/cm^2 energy densities and developed in the alkaline solution until saturation in diffraction efficiency is observed*

4.3.2. AFM scans and SEM images of the 1D relief gratings

After the chemical development process, the relief topology of the gratings was examined by atomic force microscopy (AFM) and scanning electron microscopy (SEM). The relief gratings patterned after chemical development of samples inscribed with 124mJ/cm^2 in solutions with concentration 2M, 1.5M and 1M are presented in Fig. 4.11 and Fig. 4.12. The topological data presented in the Fig. 4.11 suggest that for the case of development in solutions of high molar concentrations, the relief patterns obtained are of rather similar fringe morphology. Therefore, the different values observed in diffraction efficiencies may be primarily attributed to the difference in grating depth (see Fig. 4.8). It must be underlined here, that the AFM scan is not the most suitable approach to measure the grating depth, since it refers only to a small part of the irradiated surface, ignoring other variations and singularities. Beam irregularities in the form of hot spots or dark areas may cause variations in the depth of the interference fringes and hence the resulting grating depth. In order to get such a kind of averaged information, the diffraction efficiency measurements are employed (Fig. 4.8 and Fig. 4.9). The derivation of grating depth from the diffraction efficiency provides us with a more reliable average value concerning all the inscribed area.

On the other hand, we can observe differences in the shape of the profile between the gratings presented in Fig. 4.11 and that in Fig. 4.12. The cross-section profiles of the gratings developed in 2M KOH and in 1M KOH solutions are presented in Fig. 4.13. We observe that the development in the solution of high concentration results in a "notch-like" profile while the development in the solution of low concentration results in a "sinusoidal-like" profile. Additionally, in Fig. 4.8 it is shown that the grating developed in the solution of low concentration needs much more development time in order to saturate. Thus, we can assume that KOH alkaline solutions at low molar concentrations are less aggressive to the IOG-1 glass and a more selective etching processing can be achieved in such an approach.

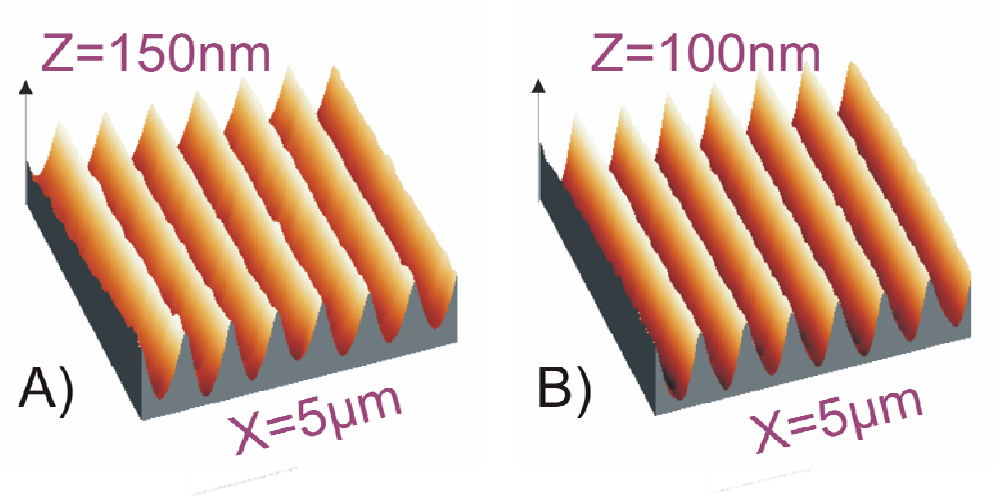

Fig. 4.11 *AFM scans of gratings inscribed with the same energy density 124 mJ/cm^{2}and developed in A) 2M KOH aqueous solution for 4 minutes, B) 1.5M KOH aqueous solution for 4 minutes.*

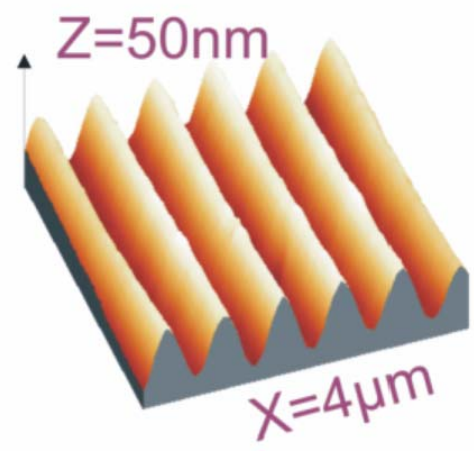

Fig. 4.12 *AFM scan of grating inscribed with 124mJ/cm^2 and developed in 1M KOH aqueous solution for 35 minutes.*

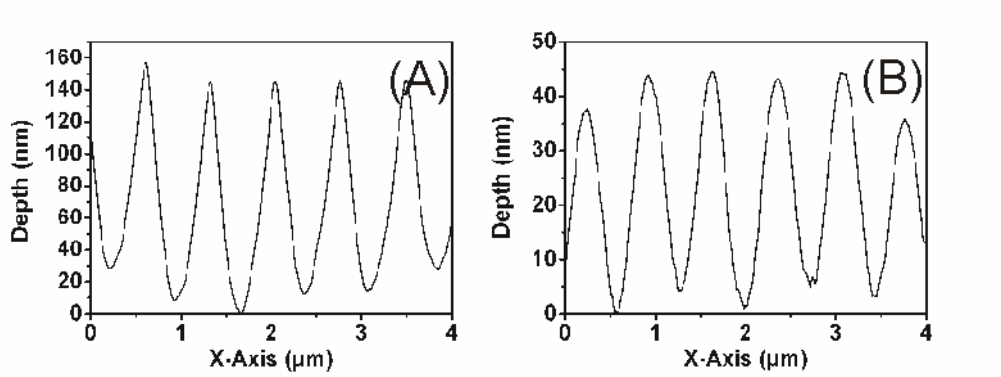

Fig. 4.13 *Profile analysis of two gratings inscribed with 124mJ/cm^2 and developed in A: 2M KOH aqueous solution for 4 minutes, B:1M KOH aqueous solution for 35 minutes.*

AFM scans obtained at different instances of the chemical etching process, of a sample that was exposed with 161mJ/cm^2 energy density and developed in 2M KOH solution, are presented in Fig. 4.14. The scan (A) was taken at the 1st minute of the chemical development while the scan (B) at the 6th minute. As it is shown in Fig. 4.9 the diffraction signal decreases after two minutes of chemical development, which is an evidence that the grating pattern is over-etched. As it is illustrated in Fig. 4.14 the over-etched grating pattern corresponds to a "notch-like" profile.

A large area AFM scan of the sample inscribed with 208mJ/cm^2 and developed in 2M KOH for 1.5 minute is presented in Fig. 4.15. A smooth and continuous structure is revealed, without debris deposition or other stitching error features. The quality of the structure appears to be superior compared to gratings patterned with other methods, like direct ablation [11]. The high quality of the patterned grating is also verified by SEM scans (see Fig. 4.16).

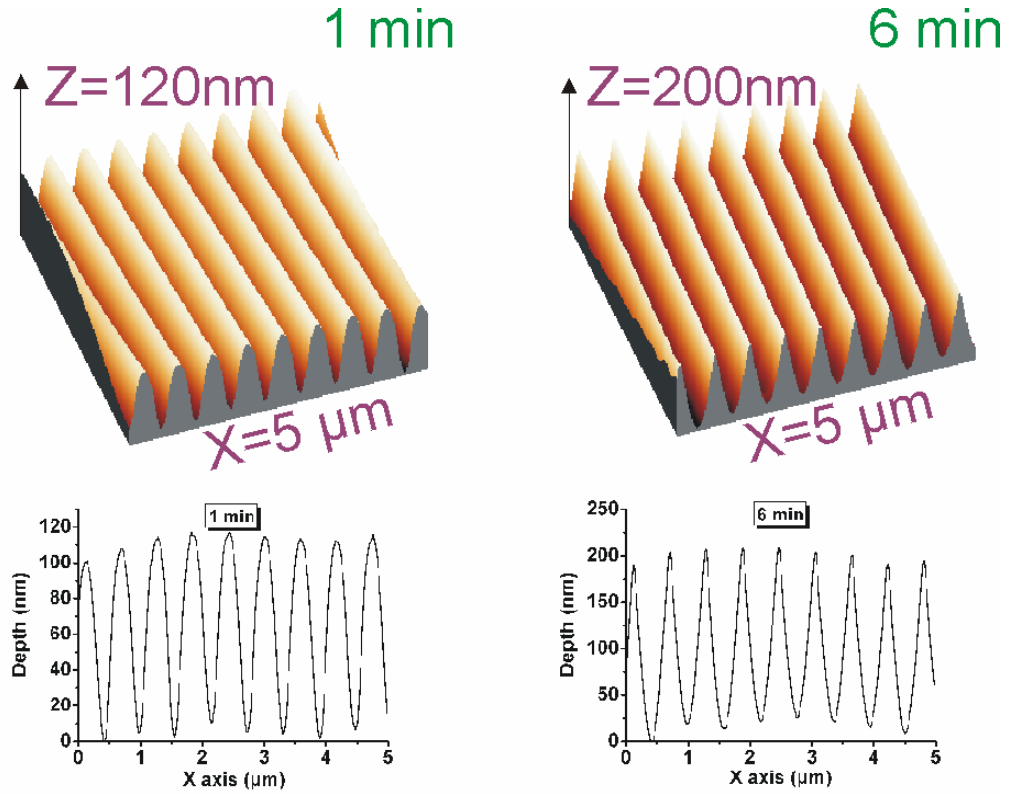

Fig. 4.14 *AFM scan of a grating inscribed with 161mJ/cm^2 and developed in 2M KOH aqueous solution. Left: the grating pattern and the profile after 1 minute of chemical development, Right: the grating pattern and the profile after 6 minutes of chemical development.*

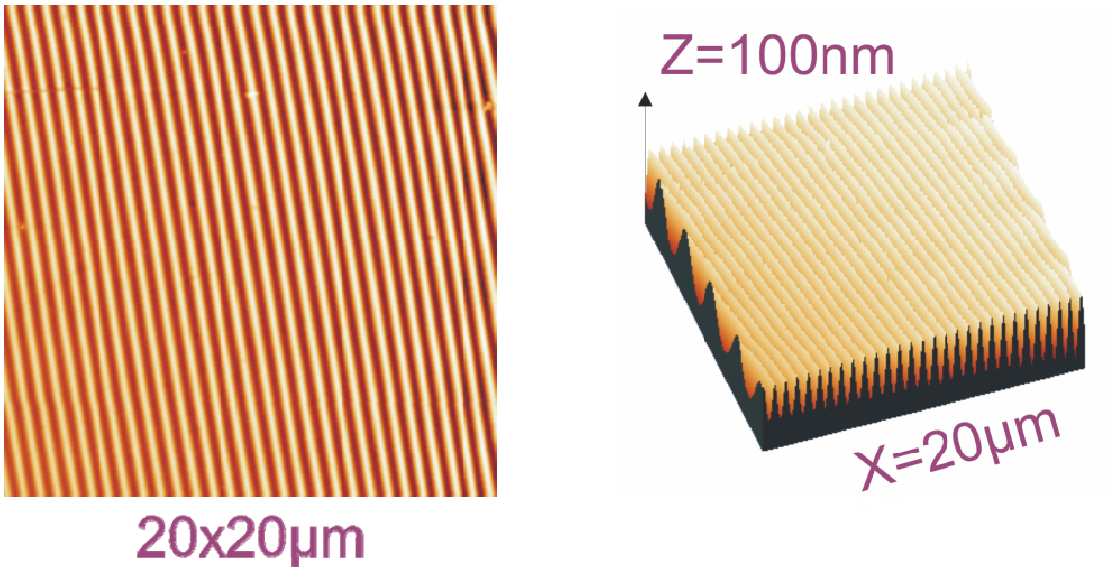

Fig. 4.15 *Large area scan and 3D representation of the grating inscribed with 208mJ/cm^2 energy density and developed in 2M KOH for 1.5 minute.*

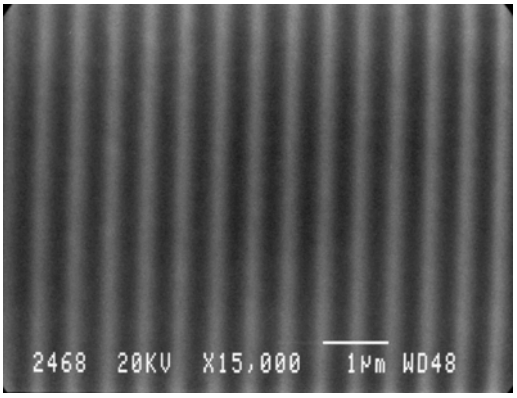

Fig. 4.16 *SEM image of a grating inscribed with 161mJ/cm^2 and developed in 2M KOH aqueous solution for 6 minutes.*

4.4. Grating patterning result analysis

The selective wet etching process in the alkaline solution yielded structures of higher quality compared to the structures obtained with the acidic solution. A profile analysis (see Fig. 4.17) indicates that, for gratings inscribed with the same value of the energy density (161mJ/cm^2), the periodic pattern obtained after chemical etching in KOH solution is smoother and significantly deeper. There is also observable difference in the morphology of the profiles with that of the grating developed in the acidic solution being more identical to the theoretically expected. In order to estimate the theoretically expected pattern we firstly calculated the intensity distribution on sample surface (calculated as $I = \left\langle \left| E_0 \cos(kx \sin\vartheta) + E_0 \cos(-kx \sin\vartheta) \right|^2 \right\rangle$, where E_0 is the electric field, k is the wavenumber and θ is the interference angle). The recorded pattern can then be simulated by correlating the intensity distribution with a logarithmic absorption function of the form [5]:

$$h = a^{-1} \ln(F / F_n) \qquad \textbf{Eq. 4.1}$$

where h is the absorption depth, α is the absorption coefficient and F_t is the threshold fluence. The resulting pattern is demonstrated in Fig. 4.17. From the profile comparison in Fig. 4.17 we see that the acidic development results in rather similar pattern to the theoretically evaluated, in contrast to that obtained for the alkaline development. For this reason we assume that the development

in the acidic solution constitutes a more selective chemical etching process than the development in the alkaline solution.

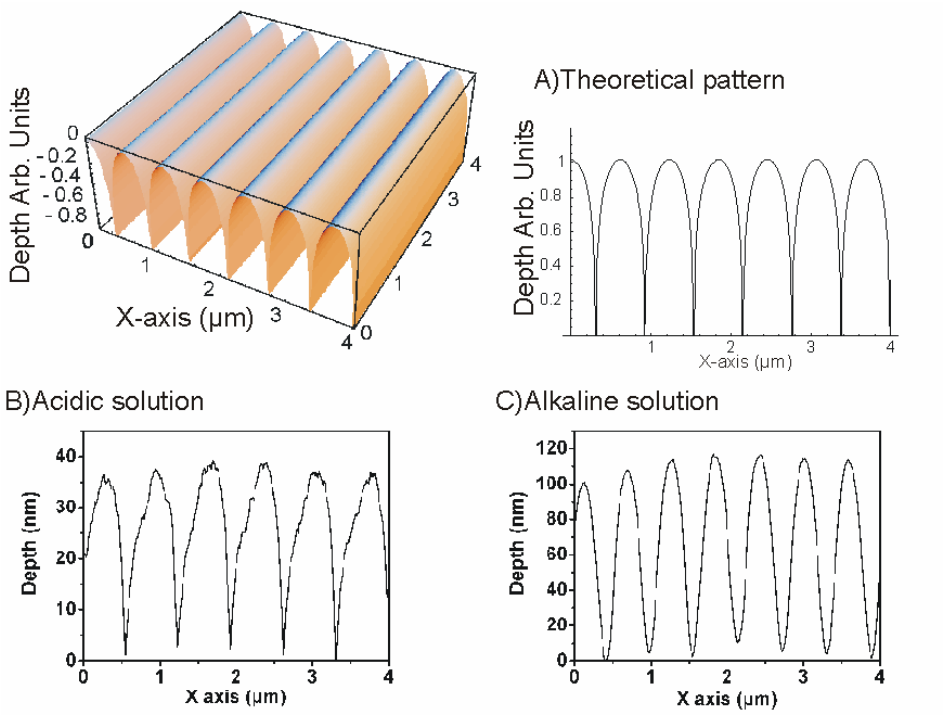

Fig. 4.17 *Profile comparison: A) 3D and 2D representation of the theoretically expected pattern, B) profile analysis of a grating developed in an acidic solution (3M HNO_3), C) profile analysis of a grating developed in an alkaline solution (1M KOH). Both of the samples presented in picture B and in picture C were irradiated with 161mJ/cm^2 energy density and 36000 pulses.*

For the two samples irradiated with the same energy density of 161mJ/cm^2 and etched in 3M HNO_3 the first and in 2M KOH the second (see Fig. 4.2 and Fig. 4.9), we see that in alkali development the diffraction efficiency increases by a factor of 4 (0.08 in KOH than 0.024 in HNO_3), the grating depth increases by a factor of 2 (100nm in KOH than 55nm in HNO_3) and the etching time decreases one order of magnitude (6min in KOH than 4 hours in HNO_3). The comparative evolution of the depths of the aforementioned gratings is demonstrated in Fig. 4.18.

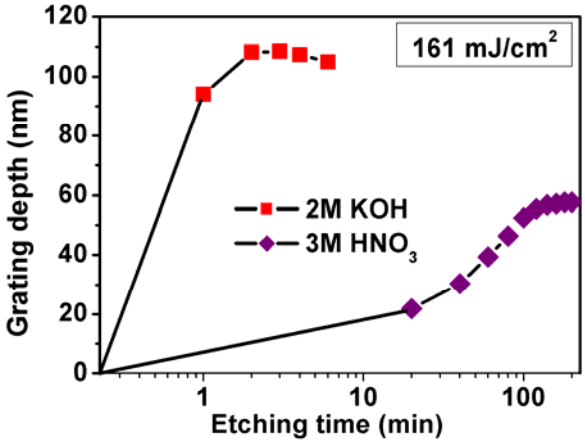

Fig. 4.18 *Grating depth vs. etching time for gratings inscribed with the same value of energy density (161mJ/cm^2) and 36000 laser pulses: The gratings are developed in two different chemical solutions (a 3M HNO_3 and a 2M KOH) until saturation in diffraction efficiency is observed.*

For the case of the wet etching in the KOH base, the prolonged immersion into the solution may increases the grating depth but simultaneously affects the shape of the grating grooves. The above phenomenon is clearly illustrated in Fig. 4.14, where the "sinusoidal-like" profile of a grating inscribed with 161mJ/cm^2 turns into a "notch-like". The above occurs because the solution, after removing the highly damaged, irradiated areas, attacks the sides of the non-irradiated areas. The shape of the profile and the width of the grooves are important parameters which affect the performance of the Bragg reflectors. The morphology of a periodic structure is described by a parameter called as the duty cycle. The duty cycle (DC) is the relative position of an index of refraction transition defined by its two boundaries. For example a duty cycle value equal to 0.5 means that the transition of the index of refraction occurs at the 50% of the period. For the gratings which are examined in the present study, we define the duty cycle as the width of the grating at FWHM (full width at half maximum) over the periodicity Λ:

$$DC = W_{FWHM} / \Lambda \qquad \textbf{Eq. 4.2}$$

The duty cycle values which were estimated in the present study are varying from 0.44 for the grating exposed to 124mJ/cm^2 energy density and developed for 4 minutes in 2M KOH, to 0.77 for the grating exposed to 161mJ/cm^2 energy density and developed for 3 hours in 3M HNO_3 acidic solution.

A perfect sinusoidal profile of optimum/maximum diffraction efficiency corresponds to a duty cycle value equal to 0.5. Deviations form this value result in degrading of the efficiency of the relief grating. The diffraction efficiency curves of a grating with a perfect "sinusoidal-like" profile (duty cycle equal to 0.5) and a grating with a "notch-like" profile (duty cycle lower than 0.5), are presented in Fig. 4.19. The *GSolver V4.20c* [6] commercial software was employed for performing the above calculation. The "notch-like" profile was specially designed in order to approach the corresponding structures presented in the present study. As it is illustrated in Fig. 4.19 the "harmonic" gratings with a duty cycle equal to 0.5 are more efficient in comparison to gratings with a duty cycle different than 0.5 and the same grating depth.

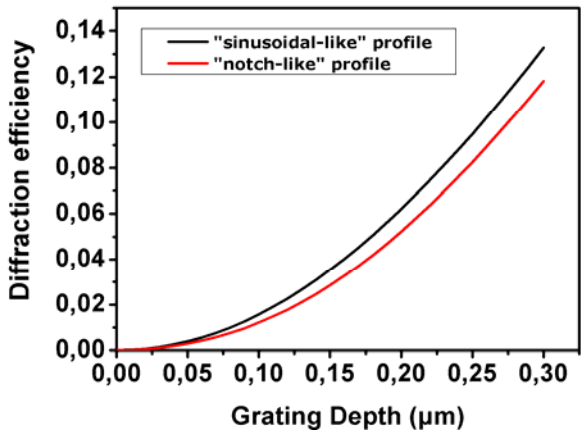

Fig. 4.19 *Comparison of the theoretically estimated diffraction efficiency of a perfect "sinusoidal-like" profile and a "notch-like" profile: The GSolver V4.20c commercial software was employed for performing the above simulation.*

In the case of the grating inscribed with 124mJ/cm^2 energy density and developed for 35 minutes in KOH alkaline solution of concentration 1M, a duty cycle of approximately 0.5 was estimated. Thus, we suggest that the development in the alkaline solution of low concentration results in a pattern comparable to a perfect "sinusoidal-like" surface structure (see Fig. 4.13B).

The maximum etching depth (and at the same time diffracted signal) is reached in the case of the grating inscribed with the higher value of the energy density (208mJ/cm^2) and developed in the 2M KOH alkaline solution. The duty cycle of this grating was measured to be of about 0.48. However, the fabrication of relief

structures by employing the above parameters can be characterized as an etching process of low selectivity, which can not be controlled in the most precise way. The glass is quite vulnerable to the solution and the diffracted signal degrades significantly, only a few seconds after reaching the maximum level.

4.5. Laser assisted wet etching mechanism for IOG-1 phosphate glass

The basic structural unit in phosphate glasses is the PO_4^{3-} group which can be attached to maximum of three neighboring groups forming long polymeric chains [7][8]. The addition of modifiers in the glass, which are in our case the Al_2O_3 and the Na_2O, result in the cleavage of P-O-P linkages [1][9] and the creation of non-bringing oxygens as shown in Fig. 4.20.

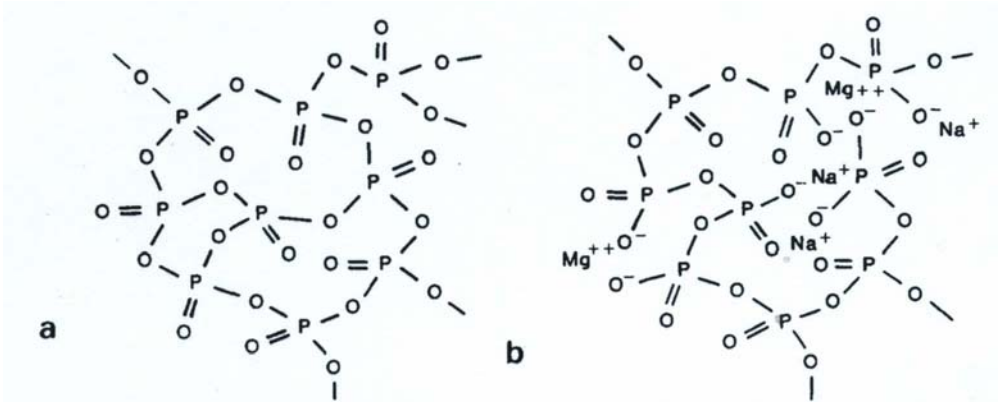

Fig. 4.20 *Phosphate glass structure, by B.C. Bunker et al.[1], (a) PO_4^{3-} group can be connected with three neighboring groups, with an infinite cross-link density, (b) The addition of modifiers disrupts bonds, lowering the cross-link density and increasing the number of anionic non-bridging oxygens present in the glass.*

Theoretical models have been developed [1] in order to approach the average length of the polymeric chain in phosphate glasses as a function of the mole fraction of the monovalent and polyvalent cations. The experimental results, however, provide evidence that the lengths are shorter than those predicted [1]. This can be attributed to the incorporation of structural water into the glass during melting. Structural water can behave like a glass modifier, hydrolyzing the P-O-P bond to produce two chain terminating P-OH bond [1]. Therefore, the

phosphate glass is considered to be composed by phosphate polymeric chains, terminated by two P-OH bonds:

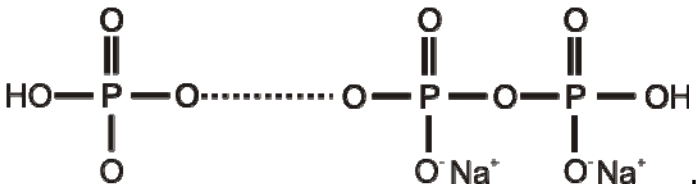

In paragraph 2.3, we mentioned that the Al_2O_3 was added into the IOG-1 glass matrix in order to increase its chemical durability. Van Wazer [10] proposed that cations can serve as ionic cross-links between the non-bringing ions of different chains:

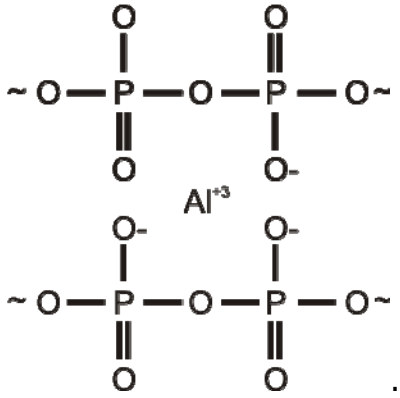

This way, the long polymeric phosphate chains are connected to one another by ionic bonds to the modifier cations and this is the reason why they are exhibiting increased chemical durability compared to the undoped phosphate glasses.

The dissolution mechanism of phosphate glasses having the above structure, in chemical solutions, can be divided in two main categories: in acidic/base reactions and in hydrolysis triggered reactions. In the study performed by Bunker *et al*, [1], it was found that the hydrolysis of the linear polymeric phosphates is accelerated in acids with a fractional dependence on the $[H^+]$. On the contrary, the hydrolysis reaction does not appear to be accelerated in basic solutions. Thus, we assume that the main dissolution mechanism in the presence of HNO_3 is the:

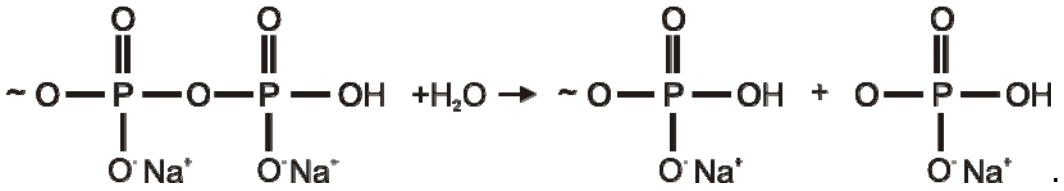

In the presence of the acid the phosphate chains are protonated and this result in the cleavage of P-O-P bonds. The water can then penetrate the glass faster and the dissolution rate increases. In the analysis performed in Chapter 2, we suggested that UV irradiation interacts strongly with the P-O bond, making the chain more vulnerable to hydrolysis and for this reason the etching rate increases.

The dissolution in alkali environment is more likely to be connected with a base reaction. Studies on short chain polymers indicate that there are different types of acid/base sites on polymeric phosphate [1]:

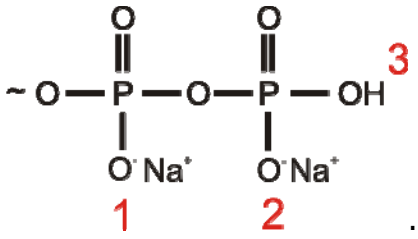

The middle sites (1) were found to be in the anionic form when the solution pH is higher than 2. The chain terminating type (3) is a weak diprotic acid, allowing the following acid/base reaction in the presence of KOH:

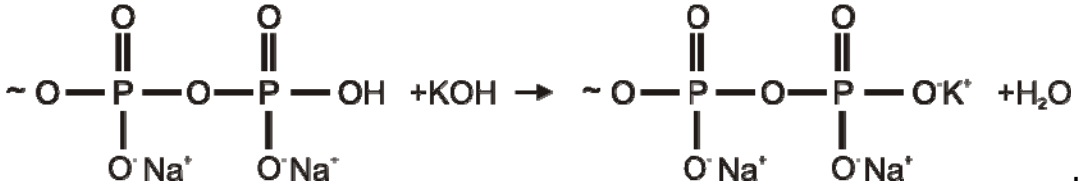

Bunker, *et al* suggested that the chemical durability of the phosphate glass is maximized when each terminal phosphate has one proton associated with it. It is assumed that the chain ends can then be interconnected by hydrogen bonding:

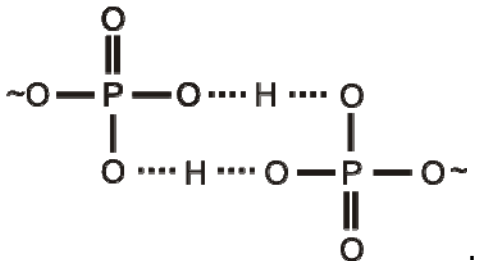

The acid/base reaction destroys the hydrogen bonding and results in a more dissolvable salt. Additionally, the more populous middle sites are in anionic form when the pH of the solution is higher than 2, facilitating the separation and thus the dissolution of polymeric phosphate chains.

In both occasions, the UV irradiation increases the dissolution rate of IOG-1 glass. In Chapter 2 we asserted that the UV irradiation interacts with the single and the double covalent bonds in the phosphate polymeric chains. Urbach Tail analysis revealed measurable structural changes that were attributed to the cleavage of P-O bonds. This could result in the cleavage of long polymeric chains in shorter ones which can be dissolved more easily. Lastly, from the comparison of the resulting grating profiles with the theoretically expected, which was performed in paragraph 4.4, we may conclude that the development in the acidic solution and thus the hydrolysis reaction is a more selective process than the base reaction.

4.6. Conclusions

In the present chapter we demonstrated the fabrication of 1D Bragg gratings in IOG-1 Er/Yb-codoped phosphate glass by employing a post-exposure selective chemical etching method. The interference technique described in Chapter 3, was employed in order to periodically photo-induce volume damage into the glass substrates. The samples were irradiated with energy densities bellow the ablation threshold. Subsequently, a chemical development technique was employed in order to selectively remove the irradiated areas.

The relief patterns were developed by employing different concentrations of an acidic (HNO_3) and an alkaline solution (KOH). Generally, the quality of the

gratings developed in alkaline solution was proven to be superior in terms of the diffraction efficiency, the surface smoothness and the symmetry of the grooves, compared to those obtained by development in the HNO_3 acid. For gratings inscribed with the same energy density ($161mJ/cm^2$), the sample developed in alkaline solution exhibited 4 times higher diffraction efficiency, 2 times deeper structures and one order of magnitude less developing time, compared to the sample treated with the acid. The maximum diffraction efficiency obtained was 0.1, corresponding to an average grating depth of about 120nm and an etching time of 1 minute.

The differences observed between the alkaline and the acidic treatment, were attributed to the different dissolution mechanisms that are taking place. The alkaline etching environment possibly triggers an acid/base reaction, while the acidic is probably connected with a hydrolysis reaction. In both cases, the UV induced damage increases the etching rates, cleaving the long polymeric chains into smaller parts which can be dissolved more easily in the aqueous solutions. However, the comparison of the resulting patterns to the theoretically expected leads to the assumption that the development in the acidic solution constitutes a more selective chemical etching process than the alkaline development.

Large area AFM scans and SEM images revealed that the alkaline development leaded to the formation of high quality continuous relief structures with no debris deposition or other parasitic features. The above experimental finding concludes to the fact that the method deployed and investigated here appears to be superior compared to other patterning techniques such as those based on direct ablation processes [11].

4.7. References

[1] B. C. Bunker, G. W. Arnold and J. A. Wilder, Phosphate Glass Dissolution in Aqueous Solutions, J. Non-Crystalline. Solids, **64**, 291-316 (1984)

[2] A. S. Barnes, C. G. Pantano, S. D. Conzone, Surface Cleaning and Etching of Rare-Earth Doped Phosphate Glass, proc. SPIE, Inor. Opt. Mat., **4452**, 115-125, (2001)

[3] N. E. Alekseev, A. A. Izyneev, V.B. Kravchenko, Y. S. Milyavskii and S.P. Rozman, Etching of Phosphate Glasses, Translated from "Steklo I Keramika", **7**, 11-12, 1983

[4] www.us.schott.com/optics_devices

[5] P.E Dyer, Excimer Laser Polymer Ablation: Twenty Years On, Appl. Phys. A, **77**, 167-173 (2003)

[6] Gsolver V4.20c, www.gsolver.com

[7] U. Hoppe, A structural Model for the Phosphate Glass, Jour. Non-Crystalline. Solids, **195**, 138-147 (1996)

[8] J. Van Wazer, K.A. Holst, Structure and Properties of the Condensed Phosphates. I. Some General Considerations about Phosphate Acids, J. Am. Chem. Soc., **72**, 639-644 (1950)

[9] R.K. Brow, C.A. Click, T.M. Alam, Modifier Coordinator and Phosphate Glass Networks, Jour. Non-Crystalline. Solids, **274**, 9-16 (2000)

[10] J. Van Wazer, D.A. Campanella, Structure and Properties of the Condensed Phosphates. IV. Complex Ion Formation in the Polyphosphate Solutions, Jour. Am. Chem. Soc., **72**, 655-663 (1950)

[11] S. Pissadakis, M.N. Zervas, L. Reekie, J.S. Wilkinson, High reflectivity Bragg Gratings Fabricated by 248nm Excimer Laser Holographic Ablation in Thin Ta_2O_5 Films Overlaid on Glass Waveguides, Appl. Phys. A, **79**, 1093-1096, (2004)

Chapter 5. Fabrication of 2-dimensional Bragg reflectors in Er/Yb-codoped IOG-1 glass slabs

5.1. Introduction

In the previous chapter we demonstrated the fabrication of 1D relief periodic structures in the IOG-1 glass. The structures were recorded as a periodic perturbation in the optical density and the structural order of the glass by employing a 2-beam interferometric technique. Then, the relief structures were patterned by following a selective chemical etching process. Different concentrations of acidic and alkaline solutions, and exposure conditions were tested, in order to optimize the development procedure, as far as, it concerns the surface quality of the structures, the diffraction efficiency and the etching selectivity. The selectivity, is defined as the ability of the solution to selectively remove the damaged area, leaving the non-irradiated areas intact.

The perspective to exploit this selective etching mechanism for fabricating more complicated periodic structures appears quite challenging. In this chapter we will focus our efforts in the fabrication of 2D photonic crystals in the IOG-1 phosphate glass. In Chapter 1, we mentioned that photonic crystals are emerging as attractive integrated optical elements for applications in dispersion compensation [1], low-threshold lasers [2][3] and fluid-detection systems [4]. Amongst their properties, which make them desirable in the aforementioned applications, is their ability to bend the light in very small radii, their dispersion angle (grater than in conventional optic devices), their ability to be used as polarization demultiplexers and their ability to trap the light preventing it to escape from the crystal. The last, parameter is very important because it enables the miniaturization of optical components in order to develop multifunctional, active integrated optical circuits.

In the present chapter we will demonstrate the fabrication of 2D photonic crystals by using a 4-beams interferometric technique in combination with the

selective etching method described in Chapter 4. The interference pattern of four monochromatic waves emitted from the 213nm laser source, will be recorded in the bulk of the IOG-1 glass samples. The diffracted signal of the 2-dimensional gratings is measured and quantified by employing a simple diffraction setup, while the interference effects observed in the patterning process are simulated using multi-beam intensity super-position. In addition, the topology of the periodic structures is examined by atomic force and electron beam microscopy.

5.2. Experimental apparatus for the inscription of 2D periodic structures

The development of straightforward, versatile and reliable fabrication techniques for structuring photonics crystals is of high importance. In Chapter 1 it is mentioned that, holographic lithography attracts great interest. However, there are few examples in the literature where such approach is applied for the structuring of "hard" materials, like silicate glasses. Such an approach predominantly requires a light source which is capable of providing high energy densities per pulse and sufficient coherence (temporal and spatial) in order to be used in an open interferometric cavity. In our study we have used the 213nm, 150psec Nd:YAG laser employed previously to perform the 2-beam holography.

The experimental apparatus is shown in Fig. 5.1. The beam emitted from the laser complex was firstly focused with a 60cm focal length lens and then separated in multiple beams using a beam splitting element (BSE). The splitting element consisted of two phase masks attached in contact mode. The periodicities of the phase masks used, were 1062nm and 1054nm and they were being both optimized for laser illumination at 248nm.

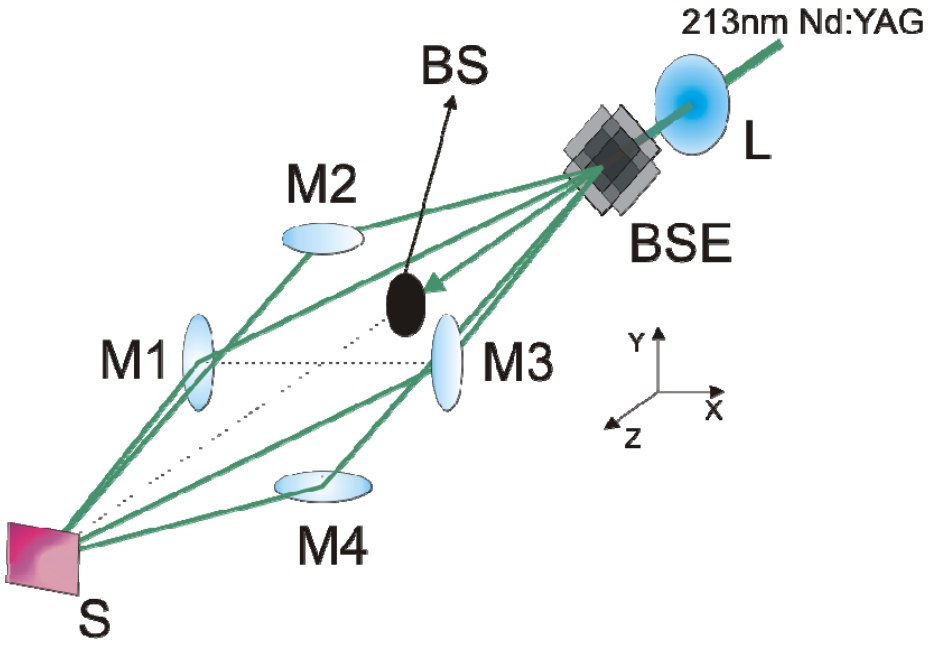

Fig. 5.1 *Four-beam interferometric setup. A beam splitting element is employed to split the beam emitted from the 213nm, 150psec Nd:YAG laser into multiple beams. A beam selecting aperture allows the ±1 first diffraction orders to propagate. In the above figure for simplicity and clarity purposes the beam selector is shown to block only the zeroth diffraction order. The focusing system, used for sending the diffracted orders onto the samples surface, consists of 4 Al-coated mirrors. (L) 60cm focal length lens, (BSE) beam splitting element, (BS) beam selector, (M1, M2, M3, M4) metal coated mirrors, (S) sample.*

The grating lines and thus, the direction of diffraction of the gratings were adjusted perpendicular to each other. For this reason a specially designed holder was developed for hardly clamping the phase masks in absolute contact. A schematic diagram of the two phase masks attached in contact mode and the principal diffraction orders scattered are presented in Fig. 5.2.

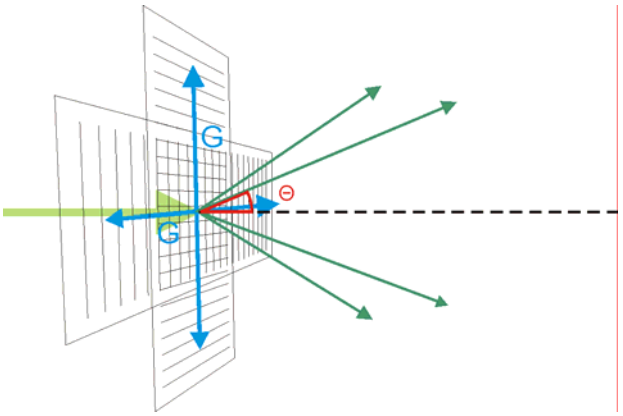

Fig. 5.2 *Two phase masks placed perpendicular to each other and attached in contact mode. The four principal diffraction orders are also presented. G: periodicity of the phase masks, Θ: angle of diffraction*

A beam selector (BS) was placed after the BSE in order to select the ±1 diffraction orders in x and y axis. A system of 4 Al-coated mirrors was placed on the path of each diffracted order, for refolding the beams onto the sample (S) surface. The 4-mirror system was positioned in the middle of the distance between the (BSE) and the sample (S). Theoretically, after the alignment of the optical elements, by just placing the (M1) and (M3) mirrors parallel to the yz plane and (M2) and (M4) mirrors parallel to xz plane an interference angle the same as the diffraction angle (measured to be $34^{o}56''$) should be obtained. In fact, slight adjustments of the gimbaled stages where each of the Al-mirrors was placed on, were required in order to achieve a complete overlap of the four beams. The perfect alignment of the optical setup is very important because slight differences in the optical paths could induce significant changes in the interference pattern. Thus, a significant amount of effort was made in order to reassure the complete overlap of the four beams, first by checking the overlap of the fluorescence spots on the surface of the sample and afterwards by checking the overlap between the beams reflected from the sample and those directed towards the sample. Ideally, a beam coming from a mirror (for example M1) and reflected on sample's surface should then follow the same path as the beam coming from the mirror which is placed in the opposite side (M3).

One of the major difficulties that frustrated the easy deployment of the experiment for inscribing gratings with 2D periodicity, was that of the significant energy losses of the diffracted beams. A part of the initial pulse energy is wasted to zero order transmission and to higher order diffraction. Additionally, the Al-coated mirrors are not optimized for maximum reflectivity at 213nm, resulting in extra energy losses of the incident energy. Finally, the back reflection from the phase masks and the lens are also accounted to be loss factor. To provide some numbers, for laser energy pulse of 8.5mJ measured after the laser aperture, only 1.5mJ finally reaches the target. Thus, in order to achieve high values of energy density the beam must be focused in small areas on sample surface. The beam diameter on the sample was set to be slightly bigger than 1mm resulting in an estimated value of energy density of $134mJ/cm^2$. kept the rest of the exposure conditions the same as in the Chapter 2 (1hour exposure with a repetition rate of 10Hz).

5.3. Inscription of 2D periodic structures in the IOG-1 phosphate glass

Theoretically, the intensity distribution I(**r**) on the sample surface, for multi beam interference is expressed as

$$I(\vec{r}) = \left\langle \left| \sum_i E_i(\vec{r}) \right|^2 \right\rangle \quad \textbf{Eq. 5.1}$$

where

$$E_i(\vec{r}) = E_i^0 \cos(\vec{k}_i \vec{r} - \omega t - \phi_i) \quad \textbf{Eq. 5.2}$$

is the electric field of each interference beam, E_i^0 and ϕ_i are the electric field strength and the optical phase of the i^{th} beam respectively. By assuming that $\phi_i = 0$, the recorded pattern into the bulk of the glass, can be simulated by employing the Equation 4.1: $h = a^{-1} \ln(F / F_n)$. In Fig. 5.3 is presented the 3D representation and the profile analysis of the theoretically calculated pattern. In this figure, the profile (B) was calculated assuming that the electric field strength is the same for each interfering beam, whereas the profile (C) is calculated according to our experimental measurements. The period of the lattice is calculated from Fig. 5.3 to be of the order of 500nm in the x and y axes. (the x and y axes are defined in Fig. 5.1). By increasing the interference angle, smaller periods can be obtained.

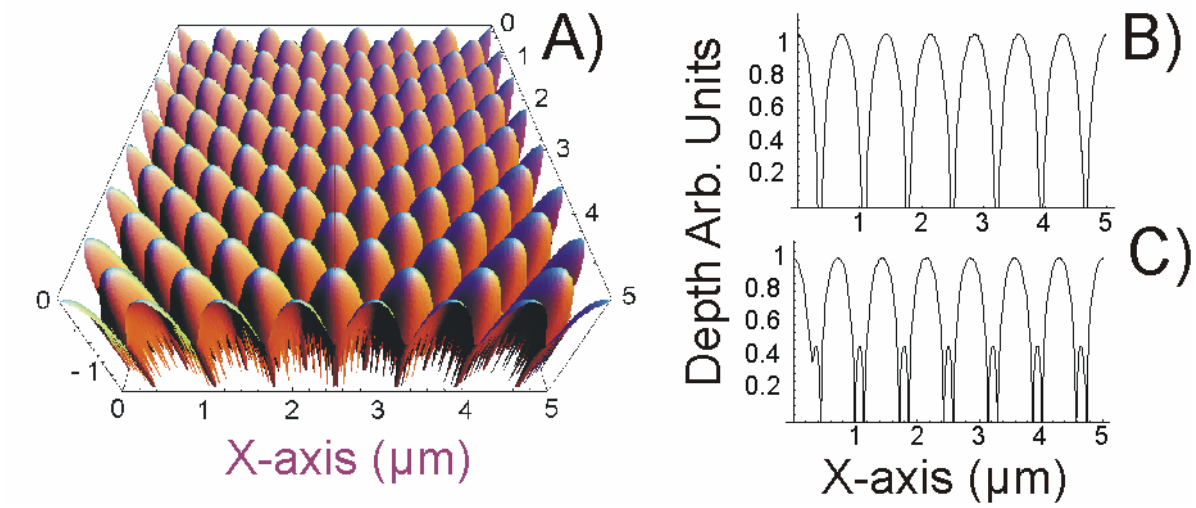

Fig. 5.3 *3D representation and profile analysis of the theoretically calculated pattern of the photonic crystal: A) 3D representation of the photonic crystal, B) profile analysis assuming equal electric field strength for each interfering beam, C) profile when the electric field strength is not the same for each interfering beam. The pattern C was calculated according to our experimental results.*

5.4. Chemical development of 2D periodic structures inscribed in IOG-1 glass

In the analysis carried out in Chapter 4, we concluded that: a) the chemical development in alkaline solutions appears to produce more qualitative structures (in terms of the diffraction efficiency and the smoothness of the grooves) in comparison to acidic solutions, b) the development time required in an alkaline solution is much shorter than in acidic solution.

The above findings revealed that the alkaline solution is preferable for the development of relief structures in the IOG-1 phosphate glass. In the 2D grating inscription process we use a KOH aqueous solution of 1M molarity. In the alkaline solution we have also added 0.4M Na_2EDTA for preventing leach deposition onto the etched surface. We chose 1M KOH alkali solution because it exhibited high selectivity, being aggressive mostly to the damaged areas instead of the non-exposed. Additionally, as it is illustrated in Figure 4.8, the etching rate is much slower in comparison to the rate measured in higher concentrations and thus, the whole procedure is more controllable. During the development procedure the temperature of the alkali solution was kept stable at 40^{o}C, as in the case of the 1D gratings.

The development procedure was interrupted at fixed time intervals; the sample was washed in deionized water, dried with a nitrogen gun and subsequently mounted in a diffraction efficiency measurement setup similar to that described in Figure 3.5. The output of an Ar-ion laser emitting at 496.5nm was used for probing the grating area. The incident angle was at 32^{o} with respect to the yz plane. The first diffraction orders and the zero order were projected on a screen as shown in the Fig. 5.4. We call the diffraction order projected above the plane of the incidence as (1,1) and the diffraction order projected below as (1,-1). The main diffraction orders were separated in smaller, which are going to be denoted using indexes. For example the main diffraction order (1,1) consists of the $(1,1)^{\pm 1}$, $(1,1)^{\pm 2}$ and $(1,1)^{\pm 3}$ orders as demonstrated in Fig. 5.5.

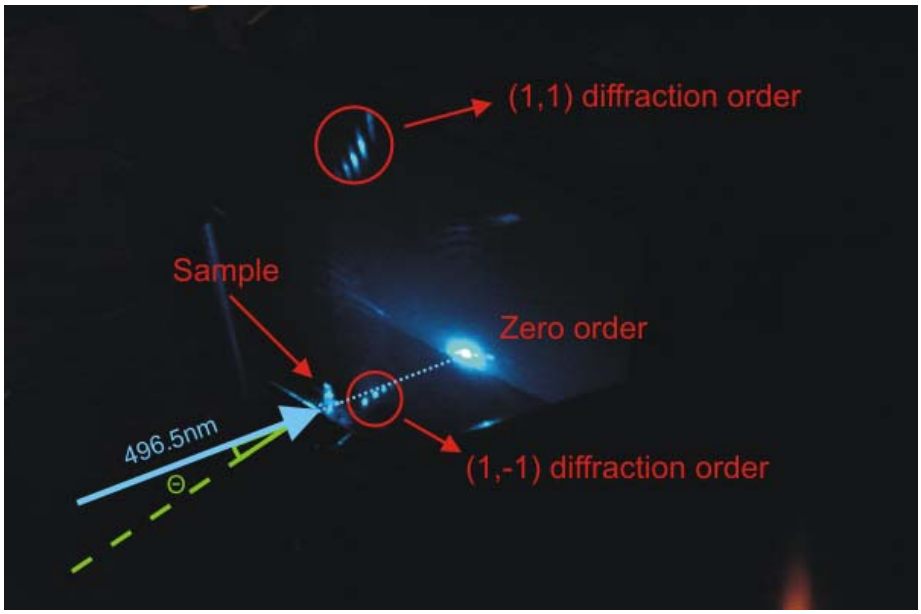

Fig. 5.4 *Photograph of the diffraction setup. A beam coming from an Ar-ion laser emitting at 496.5nm is diffracted on the grating. The incident angle is $32^{o}$with respect to the yz plane. Two main diffraction orders [(1,1) & (1,-1)] and the zero diffraction order are projected on a screen placed behind the sample. The main diffraction orders are appeared separated in smaller orders. The grating was inscribed with 136mJ/cm^2 and developed in 1M KOH aqueous solution for 45min.*

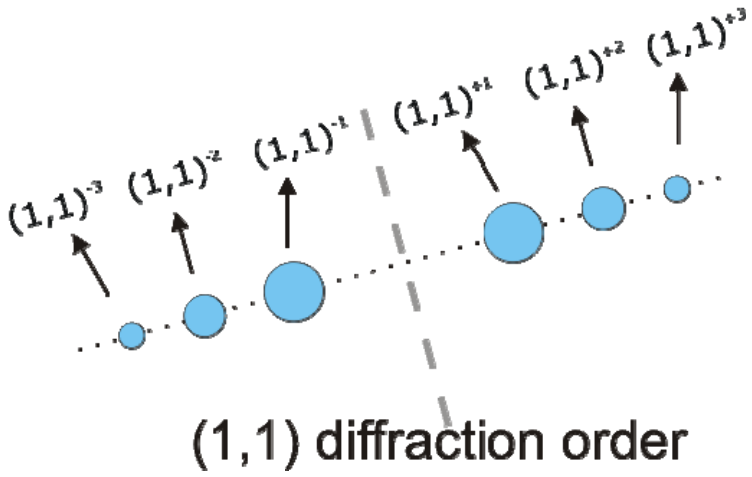

Fig. 5.5 *Schematic representation of the separation of the (1,1) main diffraction order in smaller orders. Each one of the smaller diffraction orders is denoted using an index.*

The total diffracted power was recorded at fixed time intervals. The diffraction efficiency of (1,1) and (1,-1) diffraction orders as a function of etching time is presented in Fig. 5.6. To facilitate comparison, the diffraction efficiency of the (1,-1) order is presented with negative values.

The $(1,1)^{\pm1}$ and $(1,-1)^{\pm1}$ orders saturate after 45 minutes of chemical development. Nevertheless, the total signal (black squares in Fig. 5.6) still increases and this is mainly attributed to the $(1,1)^{\pm2}$, $(1,-1)^{\pm2}$ orders. The power diffracted from each one of the main diffraction orders slightly differs. This is maybe an evidence that the polarization of the Ar-ion laser is not totally aligned with one of the axes of the 2D structure, during the diffraction efficiency measurement. Also, it maybe an evidence that the structure is not homogeneous due to deviations from perfect alignment during the inscription. The total value of the diffraction efficiency evaluated by adding the two diffraction orders, is 0.05, approximately.

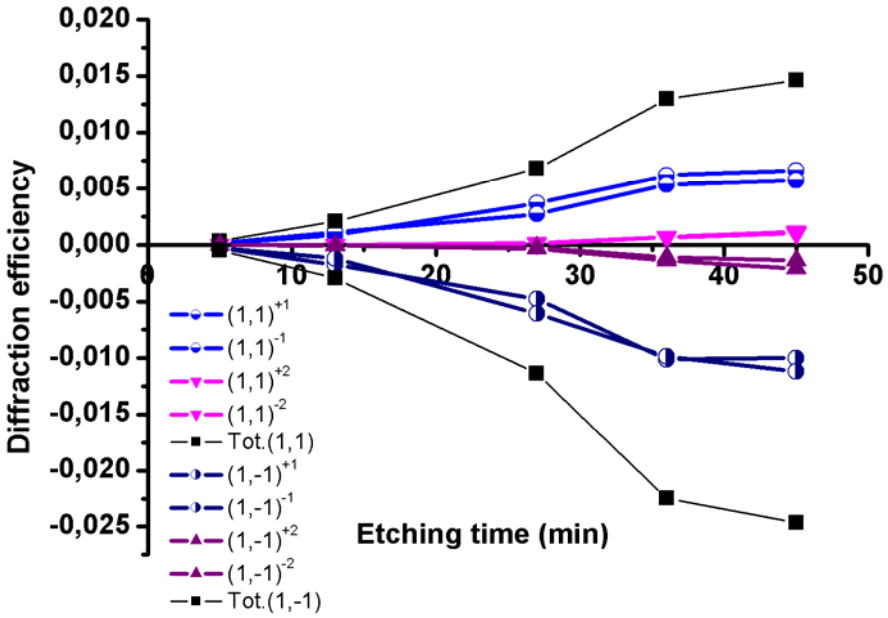

Fig. 5.6 *Diffraction efficiency as a function of etching time for a 2D periodic structure inscribed in IOG-1 glass with 136mJ/cm^2 and 36000 pulses. The sample was developed in 1M KOH aqueous solution. The smaller diffraction orders are represented with the colored points and the black squares denote the total diffraction efficiency, which corresponds to the main orders (1,1) and (1,-1). The (1,-1) diffraction order is presented with negative values to facilitate comparison.*

5.5. AFM scans and SEM images of the 2D relief gratings

During the etching procedure the relief shape of the structure was regularly examined. The AFM scans taken in the begging (5th minute) the half time (27th minute) and during the saturation (36th and 45th minute) of the chemical development process are presented in Fig. 5.7. The corresponding profiles of the gratings are presented in Fig. 5.8. As it was previously mentioned, AFM scans is not the optimum way to measure the mean depth of the relief structure because it refers to only a small part of the irradiated area. Nevertheless, Fig. 5.7 and Fig. 5.8 reveal that grating depths of the order of 200nm can be achieved. Another interesting point, is that at the early stages of the chemical etching (5th minute), the structure appears to be rather rough compared to the picture taken after of 31 more minutes of chemical development.

It is quite important to notice the difference between the shape of the peaks at 27 minutes and the shape at 36 and 45 minutes of chemical development. For 27 minutes immersion in the KOH solution, the grating peaks appear to be sharp, nonetheless they become smoother and rounder as the development progresses. On the other hand, the diffraction efficiency increases (see Fig 5.6) and this is an evidence of an increasing etching depth. But while the etching depth increases, the non-irradiated areas, depleted from the irradiated parts, are more vulnerable to the solution and the sharpness of the peaks disappear. This evolution mechanism is fully illustrated in Fig. 5.7 and Fig. 5.8.

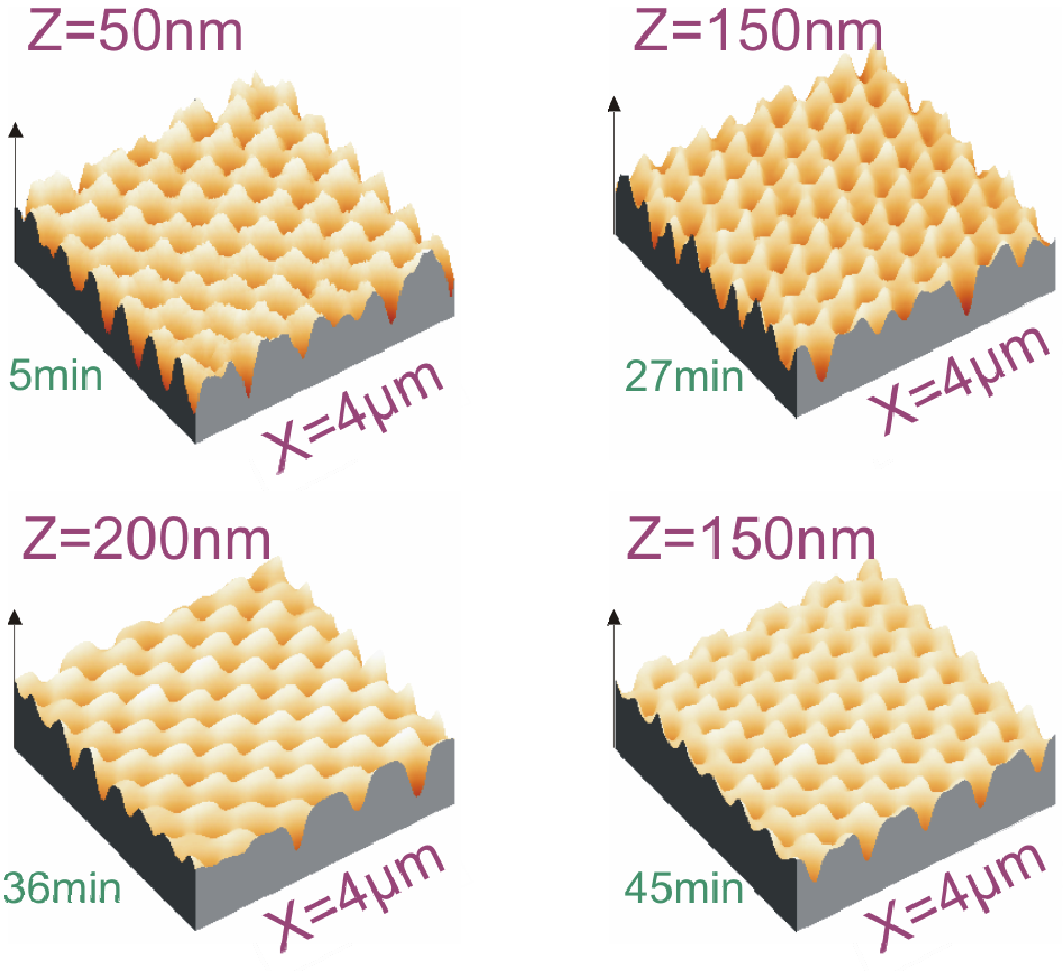

Fig. 5.7 *AFM scans of the same sample inscribed with 136mJ/cm^2 and 36000 pulses. The scans were performed at the begging (5th minute) the half time (27th minute) and during the saturation (36th and 45th minute) of the chemical etching process. The solution used was a 1M KOH aqueous solution.*

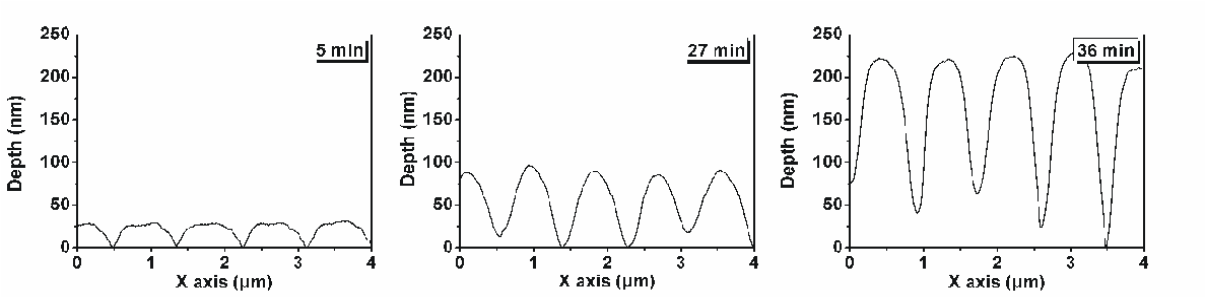

Fig. 5.8 *Profile of the grating inscribed with 136mJ/cm^2 after 5, 27 and 36 minutes of chemical etching in 1M KOH aqueous solution.*

AFM scans of larger areas revealed that the plane shape of the structure is lost if the sample is immersed in the solution for more than 27 minutes. As it is presented in Fig. 5.9 a wavy pattern appears in the surface of the structure for development times of 45 minutes. In Fig. 5.10 is presented a more detailed representation of the plane structure taken after 27 minutes of chemical etching. A high quality periodic and clean structure is revealed. No perturbations of the periodicity are observed in small or large scale or presence of defects of any kind.

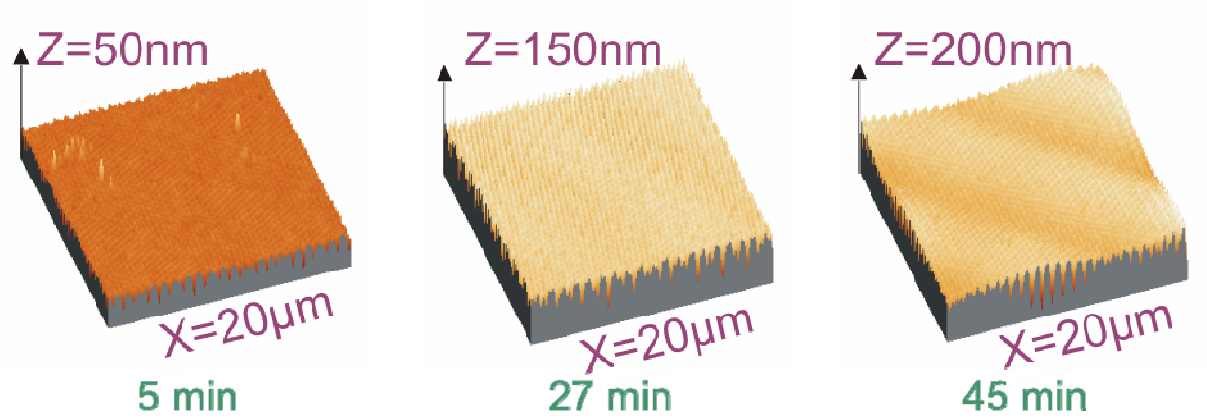

Fig. 5.9 *Large area AFM scans of the IOG-1 sample inscribed with 136mJ/cm^2 and developed in 1M KOH aqueous solution. For development time of more than 27 minutes a wavy pattern appears on the surface of the structure.*

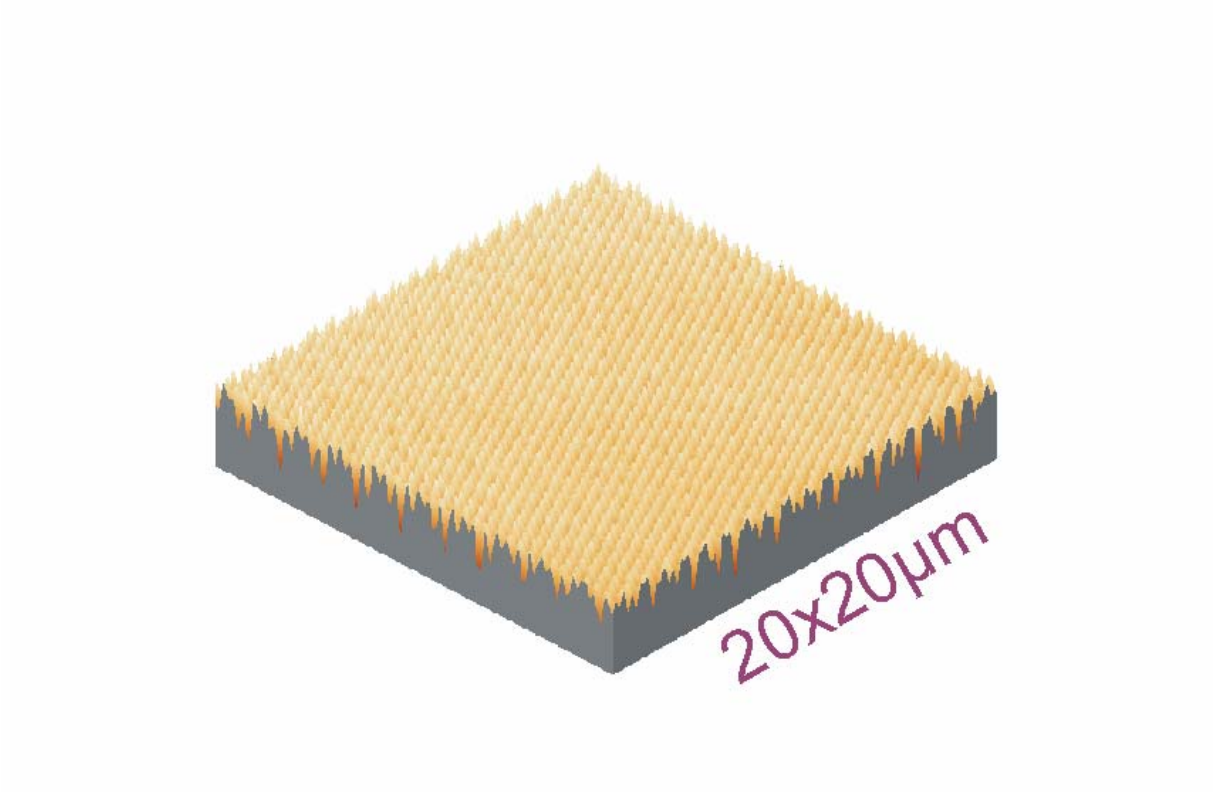

Fig. 5.10 *Detailed image of the AFM scan of the sample developed for 27 minutes in 1M KOH aqueous solution. A high quality photonic crystal is revealed with no presence of any kind of defects.*

5.6. Result analysis and discussion

Fourier transform is a useful mathematical tool for the characterization of periodic variations [5]. The forward Fourier transform (FFT) converts a periodic function from the space (or time) domain to the frequencies and the inverse Fourrier transform (IFT) does the vice versa. By applying FFT, a composite waveform, consisted of a sum of harmonic waves, can be decomposed in the same number of discrete frequencies, suitable for further processing. The *WSxM AFM* image browser [6], which has been already used for the AFM scan analysis, provides a function that enables the application of 2D FFT in periodic patterns. The resulting graphs for the 2D grating inscribed in IOG-1 glass and developed in the chemical solution for 27 and 45 minutes are presented in Fig. 5.11. At the left part of the Fig. 5.11 is presented the top view of the grating and in the right part the corresponding periodicities after a linear FFT transformation are presented. The discrete, singular orders presented in the right graphs depict the

similarity of the inscribed pattern to a single harmonic profile. There is a direct correspondence between the orders observed in Fig. 5.11 and the diffraction orders shown in Fig. 5.4 and for this reason we use the same notation. In Fig. 5.4 we observe only the diffraction orders [(1,1) , (1,-1)] for which the Bragg condition is satisfied. A weak signal from (1,0), not well distinguished in the photograph, was also appeared on the screen.

The application of the above analysis in the 2D periodic structure which contained the wavy pattern and obtained after 45 minutes of chemical treatment provided further clarification related to the origination of the smaller diffraction orders (see Fig. 5.4). When a large periodicity interferes in the pattern, diffraction orders corresponding to longer wavelengths are appeared in Fig. 5.11.

These orders, which are not readily visible in Fig. 5.11, are indicated with yellow arrows. As observed in the picture, the big periodicity forms a 1D grating on which the 2D grating is inscribed. It is possible that the orders correlated to the long periodicity are positioned in a direction parallel to the direction of the 2D grating. Additionally, all the main diffraction orders are appeared to be separated in smaller orders in the same direction (parallelism). The red dashed circles indicate the orders fro which this separation is more prominent. The direction of the separation remains the same as the direction of the 1D long modulation grating. From the above analysis we conclude that the separation of the main diffraction order to smaller diffraction orders is a result of the 1D grating that is strengthens after prolonged chemical development.

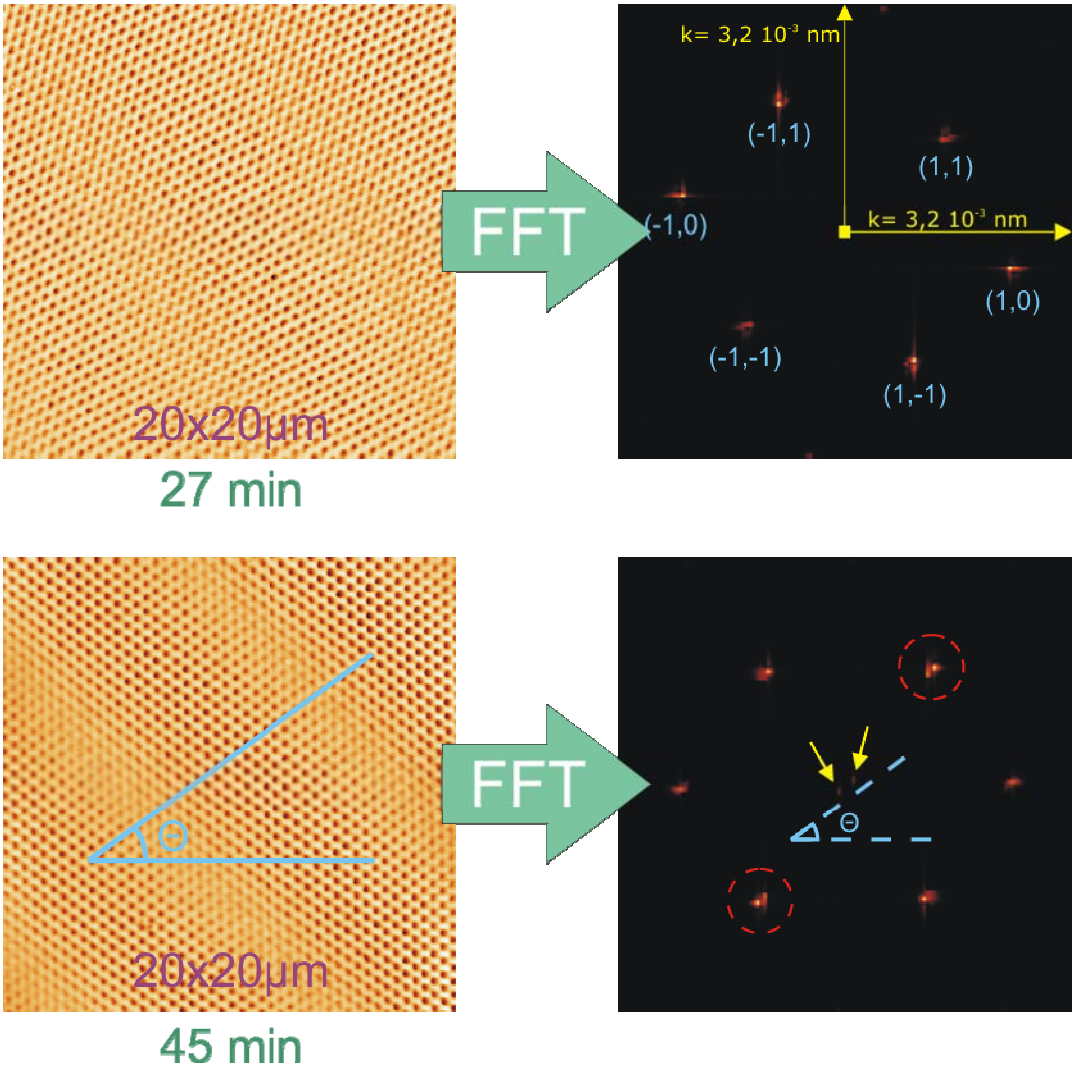

Fig. 5.11 *Forward Fourier transform (FFT) applied to the grating inscribed in IOG-1 glass after 27 (above) and 45 (below) minutes of chemical development in 1M KOH aqueous solution. Above: the Fourier transform reveals the periodicities corresponding to the periodic pattern. There is a direct correspondence between the above orders and those observed using the diffraction setup in figure 5.4, so the same notation is applied. Below: the 1D fluctuation appeared after prolonged chemical development induces more orders in the graph corresponding to smaller wavelengths. These orders (of low visibility) are indicated with yellow arrows. The main diffraction orders are also separated in smaller and the red dashed circles are used to denote the orders for which the separation is more prominent. The direction of the new orders and the separated ones is the same as the direction of the grating (see angle Θ)*

5.7. Analysis on the long period wavy pattern in the periodicity of the photonic crystal

SEM images of the 2D periodic structure inscribed in the IOG-1 glass sample with 134mJ/cm^2 energy density and 36000 pulses, and developed in 1M

KOH aqueous solution for 45 minutes are presented in the Fig. 5.12 In the SEM pictures of Fig. 5.12 it is observable, that in addition to the rhombic crystal pattern, changes in the depth and shape occur, which are in coherence with the long range mono-dimensional periodic modulation.

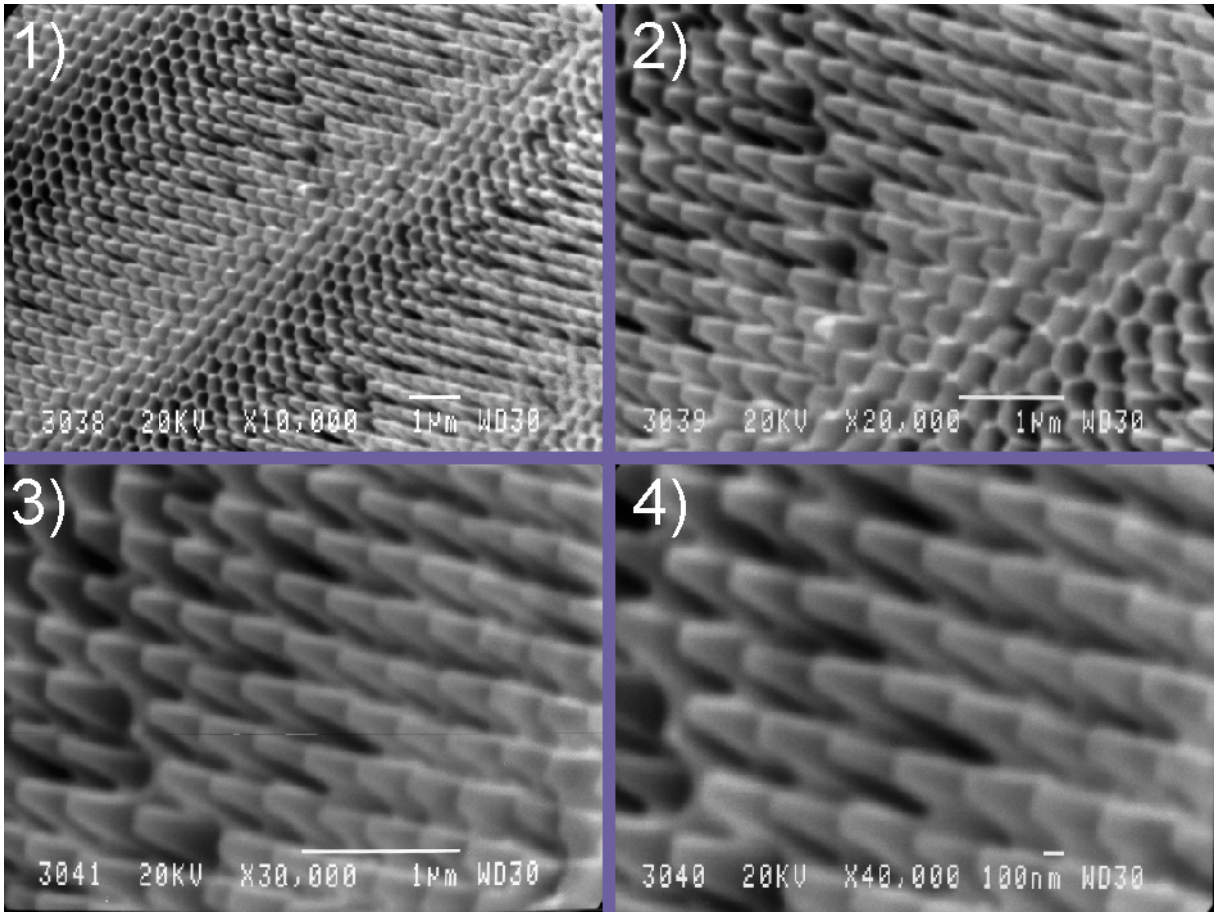

Fig. 5.12 *SEM images of the photonic crystal inscribed with 134mJ/cm^2 and developed in 1M KOH aqueous solution for 45 minutes. Each image corresponds to a different magnification factor from 10000 to 40000.*

In order to obtain additional information about the morphology of the surface a large are AFM scan is presented in Figure 5.13. In Figure 5.13, we observe that the long range mono-dimensional periodic modulation alters the depth of the photonic structure in a periodic way.

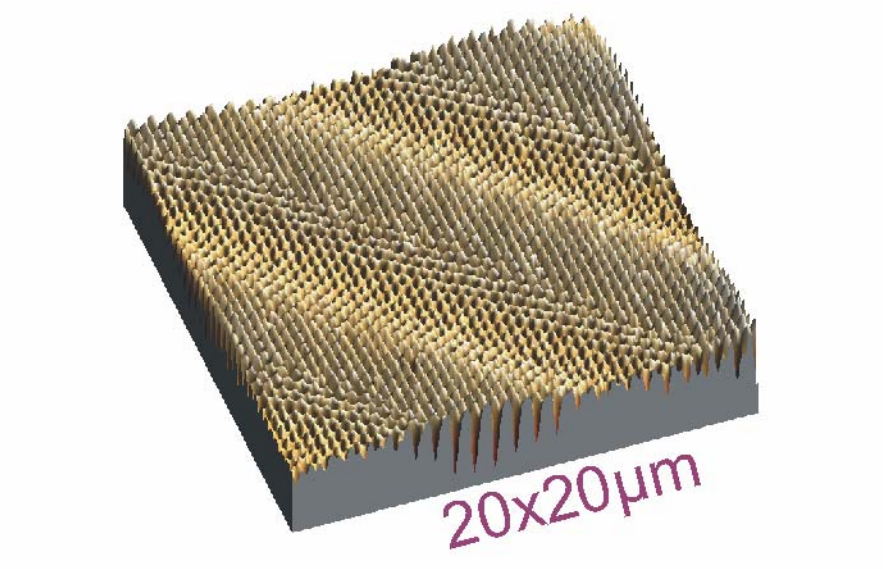

Figure 5.13 *Large area AFM scan of a photonic crystal inscribed with 134mJ/cm^2 energy density and developed in 1M KOH alkaline solution for 45 minutes*

The origin of this periodic perturbation is an issue for further investigation. One possible explanation may attribute this parasitic long range modulation to differences of the paths of the optical beams; which in turn are translated to a phase difference. Klein-Wiele *et al,* [7] demonstrated that a phase shift from 0 to 0.5π in the optical phase of the interfering beams, can alter the shape of the structure from an array of microcavities to an array of peaks. Such alterations are observable in Fig. 5.12. A second parameter that may be associated with such modulation may be that of *beam misalignment in pairs*. In such a case, the beams which interfere by two in opposite directions, form a plane where the phase vector lies slightly inclined with respect to the sample plane. This abnormal case is presented in Fig. 5.14. If this assertion holds for both of the pairs of the interfering beams, a long range modulation, similar to that presented here, can appear. For further investigation, a long range 1D periodicity was superimposed on the crystal presented in Fig. 5.3 and the resulting pattern is demonstrated in the Fig. 5.15. A pattern rather identical to those presented in Fig. 5.12 and Figure 5.13 is observed.

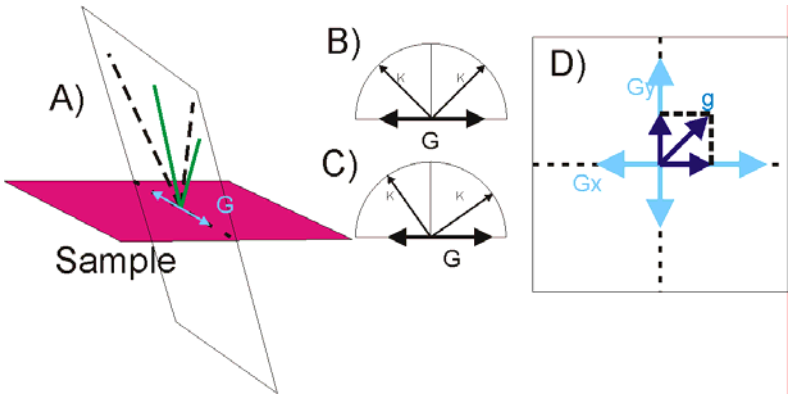

Fig. 5.14 *In picture A, the case where the beams which interfere by two in opposite directions (green continuous lines) form a plane where the phase vector lies slightly inclined with respect to the sample plane is presented. Picture B and C represent the k-vector analysis in the cases where the phase vector lies non-inclined (B) and inclined (C) with respect to the sample plane. Picture D represents the resulting long range modulation* ***g****.*

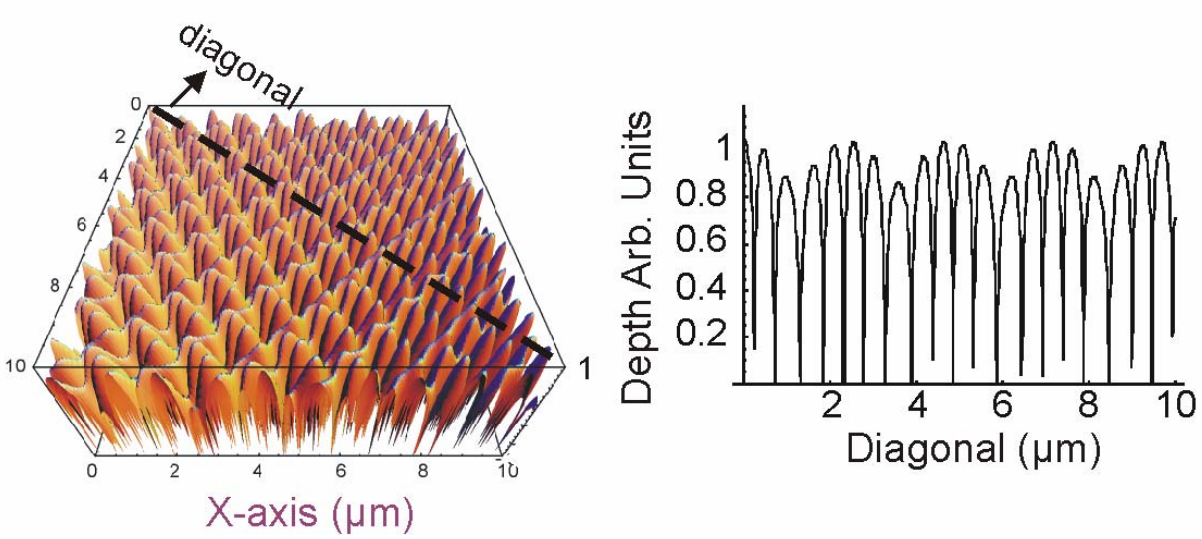

Fig. 5.15 *3D and 2D representation of the photonic structure when a long range 1D periodicity is superimposed on the periodic pattern.*

5.8. Conclusions

A two-dimensional photonic crystal in IOG-1 phosphate glass was successfully patterned by employing a 4-beam interferometer and the output of a 213nm, 150ps Nd:YAG laser. The interference pattern was recorded into the bulk of the material and afterwards the exposed areas were selectively removed by employing a chemical development technique in 1M KOH aqueous solution. The period of the structure was of the order of 500nm in the x axis, while the

etching depth was of the order of 200nm. AFM scans revealed high quality structures in terms of the smoothness and the symmetry of the peaks.

After 27 minutes of chemical development a high quality homogeneous photonic crystal was patterned. The depth of the relief structure was of the order of 100nm. Prolonged development in the alkaline solution resulted in the appearance of a 1D long range periodicity, superimposed on the rhombic two dimensional lattice. This periodicity was proven to result in the separation of the main diffraction orders into secondary ones. We believe that the origin of this perturbation is the differences in the optical paths between the beams converging in the xz plane and those converging in the yz plane. The origin and quantification of the long range modulation that is superimposed on the 2D photonic crystal is currently under further investigation.

The patterning technique presented here must be further optimized in order to obtained photonic crystal structures of improved quality and tailored diffraction. The technique exhibits many advantages over other photonic crystals fabrication methods, since it is a few step procedure, scalable for large scale production while its application does not rely on expensive laboratorial facilities, such as clean rooms and ultra-short wavelength lithographic equipment.

5.9. References

[1] L. Wu, M. Mazilu, T.F. Krauss, Beam Steering in Planar-Photonic Crystals: From Superprism to Supercollimator, J. Lightwave Technol., 21, 561-566 (2003)

[2] O. Painter, R.K. Lee, A.Scherer, A. Yariv, J.D. O'Brien, P.D. Dapkus, I. Kim, Two-Dimensional Photonic Band-Gap Defect Mode Laser, Science, **284**, 1819-1821 (1999)

[3] H. Park, S. Kim, S. Kwon, G. Kim, S. Kim, H. Ryu, S. Kim, Y. Lee, Single-Mode Operation of Two-Dimensional Photonic Crystal Laser with Central Post, IEEE Photon. Technol. Lett.,**15**, 1327-1329 (2003)

[4] J. Topol'ancik, P. Bhattacharya, J. Sabarinathan, P.-C. Yu, Fluid Detection with Photonic Crystal-Based Multichannel Waveguides, Appl. Phys. Lett., **82**, 1143-1145 (2003)

[5] A. Papoulis, Probability, Random Variables and Stochastic Processes, McGraw-Hill Companies, 3rd edition (1991)

[6] www.nanotec.es

[7] J. Klein-Wiele, P. Simon, Fabrication of Periodic Nanostructures by Phase-Controlled Multiple-Beam Interference, Appl. Phys. Lett., **83**, 4707-4709 (2003)

Chapter 6. Conclusions

In the present thesis, the fabrication of 1D relief Bragg gratings and 2D photonic crystal structures in Schott USA IOG-1 Er/Yb-codoped phosphate glass, by employing laser interferometric techniques, were demonstrated. Holographic lithography is rarely applied in the photonics and materials processing literature for the inscription of high quality relief periodic structures in "hard" optical materials like phosphate glasses. To the best of our knowledge it is the first time that a relief 2D photonic crystal is inscribed in glass substrates by employing the method presented.

6.1. Summary of results

The laser source used for grating inscription was a high intensity pulse 213nm, 150psec Nd:YAG laser. The UV induced photosensitivity was studied by employing spectrophotometric and diffraction efficiency measurements. Strong absorption bands in the visible range of wavelengths were induced by the exposure to the 213nm radiation. The absorption band in the visible range was attributed to hole center defects generated by the cleaving of the double covalent bond between a phosphorous and an oxygen ion. Kramers-Kronig analysis revealed changes in the refractive index after laser irradiation. These changes were correlated with the induced absorption bands by applying a diffraction analysis. In addition, radiation induced structural changes in the exposed material were investigated by employing examination of the ultraviolet Urbach tail slope. We believe that the structural changes created are more likely to be connected with electron center defects. Such a kind of defects can be generated by the cleavage of a single covalent bond between phosphorous and a bridging oxygen. That bond cleaving procedure results in polymeric phosphate chains of shorter lengths. Whatever the nature of the defects is, the defect population was found to increase linearly with the induced energy density, denoting a single-photon absorption process.

The interference pattern of two or more laser beams was inscribed in the glass volume in the form of a periodic perturbation in the optical and structural properties of the material. Subsequently a chemical development technique was applied in order to selectively remove the irradiated areas. Selective removal is preferable than direct ablation because in such an approach strong interactions between the laser irradiation and the material are avoided, resulting in reduced optical damage, stitching errors and debris deposition.

In our work, an acidic (HNO_3) and an alkaline (KOH) solution with different concentrations, were employed for developing the laser induced structures. The dependencies of the depth and the shape of the grooves upon the energy density of the irradiation and the concentration of the solutions were studied. The development in the alkaline solution yielded smoother and deeper patterns compared to those obtained with the acidic one. For the case of 1D Bragg reflectors, the maximum diffraction efficiency obtained was 0.1 corresponding to an average grating depth of about 120nm and 1 minute developing time in KOH. Our experimental data confirm that the method described above, constitutes a straightforward and relatively low cost approach, for the fabrication of high quality relief patterns in "hard" materials.

The fabrication of more complicated 2D photonic crystals was also demonstrated. A rhombic lattice 2D photonic crystal with average depth of about 200nm was successfully fabricated. The scattered orders of the periodic structure were examined by employing diffraction efficiency measurements and Fourier transform analysis. AFM and SEM analysis revealed that for prolonged immersion into the alkaline solution a long-period wavy pattern is generated. This unexpected artifact is due to imperfect alignment between the interfering beams. A more strict alignment of the optical setup is necessary in order to eliminate the presence of this undesirable defect.

Holographic UV laser lithography may attract an increased interest because it exhibits many advantages over other patterning techniques for fabricating periodic structures in planar samples. It constitutes a few step, mask-less procedure, of reduced stitching errors creation, while it does not require

expensive and complicated laboratorial facilities. In addition, it is relatively straightforward, thus, potentially suitable for large scale production.

On the other hand, rare earth doped phosphate glasses arise as front-running candidates for the development of high power, low pump waveguide lasing and amplification devices with numerous applications in the fields of telecommunications, sensing and spectroscopic devices. The phosphate glass used in the present study (Schott USA IOG-1) is a highly optimized glass for the realization of waveguide lasers and amplifiers. The composition of this glass allows the incorporation of rare earth ions at high concentrations and exhibits improved chemical resistance when treated with alkaline or acidic aqueous solutions. As far as, it concerns the laser properties, the transition lifetime of the material is relatively long compared to the lifetime of the pump level and the energy transfer efficiency from the sensitizing ion Yb is near unity. The inscription of Bragg reflectors in the IOG-1 phosphate glass could lead in the implementation of high gain lasers or amplification devices of low pumping power needs. For this reason high yield and easy to applied patterning techniques like the one described above could attract the interest for commercial applications and large scale production.

6.2. Future Plans

As it was mentioned previously, prolonged development of the 2D photonic crystal structure into the alkaline solution results in an undesirable wavy pattern, which convolutes with the short range periodicity and destroys the uniformity of the crystal. Experimental findings support that this is a result of an imperfect alignment of the optical setup. A more careful aligning and balancing of the optical paths of the interfering beams, will lead to the fabrication of perfect and uniform, continuous periodic patterns. A more compact beam-folding system may constitute a more reliable solution. In our intentions is to substitute the four-mirror system with a CaF_2 square pyramid prism (see Figure 6.1). We believe that this will simplify the alignment procedure and reduce the energy losses.

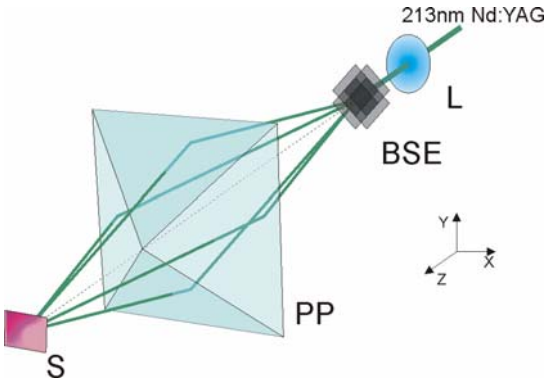

Fig. 6.1 Four-beam interference setup based on a CaF_2 square pyramide prism beam-folding system; (S) sample, (PP) pyramide prism, (BSE) beam splitting element, (L) lens.

A perfect relief photonic crystal inscribed in IOG-1 Er/Yb-codoped phosphate glass can constitute the base for the realization of high gain 2D lasers. A future plan is to cover the grating pattern with a polymeric layer with a refractive index greater than that of the phosphate glass (see Figure 6.2). This layer should be optimized for monomode guiding at the band of 1550nm. Lasing pump at the wavelength of 980nm can excite the underlying structured phosphate substrate. In addition, a point defect in the periodic structure may define a laser cavity. A sharp optical fiber tip of fine dimension in contact mode with the structure overlaid waveguide may act as such kind of defect.

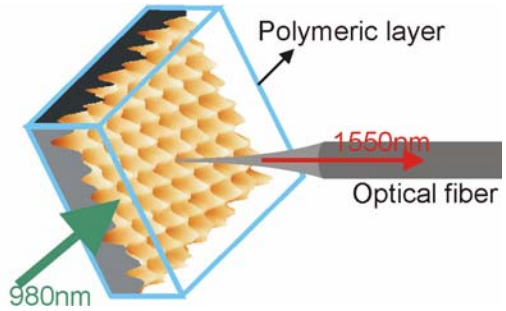

Fig. 6.2 2D laser device based on a 2D photonic crystal covered with a polymeric layer; the crystal is pumped at the wavelength of 980nm. Lasing is stimulated and amplified in the external induced cavity and outcoupled from the waveguide into a tipped fibre.

Lasing may be stimulated and amplified in that externally induced cavity, while laser emission at the 1550nm may outcouple from the active waveguide into the tipped fibre. Such a waveguide device may find application in sensing or optical communication applications.

Chapter 7. List of Publications

7.1. Journal Publications

1. C.Pappas, S.Pissadakis, UV-assisted selective chemical etching of submicron period relief gratings in Er/Yb-codoped IOG-1 phosphate glass, J. Phys. (submitted)

2. C. Pappas, S. Pissadakis, A Laser assisted Selective Chemical Etching Method for Micro-Structuring Phosphate Glasses: UV Induced Volume Damage Effects and Correlation with Chemical Etching Processes (to be submitted to JOSA B)

7.2. Conference Publications

1. C.Pappas, S.Pissadakis, 2-D Grating Reflectors in Er/Yb-codoped Phosphate Glass using Multi-beam UV-laser Holography and Selective Chemical Etching, 1st International Workshop on Advances in Nanophotonics (PHOREMOST), Heraklion, Greece (poster presentation) (2005)

2. C.Pappas, S.Pissadakis, Periodic Nanostructuring of Er/Yb-codoped IOG1 Phosphate Glass using UV-assisted Selective Chemical Etching, 3rd International Symposium on Nanomanufacturing (ISNM), Limassol, Cyprus (poster presentation), **TMP4,** p.66 (2005)

3. C.Pappas, S.Pissadakis, UV-assisted selective chemical etching of submicron period relief gratings in Er/Yb-codoped IOG-1 phosphate glass, 8th International Conference on Laser Ablation (COLA), Banff, Canada (poster presentation), **TuPO17.144**, p.241 (2005)

4. S.Pissadakis, C. Pappas, Two-Dimensional Bragg Reflectors Fabricated in IOG-1 Phosphate Glass using Multi-beam UV-laser Interference, Photonics Europe, Strasburg, France, April 2006 (accepted for oral presentation)